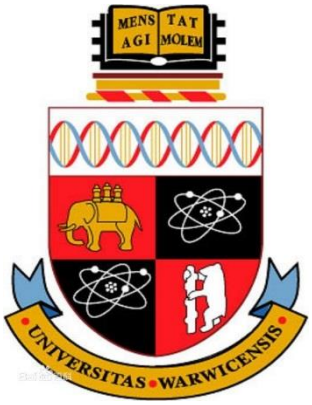

Strategic Placement of Viscous Dampers in Steel Buildings under Strong Earthquake Ground Motions

A thesis Submitted to the

University of Warwick

for the degree of

Doctor of Philosophy

by

Xiameng Huang

School of Engineering

Supervised by

Prof Theodore Karavasilis and Prof Toby Mottram

March 2018

Table of Contents

List of Illustrations and Tables

Chapter 2

Chapter 4

Chapter 5

Chapter 6

Chapter 7

List of Abbreviations

Abbreviation	Explanation
BSE	Basic Safety Earthquake
CDF	Cumulative distribution function
CMR	Collapse margin ratio
DBE	Design Based Earthquake
DM	Damage Measure
EA	Evolutionary algorithm
EC	Eurocode
EDP	Engineering Demand Parameter
FOE	Frequently Occurring Earthquake
FVD	Fluid viscous dampers
GA	Genetic algorithm
IDA	Incremental Dynamic Analysis
IM	Intensity Measure
MCE	Maximum Considered Earthquake
MRF	Moment-resisting frame
NRH	Nonlinear response history
PBSD	Performance-based seismic design
PGA	Peak Ground Acceleration

PGV	Peak Ground Velocity
PSA	Pseudo-spectral acceleration
SDOF	Single-degree-of-freedom
SF	Scale Factor
SSA	Sequential search algorithms
SSSA	Simplified Sequential Search Algorithm
TMD	Tune-Mass Damper

Acknowledgements

Many people and organizations have supported me and helped me to make this work become possible. I would like to express my special appreciation and thanks to the China Scholarship Council and the School of Engineering in the University of Warwick who provided me the funding opportunity and the academic research support for my PhD study.

First and foremost, I would like to thank my supervisor Professor Theodore Karavasilis, who kept guiding and motivating me throughout the period of my PhD study. I am sincerely grateful for his continuous support and encouragement when I met barriers in the research work. His assistances and suggestions allowed me to form my own research path and provide me a remarkable learning experience. I would also like to thank Professor Toby Mottram who acted as my formal supervisor in my final year's PhD study. I owe sincere gratitude to his guidance and suggestions that helped me complete the writing of my thesis. His encouragement and trust on my academic writing helped me overcome the most difficult time when I started to write the thesis.

Besides my main supervisors, I also thank my co-supervisors Dr Mohaddeseh Mousavi Nezhad and Dr Irwanda Laory for their valuable guidance and supports at the beginning of my PhD research. I would like to gratefully acknowledge Mr Kostas Kariniotakis, for his many hours' assistances on my learning of research techniques. His valuable suggestions helped me correct the mistakes in my research work. I would also like to thank my panel members Professor Wanda Lewis and Dr Xueyu Geng for their insightful comments and encouragement. My sincere thanks also go to the researchers

in the Civil Research Group and the members of the Resilient Steel and Steel-Concrete Structures Lab, who provided me with any kind of assistance during my research study.

Last but not the least, I would like to express my gratitude to my parents, for their spiritual support and guidance on my life journey. I would also like to thank my fiancé Miss Dan Wang for her consistent accompany and care during my study in the UK, especially in the days when I wrote my thesis.

Finally, I would like to dedicate this thesis to my grandmother, Qinxiang Jiang (1941-2016), who pushed me away from her sickbed and sent me back to the world of research.

Declaration

This thesis is submitted to the University of Warwick in support of my application for the degree of Doctor of Philosophy. It has been composed by myself and has not been submitted in any previous application for any degree.

29 November 2017

Xiameng Huang

Abstract

Supplemental passive dampers are generally considered as an effective tool to control the seismic response of multi-storey buildings. Since the optimum placement of passive dampers in buildings can potentially improve the structural performance or reduce construction cost, there is an increasing number of researchers engaged to optimize the damper placement in buildings. Given that a large number of studies have been conducted to investigate damper placement methods, a systematic method or a clear conclusion for strategically distributing dampers in buildings is not presented in any building guidelines. The main limitations of current damper placement studies may include the lack of focus on collapse resistance of retrofitted buildings, on beam and column nonlinear behaviors, and the lack of considering the variations of earthquake characteristics and intensity levels. The fundamental damper placement issue can be separated as the distribution of dampers throughout the height of the buildings and the distribution of dampers in different bays in building frames. In this research, both distributions are explored and their effect on the collapse performances of buildings under strong earthquakes is thoroughly studied. The effectiveness of advanced damper placement approaches is evaluated by comparisons with classical damper placement methods. Considering the uncertainty in earthquake ground motion characteristics, multiple ground motions scaled to various intensity levels are involved to evaluate the seismic performance of buildings. Finally, major conclusions towards the philosophy of the strategic damper placement in practical building constructions are presented in terms of the overall structural performance under strong ground motions.

Charter 1

Introduction

Seismic retrofit with supplemental energy dissipation devices has been proven to be an effective way for mitigating the dynamic response of buildings under earthquake excitations. Compared to conventional seismic design with strengthening members, supplemental passive dampers are generally considered to be more cost-effective on improving the seismic performance of structures. In recent years, there has been an increasing trend of using passive dampers to reduce the seismic response of new buildings and to rehabilitate old buildings.

The distribution of supplemental damping in the buildings may significantly influence the structural dynamic response and therefore affect the final building cost. Many damper placement and damper optimization algorithms have been proposed by previous researchers over the past decades, however, none of these approaches have been adopted by any of the existing design standards or guidelines. As Takewaki (2009) mentioned, there is a wide range of necessity for structural engineers and researchers to improve and further develop current methods for optimal damper placement.

Most of the previous studies regarding the seismic damper placement solely consider the structures under a design-level earthquake and normally ignore the variations of the seismic characteristic along with the changes of the seismic intensity levels and the earthquake components. Moreover, none of these researches has considered the global resistance of the buildings in the collapse state under strong earthquake excitations.

This research mainly focuses on exploring the strategic placement of passive dampers in steel buildings under strong earthquakes which would result in building collapse. The optimum damper distribution strategy in terms of the collapse resistance of buildings under multiple ground motions will be further investigated. Both vertical damper distribution and horizontal damper distribution are explored in buildings of different heights, under far-fault and near-fault earthquakes. This aims to provide logical and beneficial design recommendations for structural engineers to distribute passive dampers in steel buildings and drop final conclusions for the effectiveness of advanced damper placements methods through comparisons with classical damper placement methods.

The aims are achieved by firstly introducing the background of the seismic design methods and reviewing the standard applications of passive dampers, especially the basic concepts of viscous dampers in Chapter 2. A literature review of existing damper placement methods is presented in Chapter 3, where the fundamental optimization problem of damper placement is outlined and the limitations of the current damper distribution approaches are summarized. As one of the most famous and powerful stochastic optimization algorithms, genetic algorithms (GA) is adopted in this thesis to investigate the feasibility of the vertical damper distributions. To explore the constrained optimization problem in the vertical damper distribution of buildings under various seismic intensity levels, a sophisticated optimization framework which is based on the combination of genetic algorithms (GA) and nonlinear response history (NRH) analysis is presented in Chapter 4.

For evaluating the effectiveness of the GA-NRH framework regarding the height-wise damper distribution, the seismic performance of two elastic shear

buildings with GA damper distributions are compared with other damper placement methods in Chapter 5. In Chapter 6, the effectiveness of GA optimization on height-wise damper optimization is further investigated by using performance-based designed inelastic buildings. Two code-compliant realistic structures are modelled with nonlinear assumptions and optimized under ground motion suites that contain a larger number of ground motions. The collapse performances of the optimized buildings are assessed by conducting Incremental Dynamic Analysis (IDA) and the effectiveness of the GA damper distribution on building collapse is evaluated by comparisons with the classical stiffness proportional damping methods.

In Chapter 7, the performance of the passive dampers horizontally distributed in different bays of building frames is explored, regarding the load paths of the additional column loadings caused by the damper forces. Various horizontal damper distributions and the damper distribution approach using the counteraction of axial forces are investigated by assessing the probability of collapse. In addition, the plastic mechanisms of the retrofitted buildings are compared to assess the damper placement strategies.

At last, in Chapter 8, the final conclusions of the thesis are presented based on the results and the conclusions of each individual chapter.

Charter 2

Background

2.0 Introduction

This chapter mainly focuses on introducing the background of seismic design and the background of supplemental passive dampers. The fundamentals of conventional earthquake-resistant design based on Eurocode 8 and the philosophy of performance-based seismic design (PBSD) is briefly discussed in section 2.1. Incremental Dynamic Analysis is further introduced as a novel method to consider the collapse mechanism under the framework of PBSD. The mathematical theory and the construction knowledge of story-installation-type passive dampers are presented in section 2.2. Different types of energy dissipation devices and supplemental passive dampers applied to ordinary buildings are discussed. The energy dissipation mechanism of the general viscous dampers and the fluid viscous dampers (FVDs) are discussed in more detail as these are the dampers to be used in the optimization studies of this thesis.

2.1 Seismic Design

2.1.1 Background

Earthquake is one of the most intensive and unpredictable natural hazards that cause numerous loss of human lives, unrecoverable damage of infrastructures and imponderable economic losses. In accordance to Kramer (1996), the earliest earthquakes records written by human beings date back to 3000 years ago in ancient China. Kramer (1996) also notes that the practice in contemporary earthquake engineering involves the identification and the mitigation of earthquake hazards.

Earthquake-resistant design, which is generally known as seismic design, is defined by Bommer and Stafford (2009, p. 6) as "the art of balancing the seismic capacity of structures with the expected seismic demand to which they may be subjected." Specifically, seismic design of structures is a systematic design philosophy that aims to ensure safety of humans, the limitation of the structural damage and the functional continuity of infrastructure facilities.

In terms of the seismic design approaches, Constantinou et al. (1998) mention two alternative procedures. One is to dissipate the seismic energy with the ductile plastic hinges within the conventional lateral force resisting system; the other is to utilize the additional motion control devices to reduce the seismic response of the structure. For the traditional seismic design approach, the energy absorption relies on the occurrence of inelastic deformations in the beams and column bases. For the motion control systems, this task is accomplished by dissipating the energy with supplemental mechanical damping devices or utilizing seismic isolation.

2.1.2 Eurocode Force-based Seismic Design

This research mainly focuses on exploring the seismic retrofit of buildings using steel moment-resisting frame (MRF). MRFs, which have been in use in building industry over a hundred of years, are commonly considered as one of the most ductile systems to sustain the excitation from natural hazards. Eurocode 3 (BS EN 1993-1-1:2005) describes the fundamental requirements for designing a steel building, while Eurocode 8 (BS EN 1998-1:2004) presents the specific seismic design criteria for a steel structure. In accordance to the main objectives of EC8, the seismic design should ensure the protection of human lives, the limitation of the damage within the structures and the

operational state of the structures important for civil protection. These objectives are present throughout the rules and the conditions in the code and explicitly formalized as two structural design criteria for compliance:

1. **Damage limitation requirement** (Serviceability Limit State):

   In terms of ordinary structures, this requirement should be met for a moderate seismic event with a return period of 95 years. Under this seismic performance level, the structures should withstand the seismic action without permanent deformations of the elements and avoid economic losses due to the structural repair.

2. **No-Collapse requirement** (Ultimate Limit State):

   In terms of ordinary structures, this requirement should be met for an intensive seismic event with a return period of 475 years. In term of this performance level, the structures should withstand the seismic action without the global or local collapse, retain structural integrity and maintain sufficient residual load bearing capacity.

Nowadays it is widely considered that the seismic vibration of the structure at the surface is significantly influenced by the local ground characteristics. Hence to account for the ground conditions and the local seismic hazards, Eurocode 8 (BS EN 1998-1:2004) defines five fundamental ground profiles and specifies four classes of the building importance.

The seismic performance of a structure with certain site condition is generally represented by an elastic ground acceleration response spectrum, called “elastic response spectrum”. More specifically, an elastic response spectrum represents the relationship between the fundamental vibration period and the

response spectral acceleration of a linear single-degree-of-freedom (SDOF) system at a given point with varying periods under a realistic ground motion. A typical shape of elastic response spectrum is shown in Figure 2.1. In reality, most of the realistic structures experience nonlinear behaviors while resisting seismic actions. Therefore, to avoid the complexity of inelastic analysis in the structural design, a behaviour factor q is introduced to reduce a response spectrum and generate a "design spectrum" for performing an elastic analysis. The values of the behavior factor q, which account for the capacity of the structure to dissipate energy, is determined by the relevant ductile classes of the structural systems. A larger q value represents a higher ductile level of the structure. Eurocode 8 (BS EN 1998-1:2004), 3.2.2.2 and Eurocode 8 (BS EN 1998-1:2004), 3.2.2.5 explicitly describe the procedures for constructing the elastic response spectrum and design spectrum for elastic analysis respectively. Additionally, EC3 and EC8 have specific requirements for beam and column design which aim to force plastic hinges occurred in beams instead of columns and hence avoid a "soft-storey".

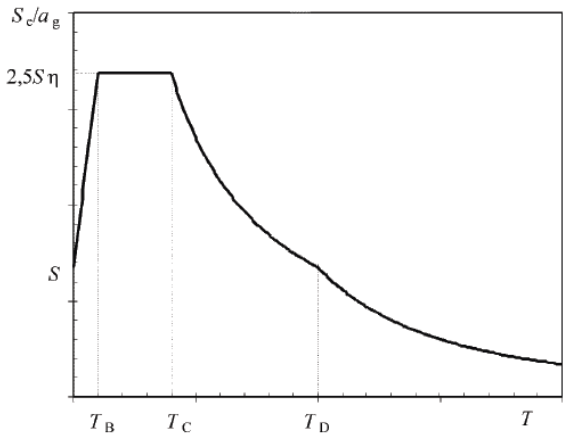

Figure 2.1 Shape of the elastic response spectrum (EC 8, BS EN 1998-1:2004)

2.1.3 Performance-based Seismic Design

With the development of advanced seismic resistance strategies, seismic design of buildings has been changed from "strength" to "performance". Rather than considering the strength of the building under the two design levels associated with the force-based seismic design philosophy in EC8, an increasing number of designers and researchers employ a multilevel performance-based seismic design (PBSD) approach to evaluate the building performance under various seismic intensity levels.

In accordance to FEMA 356 (ASCE 2000), four target building performance levels are defined for the PBSD as the 'Operational' level, the 'Immediate Occupancy' level, the 'Life Safety' level and the 'Collapse Prevention' level, while four probabilistic earthquake hazard levels are determined to have a probability of earthquake exceedance with 50%/50 year, 20%/50 year, 10%/50 year and 2%/50 year respectively. The detailed description for the target building performance levels and the seismic hazard levels are shown in Table 2.1 and Table 2.2.

Figure 2.2 provides an illustration for the relationship between the multiple seismic design levels and the seismic performance levels, which is proposed in the Version 2000 Committee prepared by the Structural Engineers Association of California (SEAOC 1995). The four building performance levels and the four seismic hazard levels presented in the illustration correspond with those defined in Table 2.1 and Table 2.2. In terms of the classification for the building importance, three structural performance objectives are defined as 'the basic objective', 'the enhanced objective 1' and 'the enhanced objective 2', corresponding to the ordinary structures, the essential structures and the hazardous structures respectively. Based on these

performance objectives, the design for a building should either increase a seismic hazard level or decrease a structural performance level when the importance of the building increases.

Table 2.1 The seismic hazard levels for PBSD (ASCE 2000)

Classification	**Seismic Hazard Levels**	**Probability of Exceedance**	**Mean Return Period (Years)**
Level 1	Frequently Occurring Earthquake (FOE)	50%/50 year	75
Level 2	-	20%/50 year	225
Level 3	Design Based Earthquake (DBE) or Basic Safety Earthquake-1 (BSE-1)	10%/50 year	500
Level 4	Maximum Considered Earthquake (MCE) or Basic Safety Earthquake-2 (BSE-2)	2%/50 year	2,500

Table 2.2 The target building performance levels for PBSD (ASCE 2000)

Classification	**Performance Levels**	**Overall Damage**	**Description of Post-earthquake Damage**
EQ-I	Operational	Very Light	No permanent drift, structure entirely maintain original stiffness and

			strength, minor cracking of structural elements, all systems are functional for operation
EQ-II	Immediate Occupancy	Light	No permanent drift, structure substantially maintain original stiffness and strength, minor cracking of structural elements, elevators and fire protection are functional
EQ-III	Life Safety	Moderate	Some permanent drift, some residual stiffness and strength, gravity resistance systems are functional, probably beyond economical repair
EQ-IV	Collapse Prevention	Severe	Large permanent drift, Little residual stiffness and strength, some exits inaccessible, building near collapse

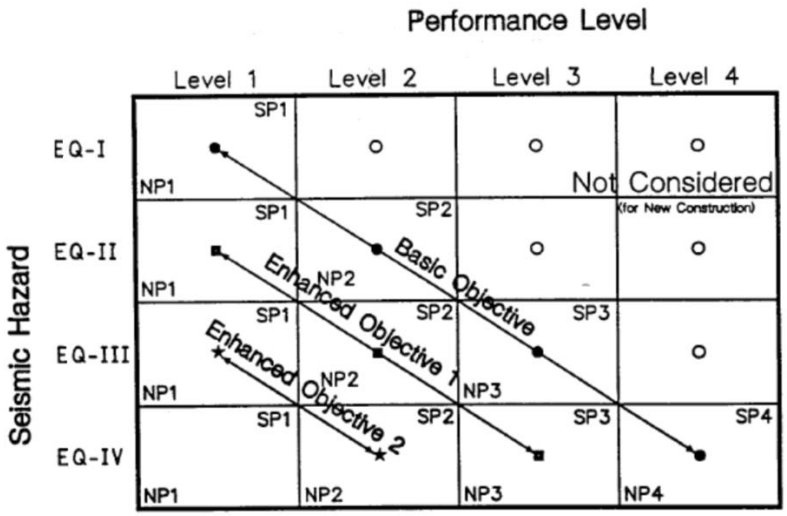

Figure 2.2 Relationship between the earthquake design level and performance level (Priestley 2000)

2.1.4 Incremental Dynamic Analysis

For evaluating the structural performance under the Collapse Prevention level, in addition to considering the local behavior of the individual structural elements, it is rather essential to consider the global collapse capacity of the structure system. For the assessment of the building collapse capacity, FEMA P695 (ATC 2009) highlights that Incremental Dynamic Analysis (IDA) (Vamvatsikos and Cornell 2002) is a cardinal solution for considering the median collapse intensity and the global collapse probability of a structure under a series of earthquake excitations. In accordance to IDA, each ground motion within the ground motion records series is scaled to increasing intensities until the extreme seismic intensity results in global collapse of the structure.

Several important control parameters defined by IDA are the Scale Factor (SF), the Intensity Measure (IM) and the Damage Measure (DM). SF is the non-negative scalar value to characterize the intensity of the natural accelerogram. IM is the selected quantity used to represent or measure the

intensity of the unscaled accelerogram which is monotonically increasing with the SF. The Peak Ground Acceleration (PGA), the spectral acceleration at the structural fundamental period $S_a(T_1)$ and the Peak Ground Velocity (PGV) are the common quantities selected for the IM. DM or Engineering Demand Parameter (EDP) is the parameter utilized to characterize the associated structural response of the building model due to the scaled seismic excitation (Vamvatsikos and Cornell 2002).

Figure 2.3 provided an illustration for a set of IDA results, where each point plotted in the figure represents the seismic intensity versus a certain structural performance level of a single nonlinear response history (NRH) analysis for a structural model subjected to a single ground motion scaled to an intensity level. In Figure 2.3, the spectral acceleration for the vertical axis and the maximum interstorey drift ratio for the horizontal axis corresponds to the seismic intensity and the structural performance level respectively. Each IDA curve is formed by connecting the points representative for a certain earthquake record in accordance to the progressively increasing trend of the spectral intensity, while the differences within the different IDA curves indicate the variety of the dynamic response for a given structural model under different earthquake excitations. Two criteria can be used to determine the occurrence of collapse failure of the structural model subjected to each ground motion. One is directly based on the limitation for the maximum lateral displacement or the maximum interstorey drift of the structural model, the other is based on the non-simulated component occurred in the computational process of the model simulation. As can be seen from Figure 2.3, the median collapse intensity $\hat{S}_{CT}$ =2.8g is defined as the spectral acceleration that 50% of the considered ground motions result in initial collapse failure of the structure. The MCE spectral intensity S_{MT}=1.1g can be

obtained from the design response spectrum of DBE or MCE earthquakes at the structural fundamental period in building design codes. The collapse margin ratio CMR, as presented in Equation 2.1 and Figure 2.3, is the ratio between the median collapse spectral acceleration $\hat{S}_{CT}$ and the MCE spectral acceleration S_{MT}. It is also important to note that CMR is the primary index for collapse safety assessment and seismic design criteria of the structure, which is normally applied to the 5% damped structures.

$$CMR = \frac{\hat{S}_{CT}}{S_{MT}} \tag{2.1}$$

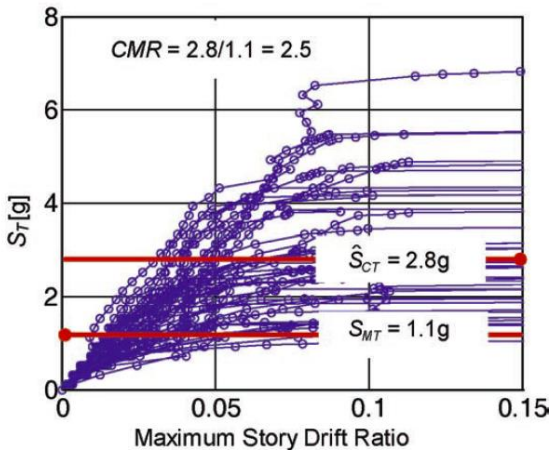

Figure 2.3 A typical set of IDA curves (ASCE 2009)

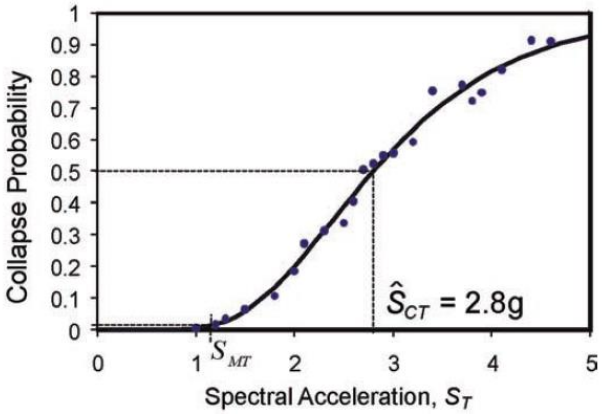

Figure 2.4 A typical collapse fragility curve or fitted lognormal CDF (ASCE 2009)

Using the information of collapse from the IDA results, the probability of collapse at a given S_a intensity level can be estimated as the fraction of records based on the percentage of earthquakes that have already caused collapse at this intensity level. As is illustrated in Figure 2.4, a lognormal cumulative distribution function (CDF) is normally fit through the fraction of collapse records to generate a collapse fragility curve (Ibarra and Krawinkler 2005). The CMR value can also be derived from the median collapse intensity $\hat{S}_{CT}$ and MCE spectral acceleration S_{MT} as indicated in Figure 2.4, while the $\hat{S}_{CT}$ corresponds to a 50% probability of collapse.

2.2 Passive Dampers

2.2.1 Background

Passive control systems or passive energy dissipation systems are generally classified as seismic retrofit systems since their function is to mitigate dynamic response of the structure under seismic excitation. Rather than dissipating the energy by the occurrence of structural inelastic deformations, passive control systems absorb the energy by the mechanical devices incorporated in the buildings and provide a supplement damping to the main structure. The term 'passive' represents that the systems do not require any externally supplied power which is distinguished from the terms of 'semi-active' and 'active' for semi-active control systems and active control system (Constantinou et al. 1998). In addition to reduce the structural seismic response, passive control systems are also effective and efficient in improving the dynamic response of building under wind excitation and other service loads.

In accordance to the present industrial application, three primary type of passive control system applied to the ordinary building structures as

illustrated in Figure 2.5 are:

1. **Story-installation-type passive dampers:**

   This kind of supplemental damper systems are normally installed within the bays throughout the height of the frames. Common examples are the viscous damper, the viscoelastic damper, the hysteretic damper and the re-centering damper.

2. **Tune-Mass Dampers (TMDs)**

   This kind of modern damper systems originate from Dynamic Vibration Absorber presented by Frahm dating back to 1909. Typically, these dampers are huge steel bodies or concrete blocks mounted in the taller stories of the high-rise buildings.

3. **Base-isolation systems**

   A seismic base-isolation system is generally installed at the base of a structure. It can partially reflect and partially absorb the earthquake energy input into the structure during a seismic excitation, by preventing the primary structure from receiving this energy directly (Constantinou et al. 1998).

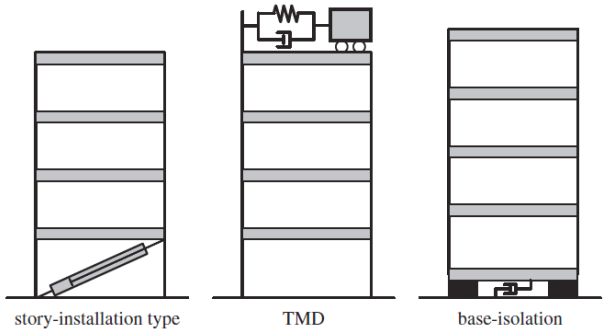

Figure 2.5 Three principal installation types of passive control system (Takewaki 2009)

In the early stage of applying passive structural control systems, the principle design philosophy solely focuses on the installation itself of passive dampers in the buildings. With the development of the damper installation techniques and the damper systems variety, it appears that the objective for the damper design is directed to the smart installation and the optimal placement of the supplemental passive dampers (Takewaki 2009). This research mainly focuses on exploring the optimal placement strategy of the story-installation-type passive dampers in the multistorey buildings. Specifically, the Fluid Viscous Damper (FVD) installed in the moment-resisting frame (MRF) is principally treated as a standard example in the present work.

2.2.2 Story-installation-type Passive Dampers

The story-installation-type passive dampers vary greatly in damping mechanism and damper material. Generally, these passive damping devices can be characterized into three main categories as hysteretic damper, viscous & viscoelastic damper and re-centering damper. The detailed principle of operation, material and technologies and performance objectives for these passive dampers are summarized in Table 2.3 respectively.

Table 2.3 Story-installation-type passive damper systems (Constantinou et al. 1998)

Classification	Principle of Operation	Material and Technologies	Performance Objectives
Hysteretic Damper	Yielding of metal	Steel or Lead	Strength Enhancement & Energy Dissipation
	Friction	Metal-to-metal or non-metal contact	

Viscous & Viscoelastic Damper	Deformation of viscoelastic solids	Viscoelastic polymers	Stiffness Enhancement & Energy Dissipation
	Deformation of viscous or viscoelastic fluids	Highly viscous fluids	
	Fluid orificing	Fluids; advance orifice designs	
Re-centering Damper	Fluid pressurization and orificing	Compressible fluids and high pressure sealing	Strength Enhancement & Re-centering Capability & Energy Dissipation
	Fiction-spring action	Metal-to-metal or non-metal contact	
	Phase transformation in metals	Shape memory alloys and superelastic behavior	

Viscous dampers have been demonstrated as an extremely effective device to dissipate seismic energy for structures. As Soneji & Jangid (2007) mentioned, fluid viscous damper (FVD) has the most rapid growth in the application of energy dissipation systems for both buildings and bridges, since it has the large capability for dissipating energy. As viscous damping devices and FVD is mainly focused to explore the damper placement method in this research, the following sections will describe the mathematical modeling of viscous dampers, the mechanical design of FVD, the installation concerns of FVD

and the industrial limitations of FVD.

2.2.3 Mathematical Modeling of Viscous Dampers

The general viscous damper system as illustrated in Figure 2.6 can be ideally modeled into two mathematical models, which is a single dashpot and a dashpot supported by a spring (Maxwell model) respectively (Takewaki 2009). For the Maxwell model, the spring represents the stiffness of the local viscous damper or the supporting system. The Maxwell model can be easily transformed to the Kelvin–Voigt model accordingly. Based on the force-displacement relationship in the frequency domain, the viscous damper force $F(\omega)$ can be expressed by

$$F(\omega) = (K_R + iK_I)U(\omega) = \frac{1}{\frac{1}{i\omega c} + \frac{1}{k_S}} U(\omega) = (k_V + i\omega c_V)U(\omega) \qquad (2.2)$$

While $K_R + iK_I$ denotes the complex stiffness of the damper system that contains the real and imaginary parts, $U(\omega)$ denote the displacement of the damper system, c and k_S denote the damping coefficient of the dashpot and the spring stiffness in the Maxwell model respectively, c_V and k_V denote the damping coefficient of the dashpot and the spring stiffness in the Kelvin-Voigt model respectively.

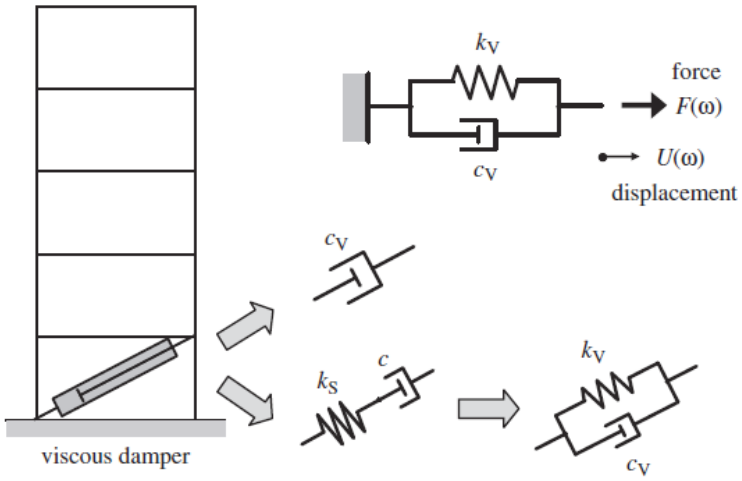

Figure 2.6 Viscous damper system modeled with dashpot model, Maxwell model and Kelvin–Voigt model (Takewaki 2009)

2.2.4 Fluid Viscous Dampers

Fluid viscous damper (FVD) is one of the most common energy dissipation devices for seismic mitigation of buildings and bridges (Symans et al. 2008). A typical FVD consist of a hollow fluid-filled cylinder as illustrated in Figure 2.7. The compressible silicone fluid is forced to flow via the action of the piston rod with a piston head. This piston head is designed with a fluidic control orifice that enable the fluid to flow through. The resulting pressure differential across the piston head can provide extreme large forces against the motion of the FVD (Lee and Taylor 2001). Additionally, the friction forces caused by the high-velocity fluid flows or the deformation of the compressible fluid can provide essential energy dissipation in the form of heat. Figure 2.8 and Figure 2.9 display two FVDs manufactured by Taylor Devices, Inc and ITT Enidine, Inc respectively.

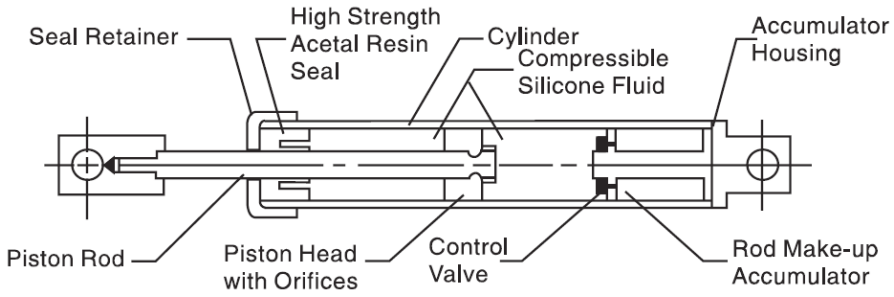

Figure 2.7 Construction of a typical FVD (Constantinou and Symans 1993a)

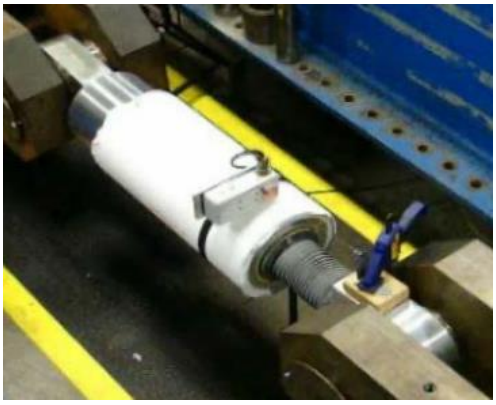

Figure 2.8 A Tested Story-installation-type FVD (Taylor 2011)

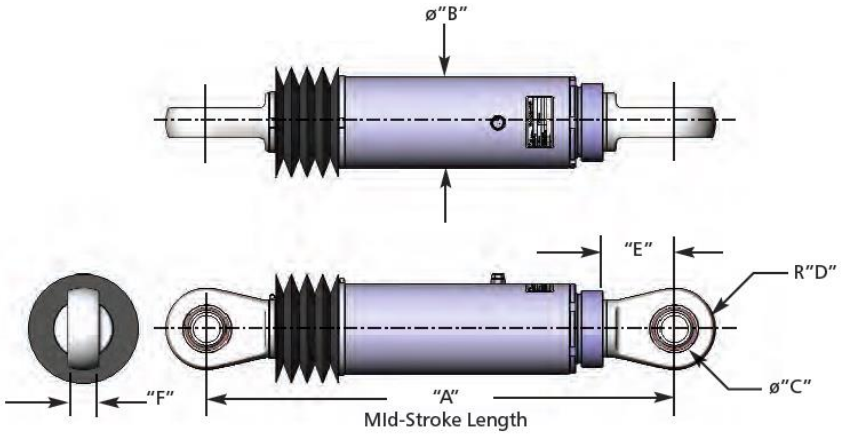

Figure 2.9 A typical FVD utilized for building application (ITT 2017)

To explore the nonlinear behavior of FVD, Seleemah and Constantinou (1997) conduct an experimental test that found out the force-velocity relationship of FVD as shown in Equation 2.3.

$$P(t) = C|\dot{u}(t)|^{\alpha}\text{sgn}[\dot{u}(t)] \quad (2.3)$$

While $P(t)$ is the damper force; C is the damping coefficient; $\dot{u}(t)$ is the piston velocity; α is an exponent related to the design of the orifices in piston head in the range from 0.3 to 2.0; sgn[ ] is the signum function. For seismic applications, the exponent α is normally in the range from approximately 0.3 to 1.0 (Symans et al. 2008). For $\alpha = 1$, the physical model of the damper can be described as a linear viscous dashpot and its idealized hysteretic behavior is shown in Figure 2.10. Antonucci et al. (2004) provide an experimental description for the hysteretic behavior of the FVDs with different α as shown in Figure 2.11. As can be seen from the figure, the FVD dissipated energy for a single cycle of harmonic motion is roughly equal to the equivalent area enclosed by the force-displacement hysteresis curve.

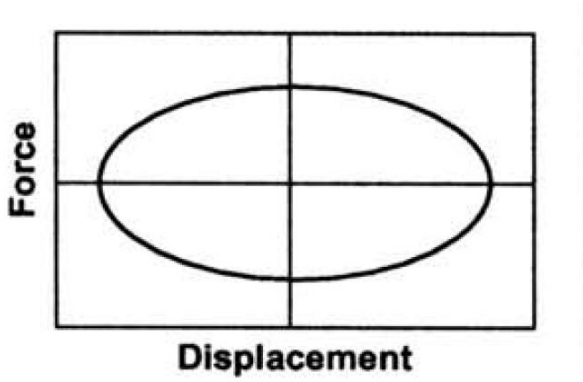

Figure 2.10 The idealized force-displacement relation of a linear viscous damper (Symans et al. 2008)

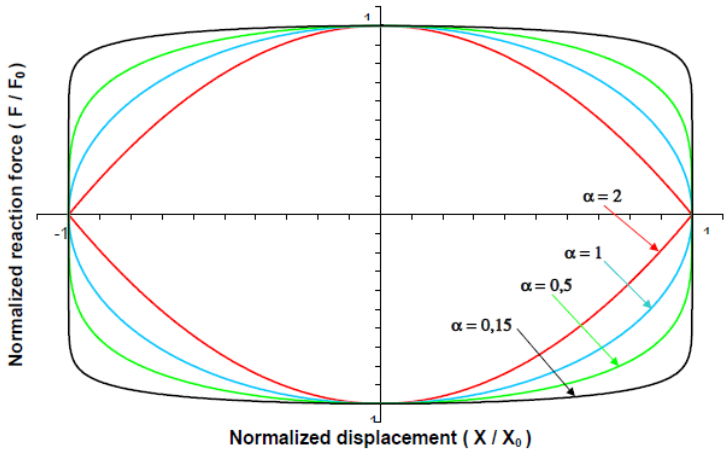

Figure 2.11 Normalised force-displacement relation of FVD with different values of the exponent α (Antonucci et al. 2004)

2.2.5 Installation of Fluid Viscous Dampers

In general, dampers are connected to the primary structural frame through a bracing system. Common bracing systems for story-installation-type FVDs include the diagonal bracing system and the chevron bracing system as illustrated in Figure 2.12 (Taylor 2002). Figure 2.13 and Figure 2.14 provide the construction detailing for a typical diagonal bracing system and a two-damper chevron bracing system. Considering that the damper effectiveness is limited by the slight motion across the damper when the FVDs are installed in a relatively stiff structural frame or when the structural frame is under wind excitation context, some novel damper bracing systems are developed to amplify the motion response of the FVDs. Examples of these novel damper bracing systems include the toggle bracing system and the scissor-jack bracing system (Symans et al. 2008). Figure 2.15 and Figure 2.16 show the construction detailing for a typical toggle bracing system and a scissor-jack bracing system with an attached FVD respectively. With these bracing systems, the displacement of the dampers can be amplified significantly and damper reaction force is therefore increased.

As the columns attached to the damper braces undertake the vertical component of the damper reaction forces, the accumulated axial loads in the base columns adjected to brace-damper bays become a critical design concern (Constantinou and Symans 1993a). Hence, strategically distributing the brace-dampers in different bays may be effective to alleviate the axial column loading. This concern is further explored in the Charter 7.

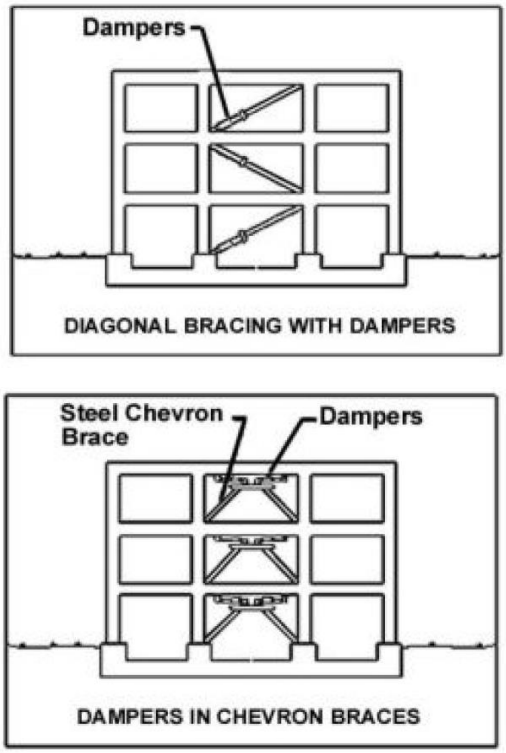

Figure 2.12 The illustration of diagonal bracing system and chevron bracing system in a structural frame (Taylor 2002)

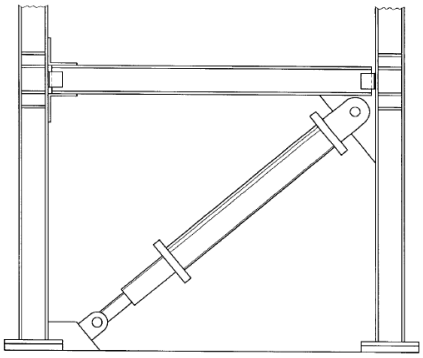

Figure 2.13 The construction detailing of a typical diagonal bracing system with a FVD (Constantinou 2002)

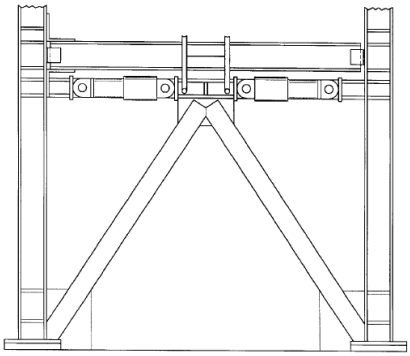

Figure 2.14 The construction detailing of a typical chevron bracing system with two FVDs (Constantinou 2002)

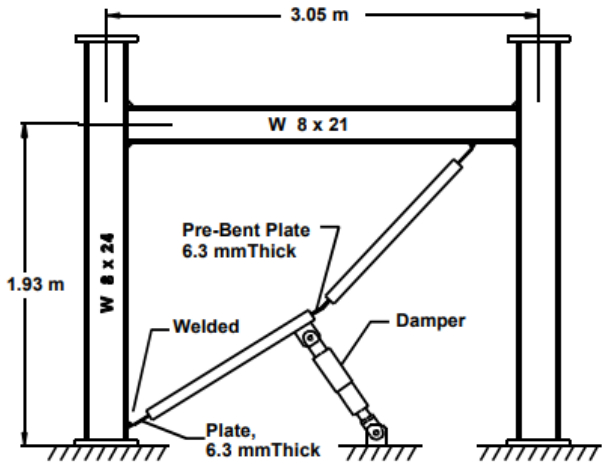

Figure 2.15 The construction detailing of a typical toggle bracing system with a FVD (Taylor 2000)

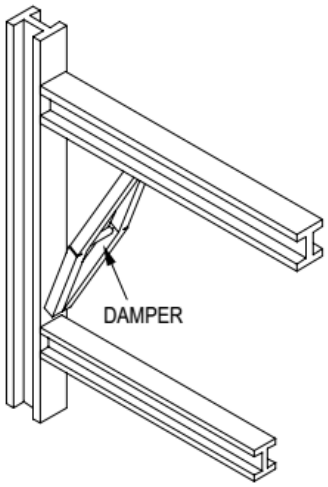

Figure 2.16 The construction detailing of a typical bracing system with a FVD (Sigaher and Constantinou 2003)

2.2.6 Advantages and Limitations of Fluid Viscous Dampers

Compared to other types of passive dampers or energy dissipation devices, a FVD contains a series of inherent and remarkable advantages. These advantages include low maintenance required, long-term lifetime, significant self-contained energy dissipation capability and damper forces being out of phase with the elastic forces in the structure (Di Paola et al. 2007). A fluid viscous damper is normally more cost-effective than other types of dampers in terms of purchase, installation and maintenance. It is possible to be reused in several severe seismic environments. Additionally, modern FVDs are generally designed with high fluid pressure that makes the dampers small and convenient for installation. Moreover, the output forces of a FVD is out of phase with the primary bending moment and the shear forces in a structure indicating that the damper force of FVD could be potentially used to reduce the structural elastic forces (Taylor and Constantinou 1998)

Given that the FVDs have various advantages for industrial application, a

fluid viscous damper becomes a superior choice for determining the energy dissipation system of an ordinary structure. However, some limitations are still existed for the popularization and the design of the FVDs. To some extent, the total cost of the FVDs installed for a taller building is relative expensive although the price of a single FVD is lower than other types of the damping devices. As Di Paola et al. mentioned (2007), another limitation is the nonlinear behavior of the seismic frames superimposed by the highly nonlinear behavior of the FVDs, makes the whole damper-structure system become a high-order nonlinear system in seismic context. This complex system results in that the response spectrum technique may not be applied to solve the differential equations of the nonlinear system. Both the limitations noted above point to a concern that whether the optimal placement of the FVDs (or other dampers) in each storey could be achieved to minimize the total damper cost for the tall buildings in earthquake environment. To find out the optimum distribution strategy is also the primary problem for all the story-installation-type passive dampers.

2.3 Conclusions

In accordance to Eurocode 8, force-based seismic design is a two-level design focusing mainly on structural strength. Performance-based seismic design is a more practical and logical methodology for seismic building design. Incremental Dynamic Analysis is widely used by researchers and designers to explore the structural performance under various earthquake intensity levels, especially those associated with building collapse.

Retrofit with supplemental passive dampers have been proven to be an effective way to improve the dynamic response of the building under earthquake excitation by increasing the total damping of structure and

dissipating the input energy. In terms of supplemental damping devices applied to each storey of the buildings, fluid viscous damper is a cost-beneficial and practical damper device for industrial application. Considering the total price cost for all the dampers installed for a building is relatively expensive, it is essential to ensure the optimal damper placement strategy for a seismic building regarding the damper size or the damping characteristic for each damper. However, the high-order nonlinearity of the damper-frame systems makes it difficult to work out the spectrum analysis and hence solve the damper placement problem.

The next chapter provides a literature review on the existing guidelines and methods for damper placement. Several methods proposed by previous researchers are introduced to prepare the foundation for exploring the design issues of optimal damper placement.

Charter 3

Review of Methods for Optimal Placement of Dampers

3.0 Introduction

The previous chapter addressed that seismic retrofitted with passive dampers is an effective approach to mitigate dynamic response of buildings. As Takewaki (2009) mentioned, although passive dampers are widely applied by engineers to design the buildings, the total costs of damping devices are still considered to be relative expensive. The optimization with respect to the distributions of passive dampers therefore becomes an important and heated research issue. The aim of this chapter is to outline the fundamental optimization problem for damper placement, point out the lack of specifications for damper placement philosophy in current building guidelines, and review conventional practices and previous research efforts of damper distribution strategy. It is also important to note that the primary damper optimization problem described in this chapter is the damper distribution along the height of the building (vertical distribution). The secondary optimization problem that distribute dampers in different bays (horizontal distribution) will be further explored in Chapter 7.

3.1 General Optimization Problem of Damper Placement

The effectiveness of supplemental dampers for improving the seismic and wind response of the building has been demonstrated through analytical and experimental studies. However, the determination of the approaches for optimally utilizing these devices is still an important research concern. As is known that the damping capacity of each damper (related to damping coefficient and damper force) throughout the building, the installation place of each damper and the total amount of supplemental damping applied to the

dampers, have significant effect on the ability to reduce the seismic response and hence to achieve the required design objectives (Singh and Moreschi 2002).

In accordance to previous studies, the fundamental and general optimization problem of damper placement with respect to seismic context is to minimize the dynamic response of the building by optimally placing the dampers throughout the height of the building. General performance indexes utilized to characterize the seismic response could be identified as peak interstorey drifts, absolute accelerations, base shear and residual drifts. The optimization objective varies greatly with these performance indexes, while the maximum peak interstorey drift of a building is one of the most popular index for constructing the objective function of structural optimization. As it is known, the damage and the serviceability check for the columns can be directly correlated to the maximum peak interstorey drift of the building (Fajfar and Krawinkler 2004). There are two alternatives for conducting a specific optimization of damper distribution. One is to constrain the total supplemental damping to a certain value and to find out the optimum distribution of dampers to achieve minimum seismic structural response. The other one is to minimize the total supplemental damping with an optimum damper distribution while meeting a targeted performance criterion of the building (Lavan and Levy 2009).

3.2 Guidelines and Provisions for Damper Placement

In order to explore the existed application of damper placement in the structure, a large number of general building guidelines and construction provisions including Eurocode 8 (BS EN 1998-1 & BS EN 1998-3), FEMA 356 (ASCE 2000), FEMA 368 (BSSC 2001), FEMA 450 (BSSC 2004),

FEMA P750 (BSSC 2009), ASCE 7-05 (2006), the International Building Code (2015) are reviewed by the author. A few of the provisions mention the retrofit solution for base isolation, while both FEMA 365 (ASCE 2000) and FEMA 368 (BSSC 2001) provide solutions for calculating the total supplemental damping contributed by supplemental passive dampers. However, none of these codes or provisions provide any specific recommendation for the strategic placement of passive dampers.

3.3 Conventional Practice for Damper Placement

In absence of a specific rationale in the provisions, it is observed that the damper placement in the buildings are normally in accordance to common accepted practices. These practices involve uniform damping distribution, stiffness proportional damping distribution and placing dampers at a single storey or a single bay.

The uniform damping method is a simple and intuitive method that uniformly distributing the total supplemental damping throughout the floors. In accordance to this method, the total damping of the supplemental dampers at each floor C_i is given by:

$$C_i = \frac{C_t}{n} \tag{3.1}$$

While C_t is the total supplemental damping of a building, and n is the number of the building stories. This damper distribution method has been applied to some buildings including the new World Trade Centre in New York and the Santa Clara County Building located in San Jose (Soong and Dargush 1997). Nevertheless, uniform damping distribution is treated as a less effective approach compared to mass proportional and stiffness proportional

damping distribution (Singh and Moreschi 2002).

Stiffness proportional damping system and mass proportional damping system are more effective to reduce the dynamic response of structure as they result in a Rayleigh-type damping matrix which does not lead to complex modes (Adhikari and Woodhouse 2000). Trombetti and Silvestri (2005) mentioned that the mass proportional damping method is impractical to implement although this method is theoretically more effective. Therefore, the stiffness proportional damping distribution of viscous dampers will be focused in this study.

The stiffness proportional damping distribution is to distribute the total supplemental damping of building proportional to the storey stiffness. In accordance to this approach, the total damping of the supplemental dampers at each floor C_i is given by:

$$C_i = C_t(\frac{K_i}{K_t}) \tag{3.2}$$

Where C_t is the total supplemental damping of a building and K_i is the lateral storey stiffness of the steel MRF at storey i. K_j can be determined by utilizing pushover analysis to obtain the ratio between the storey shear force and the interstorey drift displacement at each storey. This approach is proposed by Christopoulos and Filiatrault (2006) to determine a distribution of viscous damping coefficients of a frame. The distribution method is further adopted by Lee et al. (2009) and Karavasilis et al. (2011) to distribute the elastomeric dampers. In these studies, stiffness proportional distribution ideally results in a relatively uniform distribution of seismic drift demands throughout the height of the frame.

3.4 Previous Research for Optimal Damper Placement

Although the optimal placement of passive dampers is not addressed in the current building codes or design provisions and the placement strategies generally follow the common accepted practices in building industry, it is an essential and heated research topic regarding the seismic design of building. Previous research work in terms of the damper distribution strategy can be categorized into four optimization approaches which are parametric studies, analytical approach, heuristic approach and evolutionary algorithms (Liu et al. 2005).

Parametric study is one of the early studies that seek potential solutions by examining the relationships between different parameters. These approaches are generally not exhaustive for describing the search space of the optimization problem. Analytical approaches are numerical optimization methods that normally optimize a defined objective function with a constrained total added damping capacity (a few with constrained structural performance level). A heuristic approach is a practical method that solves the optimization problem normally based on rules of thumb without guarantee of converging at the global optimum, but with fast search speed (Pearl 1984).

An Evolutionary algorithm (EA) utilizes mechanisms inspired by biological evolution such as selection, reproduction and mutation. Based on the adaptive search algorithm, candidate solutions to the optimization problem are measured by a fitness function and the inferior solutions are weeded out during the adaptation process. Given appropriate adjustment of the operators and enough generations of the evolution, the optimization problem implemented by this evolutionary approach can converge to the relative global optimal configuration (Bäck 1996).

3.4.1 Parametric Studies

Optimal distribution of the viscous or visco-elastic dampers for the vibration reduction of seismic structures has been of interest in earlier ages. Some of the research efforts make use of parametric studies to optimize the damper distribution on the seismic response of simple shear buildings. Ashour (1987) conducted parametric studies for an idealized multi-storey building, and suggested that dampers should be distributed with the configurations where the first mode damping ratio of the building will be maximized. Hahn and Sathiavageeswaran (1992) preformed a series of parametric studies on the distribution of viscoelastic dampers, and concluded that dampers in a building with uniform storey stiffness should be placed to lower floors. It was further concluded by them that the response behaviors of tall buildings are normally more sensitive than that of the low buildings. These early attempt of damper placement studies are limited to the simple idealized structures used and single ground motion considered.

3.4.2 Heuristic Studies

Heuristic studies are generally based on a sequential search algorithms (SSA). This algorithm is introduced by Zhang and Soong (1992) for the first time to determine the optimal placement of viscoelastic dampers in multi-storey buildings. They utilized the adaptation of the controllability index to sequentially distribute the dampers at the locations where their damping effects are maximized. Shukla and Datta (1999) used an elastic single-bay shear frame to validate the efficiency and effectiveness of the SSA method. To include the torsional effects, Wu et al. (1997) used the SSA method to distribute the viscoelastic dampers in a three-dimensional model.

Simplified Sequential Search Algorithm (SSSA), which is considered as an evolution of the SSA method, is proposed by Lopez-Garcia (2001) to

determine the optimum solution for the shear frame with linear viscous dampers. The SSSA method is claimed to be more efficient than the SSA method regarding the required computational time. In terms of the convergence of optimum dampers distribution in linear structures, this method has been approved to be as effective as other complex damper placement methods such as Takewaki Method (Takewaki 1997) and Optimal Control Theory (Gluck et al. 1996). Limitations of the study on SSSA include that the optimization results are only based on four separate stochastic ground motions and the effectiveness of damper distributions are not verified for a different earthquake or a different seismic intensity level. In addition, the global equivalent damping ratios (less than 7%) assumed for the building with dampers are unrealistic.

3.4.3 Analytical Studies

Plenty of analytical studies have been conducted to find out the optimal distribution of passive dampers. These research studies proposed different objective functions to defined the optimization problems.

Some earlier analytical attempts include the study of Constantinou and Tadjbakhsh (1983) where they derived the optimum damping coefficient of a single damper installed on the first floor of a shear building by minimizing the maximum displacement under random white noise ground motions. Gürgöze and Müller (1992) minimized a constrained energy criteria to obtain the optimal damping coefficient of a viscous damper in a multi-degree-of-freedom system. These early analytical approaches are limit to the idealized structures only with a single damper.

Recent analytical damper placement approaches develop the damping distribution from a single damper to dampers placed in each floor. These

methods are based on multiple optimization principles, such as active control theory, gradient-based search methods and redesign optimization method.

Gluck et al. (1996) proposed an optimal control theory based on active control theory, using a linear quadratic regulator to optimally design the damper size of a three-storey structure. In this study, a gain matrix is obtained from the minimization of the performance objective index. Since passive dampers cannot supply feedback for all states, three approaches are presented to eliminate the off-diagonal interactions between different states. The approaches, which are the response spectrum approach, the single mode approach, and the truncation approach, are used to consider the supplemental damping for the gain matrix. The limitation of this study is the structure dominated by a single vibration mode.

Gradient-based search methods are widely applied by the previous researchers to investigate the optimal damper placement strategy including Takewaki (1997, 2000, 2009), Singh and Moreschi (2001), and Lavan and Levy (2006). A gradient-based search method is generally based on an algorithm to solve constrained minimization problems with the search direction dominated by the gradient of the function.

Takewaki (1997) introduced minimum transfer functions to minimize the sum of interstorey drifts, optimizing the damping distribution of two shear buildings with the undamped fundamental natural frequency. This method has been developed from single objective optimization to multiple objective optimization (Takewaki 2009). Based on the assumption of stationary ground motions, Takewaki's approach (refer as Takewaki Method in this research) is independent from the real ground motions, using the index of dynamic

behavior from the transfer functions. This work is limited to the stationary seismic environment and the simple elastic structure model. In addition, the sum of the performance index should be replaced by a maximum one which is more appropriate to represent the design criteria. However, the methodology that could exclude the realistic ground motions records is remarkable.

Singh and Moreschi (2001) used a gradient-based algorithm to distribute the viscous and viscoelastic dampers with a total supplemental damping constraint. They utilized a non-classically damped response spectrum approach to derive the normalized form of the performance objective function. A design-level ground motion defined by a spectral density function was used to optimize the damper placement of a 24-storey shear linear building. The input ground motion considered for this optimization is stochastic and the performance objectives are varied.

Lavan and Levy (2006) proposed a gradient-based methodology to solve the problem of minimizing the supplemental damping of two structures subject to constraints on the maximum interstorey drift in terms of an ensemble of realistic ground motions. This work exposed that the characteristics of the ground motions with respect to the structural response could vary greatly. The limitation of this work is that the selected ground motions are not sufficient to represent the integrate natural seismic environment and the earthquakes are all under the design-based intensity level. Additionally, the nonlinear behaviors of the structures are not fully considered during the nonlinear analysis.

Another analytical damper placement method is known as Fully-stressed Method which is based on redesign optimization method. It is proposed by

Levy and Lavan (2006) to minimize the total supplemental damping of the building subjected to the constrained maximal peak drift, of which the objective function is similar to the previous one with the gradient-based method. This method utilizes a recurrence relationship between the performance parameters and the supplemental damping coefficients to maximize the dampers influence on seismic response. It is implemented by a simple numerical approach which could converge after several iterations. The objective function for conducting fully-stressed methods was developed to the minimization of the maximum peak drift subjected to constrained total added damping of the building (Lavan and Levy 2009). The Limitation of this work is similar to the one of gradient-based optimization proposed by Lavan and Levy (2006).

3.4.4 Evolutionary Approach - Genetic Algorithms

Genetic algorithm (GA), which is considered as one of the most popular evolutionary algorithms for solving engineering optimization problems, is introduced to the damper placement methods recent years. GAs are general search and numerical optimization algorithms inspired by the adaptation phenomenon of species in the natural world. A typical GA normally initials with a random population that contains individuals for a number of potential solutions. Based on a defined objective function (or fitness function), each individual is given a fitness. The population is forced to experience several generations with some numerical operators (e.g. selection, crossover and mutation) that inspired by the mechanisms of natural selection and genetic inheritance. After enough generations of evolution, the individuals of the population could converge to solutions relatively closed to global optimum (Coley 1999). Since GAs contain the powerful searching ability, they are widely applied to the field of engineering global optimization problems and

the artificial intelligence programs (e.g neural network and deep learning) (Vas 1999).

Singh and Moreschi (2002) proposed a notable optimization method for damper placement based on GAs. In accordance to Singh and Moreschi (2002), there are [(m+n-1)! / (m! (n-1)!] different combinations while considering placing m identical devices in n possible storeys. Hence, GAs were considered to be superior to other search algorithms in terms of dealing with such a huge potential combinations. Singh and Moreschi (2002) employed a GA to minimize the structural performance index subjected to a constrained total number of dampers. This method was validated by a six-storey linear torsional structure and a 24-storey linear shear building with viscous and viscoelastic dampers. Both the shear reduction and the storey accelerations reduction were assessed for the performance of the optimized structure in terms of drift-based optimization and acceleration-based optimization. Compared to the study that they used the same 24-storey shear building for gradient-based analysis (Singh and Moreschi 2001), the building designed with GA yielded a similar acceleration reduction with the building designed with gradient-based search algorithms.

However, Singh and Moreschi's studies (2001, 2002) contained several obvious limitations. First of all, their studies are solely based on a stochastic design-level ground motion defined by a spectral density function. The variety of the earthquake excitations in terms of frequency level and intensity level, is not validated for the optimization of the structures. Secondly, all the buildings used to conduct optimizations were linear elastic structures which did not include complex nonlinear behaviors in the beam-column systems. Moreover, the modified GA code used for the optimization were self-defined

and might not be as powerful as the GAs coded in other official softwares. Since the convergence process of the population evolution was not provided by the authors, whether the solutions converged at the points closed to global optimum was open to doubt.

Movaffaghi and Friberg (2006) used the genetic algorithms to optimize a three-dimensional frame using the IDESIGN software interfaced with ABAQUS. The objective function defined by this study is the minimization of the sum of the three translational floor accelerations under a classical realistic ground motion. The nonlinear behaviors of the beam column systems were not explicitly considered in this work and the optimized frame was also not validated for the critical performance index regarding design concern (such as peak interstorey drift). This work claims to achieve up to 60% reduction for the fitness/cost function. However, the total supplemental damping of the structure was not constrained for the optimization which made the study less valuable and sophisticated.

GA and nonlinear response history (NRH) analysis are combined by Apostolakis and Dargush (2010) to investigate the optimal seismic design of hysteretic passive damper placement regarding both the vertical and horizontal distributions. The evolutionary approach was developed for optimizing the supplemental damping distribution of two 3-storey structures and a 6-storey structure with buckling restrained braces and friction dampers. Several classical assumptions are adopted by the authors to consider the nonlinearity of the modeled frames. The fitness function defined by this study involved the interstorey drift, the residual interstorey drift and the floor acceleration using different weighting factors. This work claimed that four earthquakes cause the greatest seismic response are selected from 25

earthquakes with a certain return period. However, the authors finally used solely one earthquake under the design basis level to optimize the frames. Since the performance of the optimized frames in terms of other ground motion records and seismic intensity levels are not included in this study, the effectiveness of the optimization respect to general seismic design is still open to doubt.

3.4.5 Comparisons of Damper Placement Methods

Although there are a large number of studies focusing on optimum damper placement strategies, only a few of them provide comparisons of the damper placement methods in terms of realistic seismic hazard levels and structural performance levels.

A notable comparison was carried out by the work of Cimellaro and Retamales (2007) that involved realistic performance objectives and seismic hazard levels to compare several advanced damper placement methods, regarding the capacities of softened stories and dampers. In this work, a set of 25 synthetic ground motion records were included to consider the performance of the optimized structures, using the mean response value.

A remarkable comparison is the study of Whittle et al. (2012) that uses NRH analysis and code-compliant building designs to compare different damper placement methods based on the realistic seismic hazard levels. Whittle et al. (2012) compared five placement methods of viscous dampers, including the uniform damping method, the stiffness proportional damping method, the Takewaki method, the SSSA method and the Fully-stressed Analysis method. Two nonlinear moment-resisting frames with linear viscous dampers were optimized with each placement technique subjected to a representative

ground motion under the intensity level of DBE. The performance objectives were defined with the peak interstorey drift. The seismic performance of the retrofitted structures was validated using the median performance index of 20 selected ground motion records (such as median interstorey drift and median absolute accelerations) under the seismic hazard levels of DBE and MCE respectively. In accordance to the study of Whittle et al. (2012), the performance differences between the damper placement methods are not significant. Compared to the performance of stiffness proportional damping distribution, the technical optimizations of the nonlinear frames under DBE did not considerably decrease the maximum interstorey drifts under both DBE (around 20% reduction for maximum interstorey drift) and MCE (around 15% reduction for maximum interstorey). The results showed that the seismic optimization under DBE might not work for higher intensity levels.

Additional comparisons are found in works of Zhang and Soong (1992), Lopez-Garcia (2001), Singh and Moreschi (2001), Liu et al. (2005), and Levy and Lavan (2009). These works provided useful conclusions for selecting the placement methods for simple shear buildings under a stochastic ground motion regarding various of performance criteria.

3.4.6 Limitations of Previous Damper Placement Studies

While plenty of studies have been conducted by previous researchers to investigate the damper placement strategies throughout the height of the buildings, there are still some reoccurring limitations within the current damper placement methods. These main limitations include the lack of collapse evaluation, large drift optimization, validations for a set of earthquake environments, code-compliant design models, realistic performance levels and hazard levels, nonlinear structural performance,

appropriate nonlinear models and practical evolutionary optimization framework.

Although excessive researchers provided their own solutions for optimal distribute the dampers in vertical direction of the buildings, most of them solely demonstrated the methods by presenting the seismic performance of structures subjected to a design-level (DBE) ground motions. Whittle et al. (2012a) developed the intensity level from DBE to MCE for the seismic performance of the optimized frames. However, the seismic response of the retrofitted frames under higher intensity levels, which are closed to collapse state, were not explicitly explored. Therefore, it can be concluded that few of the existed work provided collapse assessments for their proposed damper placement methods. Furthermore, none of the previous studies tended to optimize the building with respect to the large drift performance associated with building collapse. In contrast, current studies rely on using DBE or a stochastic ground motion not based on realistic hazard levels to optimize the building.

As is mentioned above, many of the existed damper placement methods utilized solely one or two random earthquake records to verify their solutions regarding seismic performance. Some of them claimed to use a ground motion caused the maximum response from a pre-selected ground motions ensemble to validate the performance of the retrofitted frames (e.g. Levy and Lavan 2006, Apostolakis and Dargush 2010). However, considering the variety of the earthquake characteristics in the natural world, it is more appropriate to involve as many earthquakes as it can to test the structural performance. Hence, the median or mean response of a ground motions ensemble should be used to verify the optimized frames, instead of using a single ‘active’

ground motion. Cimellaro and Retamales (2007) and Whittle et al. (2012a) ideally compared the mean (or median) performance index of the retrofitted frames for an earthquakes records ensemble. Nevertheless, the determinations of the selected earthquakes ensembles are not explicitly described.

It should also be noted that extensive previous research works on damper placement focus on simple shear buildings, which normally are not code-compliant buildings. Similarly, building performance objectives associated with the realistic hazard levels (such as achieving a desired drift level under DBE or MCE) are not regularly applied to damper placement studies.

Another limitation is the nonlinearity considered for modeling the buildings. As is noted above, many of these studies use linear shear buildings to adopt conclusions which could not describe nonlinear behaviors of the realistic buildings. While some of the recent research claimed to use nonlinear response analysis with help of different finite element softwares, the nonlinear behaviors of the structure are not appropriately considered. Many of these works could not use advanced assumptions associated with proper building design and accurate nonlinear deteriorations to simulate the nonlinear mechanisms of the building.

Finally, the existed damper placement methods are indeed limited to the difficulty of the implementation which has been addressed by some of the previous researchers. Many of the proposed search algorithms for the damper optimizations are not open source. In addition, many of these advanced algorithms are simply based on self-adapting coding which might not be as powerful as those originated from official optimization softwares (such as MATLAB Toolbox). GA is considered as one of the most powerful search

algorithms, however, a detailed optimization framework for combining nonlinear response history analysis and software-based GA does not exist.

3.5 Conclusions

A review of damper placement methods, in terms of general practices and applications, existed research efforts and the regular building standards, shows that the damper distribution strategy along the building height is a hot research topic. Hundreds of studies have been conducted to explore how to optimally distribute the dampers throughout the height of the building. Based on the differences of the optimization approaches, these studies could be divided into four different categories which are parametric, heuristic, analytical and evolutionary. Many of these research works claim their proposed methods could achieve significant improvements for the building performance. However, the absence of specific recommendations on the damper placement philosophy in building guidelines reveals that the development of this research field is indeed limited. The main limitation of the previous research studies is that none of them carried out a collapse evaluation by considering a ground motions ensemble having different earthquakes characteristics. In addition, the optimizations aimed at improving structural response under the design earthquake; however this does not guarantee an improvement of the collapse performance. Therefore, the seismic intensity levels considered for the dampers optimization should be developed from design-based level or Maximum Considered Earthquake to larger levels. Other notable weaknesses of current research include the use of linear shear frame models and less powerful search algorithms. In order to perform complex search tasks on the large-drift optimization, the following chapter will investigate an effective and advanced damper placement method based on Genetic Algorithms. A systematic methodology of combining the

constrained optimization with GAs and the nonlinear response analysis will be addressed.

Charter 4

Damper Placement Optimization with Genetic Algorithms

4.0 Introduction

Multiple search algorithms have been used by previous researchers to deal with the global optimization problem of damper placement and other science issues. Genetic algorithm (GA) is widely considered as one of the most effective tools for treating the high-order optimization problems. Nevertheless, GA has once been blamed for an excess of computational time consumed for the evolutionary convergence. With the development of the Cloud Computing and Quantum Computing recent years, the computational effort cost for the common search algorithms could be significantly shorten. GA therefore becomes a more practical and powerful tool for solving the scientific optimization problems with respect to the industrial design.

In order to investigate the damper distribution issue of mult-storey steel buildings under large seismic intensity levels, this study develops a systematic framework for working out the constrained minimization problem, based on interfacing GA with nonlinear response history (NRH) analysis. To explain the implementation concerns for this optimization methodology, this chapter will firstly describe the fundamental mechanisms of GAs, followed by the specific settings of the GA solver in MATLAB Toolbox. At last, a specific method for combing the MATLAB program and the OpenSees program will be explicitly presented and a detailed process of the tandem evolutionary optimization will be theoretically explained.

4.1 Classical Genetic Algorithms

As it has been described in the previous chapter, GAs are general search and

numerical optimization algorithms which are inspired by the species evolution in the natural world. More specifically, the GA approach imitates the adaptation phenomenon of species by both natural selection and natural genetics. After it was first introduced by Holland in 1960s, this approach has been gaining a growing following in the physical, computer systems, social science and in engineering (Coley 1999).

A classical GA initialized with a population of random guesses within the search space instead of starting from a single guess. These guesses are called as the individuals of the population and each individual represents a potential solution of the optimization problem. Typically, an individual in a population is modeled as a binary encoding string that divided into several sub-strings, which has a similar structure with a chromosome. Each sub-string simulates a single gene of the chromosome that corresponds to a true variable for an optimization problem. A typical binary encoding string or chromosome with N_{var} genes is shown in Figure 4.1. A simple GA utilizes selection, crossover and mutation as the three main operators to direct the evolution of the population. These numerical operators are developed by analogy with the mechanisms of the natural selection, genetic crossover and the genetic mutation during the species evolution. With a series of generations processed by the operators and the appropriate maintenance of population diversity, the population are normally directed towards convergence at the global optimum of the search space (Mitchell 1998).

$$chromosome = \left[\underbrace{1111001001}_{gene_1} \underbrace{0011011111}_{gene_2} \ldots \underbrace{0000101001}_{gene_{N_{var}}} \right]$$

Figure 4.1 A typical binary encoding string

4.1.1 Selection

Selection is defined as a fundamental operator to apply the evolutionary pressure upon the population similar to natural selection existing in biological systems. Individuals with poorer performance (e.g. lower fitness) in a population are weeded out during process of selection (Mitchell 1998). In contrast, individuals with better performance (e.g. higher fitness) are provided a greater probability of transferring the characteristic they contain to the next generation. In terms of engineering optimization problems, the fitness function (or cost function) for evaluating the fitness of each individual, should be established properly regarding the balance of the considered optimization objectives. Rather than using the simple method that selecting the best 50% of the individuals to reproduce and weed out the rest individuals, a more applicable and useful selection operator called fitness-proportional or roulette wheel selection is commonly recommended. With the application of this approach as illustrated in Figure 4.2, the probability for determining a selected individual is directly proportional to the fitness of this individual and hence the distinctions can be made between different fitness levels (Coley 1999).

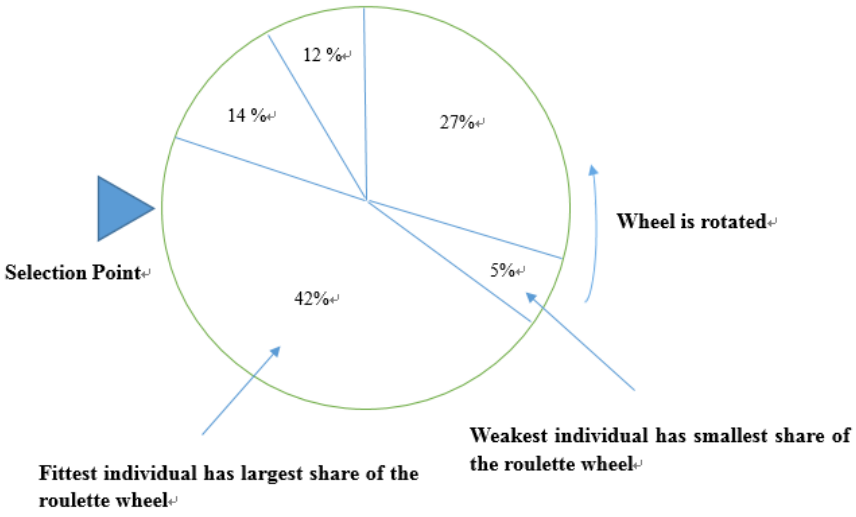

Figure 4.2 Roulette Wheel Selection

4.1.2 Crossover

Crossover makes use of the exchange of the binary sub-strings to swap the information or characteristics within pairs of individuals, which is similar to the natural organism undergoing sexual reproduction. This operator provides a method to maintain the exploration of the search space for differing the potential solutions of the optimization problem, that could be analogy with the enhancement of diversity for species population in ecological systems (Coley 1999). While there are other sophisticated recombination operators for crossover, single point crossover is still considered as a common operator of crossover. In accordance to the implementations of this operator, pairs individuals processed by the selection operator are selected and stochastically cut at a single point within the binary strings to divide them into sub-strings. Then the sub strings are forced to swap between the two individuals to create pairs of child strings. Figure 4.3 provides an intuitional explanation for the process of crossover. The probability P_C, which dominates the selections for the pairs of individuals undergoing crossover, should be normally defined around 0.4 to 0.9 (Mitchell 1998).

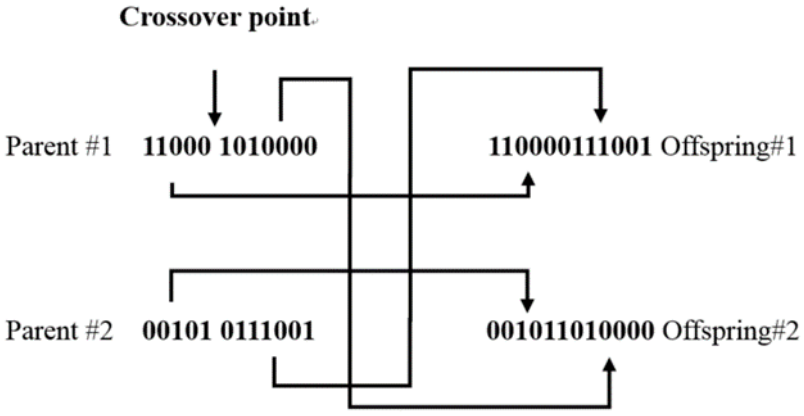

Figure 4.3 The process of crossover

4.1.3 Mutation

In the nature world, several processes can cause mutation in the procedure of

the gene replication. In terms of the representation of a binary encoding in genetic algorithms, mutation is manually implemented by flipping the values of random single bits within the individual encoding strings. In addition, the probability of mutation P_C is commonly assigned a sparing value (e.g. from 0.001 to 0.01), in order to slow down the rate of population convergence to guarantee enough exploration for the search space (Coley 1999).

4.1.4 Additional Optional Settings

As it is known, roulette wheel selection (or some other selection operators) could not always guarantee the selection for a fittest individual, unless the fitness of this individual is extremely higher than others. Therefore, the best solution in a generation and some superior solutions to the global optimization problem, that normally contain desired 'genes' can be occasionally weed out during the process of selection. This potentially slows down the convergence process of the population evolution, which results in a waste of computational time. To prevent the population from undergoing the unnecessary search space and to maintain the superior features for the population, the 'elite' individuals in a generation can be directly transferred to the next generation. This can be simply achieved by defining the number of the elite individuals to be propagated to the next generation. Ensuring the inheritance of the superior individuals for every generations is called as 'elitism' in genetic algorithms.

Another optional setting is for the initialization of the population. As is mention above, the initial population of GA is normally assigned with a series of random individuals. In attempt to improve the computational time, GA can be adjusted to initial with individuals that are estimated to have high performing values of the problem.

4.2 Generalized Optimization Problem

It has been approved by extensive studies that GAs can be applied to various of optimization problems including the nonlinear constrained optimization problems. A generalized mathematical optimization problem (or engineering optimization problem) can be expressed by

$$\begin{aligned} &\text{minimize} \quad f_0(x) \\ &\text{subject to} \quad f_i(x) \leq b_i \text{ or } f_i(x) \leq 0, \qquad i = 1, \ldots, m \\ &\qquad\qquad h_i(x) = d_i \text{ or } h_i(x) = 0, \qquad i = 1, \ldots, p \end{aligned} \tag{4.1}$$

where the function $f_0(x)$ is the objective function, the vector $x = (x_1, \ldots, x_n)$ is the variable for the optimization problem, the functions $f_i(x): i = 1, \ldots, m$ are the inequality constraint functions, the functions $h_i(x): i = 1, \ldots, p$ are the equality constraint functions, b_i are called the inequality constraints (when $f_i(x) = x$, b_i are the bounds of the variables), d_i are called the equality constraints (Boyd and Vandenberghe 2004). Base on the detailed differences between the constraint functions, the constraints on the objective functions can also be distinguished into linear constraint and nonlinear constraint.

In terms of genetic algorithms, the objective function is generally called as the fitness function.

4.3 GA Optimization with MATLAB Toolbox

As is mentioned in the introduction section of this chapter, the GA optimization conduct for this study is implemented with the help of the Global Optimization Toolbox in MATLAB. MATLAB provides a sophisticated and distinct algorithms structure for the GA solver, regarding both the mixed-

integer, the continuous-variable optimization, the unconstrained optimization and the constrained optimization. Based on the classical framework of genetic algorithms that using selection, crossover, mutation and elitism, the MATLAB GA solver involves extensive optional parameters or functions to support the evolutionary exploration. The detailed descriptions and the recommendations for all these parameters are specified in the customer document (MATLAB 2014).

The general expression of the main syntax for the GA solver in MATLAB Toolbox could be identified as:

```
[x,fval]=ga(ObjectiveFunction,nvars,[],[],[],[],LB,UB, ...ConstraintFunction,options)
```

Where x is the point at which the final value is attained, representing the vector for the optimization variables; fval is value of the fitness function or objective function at x; ObjectiveFunction is the handle to the fitness function or objective function; nvars represents the number of the variables for the optimization problem; LB represents the vector for the lower bounds of the variables; UB represents the vector for the upper bounds of the variables; ConstraintFunction is the function handle to linear constraints and nonlinear constraints excluding the bounds for the variables; option is the handle to the optimization options specified as the output of the optional functions or parameters.

Table 4.1 presents some cardinal option parameters apply to the constrained optimization problem, corresponding to the optimization problem of the damper distribution in this study. Other important parameters used to define

the population type and the penalty parameter are determined by the default settings of the MATLAB Toolbox.

Table 4.1 Description of option parameters

Optional Parameters or Functions	**Description**
InitialPopulation	The Initial population used to seed the genetic algorithm
PopulationSize	The number of individuals in the population of every generations
SelectionFcn	The handle to the selection function including various of selection operators
CreationFcn	The handle to the function that creates the initial population
CrossoverFcn	The handle to the crossover function including different crossover operators
CrossoverFraction	The fraction of the population or the probability of an individual to undergo the crossover process at a generation, not including the elite individual
Generations	Maximum evolutionary generations before the algorithm halts
MutationFcn	The handle to the mutation function containing various of optional mutation operators
EliteCount	The number of elite individuals that are guaranteed to survive to the next generation
MigrationInterval	The number of generations pass between

	migrations which is the movement of individuals between the subpopulations
TolCon	The criterion for determining the feasibility with respect to nonlinear constraints
TolFun	The criterion for stopping the algorithm with respect to the average change in the best value of fitness function

4.4 Combination of GA and NRH analysis with MATLAB and OpenSees

To evaluate the performance of a building under seismic excitation considering its nonlinear behavior during the vibration process, it is essential to include the nonlinear response history (NRH) analysis to the study. As it is mentioned in Section 3.43, NRH analysis has been utilized by Apostolakis and Dargush (2010) and Whittle et al. (2012a) to investigate the damper placement strategy. Hoffman and Richards (2014) performed a study on improving the computational efficiency of a baseline GA interfaced with the NRH analysis of tall building.

The Open System for Earthquake Engineering Simulation (OpenSees) is known as one of the most effective software for performing NRH analysis and simulating the structural behavior under the earthquake environment. It has been widely used many structural engineers to conduct research in performance-based earthquake engineering (OpenSees 2016). The optimization of the dampers distribution in this study is therefore implemented by combining the GA framework within MATLAB Toolbox and the NRH analysis framework with the help of OpenSees.

As it is known that the OpenSees program outputs results into text files after

each run of the analysis. In addition, the program can call for any model-construction commands within a text file simply by a 'source' command (e.g. 'source aaa.txt'). While the MATLAB program is able to call for a single run by a simple syntax '!opensees' (e.g. '!opensees bbb.tcl'), the parameters and values with the text files can be read and written by various of syntaxes in MATLAB. These enable the combination of OpenSees and MATLAB programing, as each single run of OpenSees can be embodied in MATLAB by self-defining a performance function. This function expresses each seismic performance value corresponding to each NRH analysis. It is constructed by writing the handle of the optimization variables into a text file used to be read by the main file of OpenSees, and then starting to run a single analysis of OpenSees, followed by extracting the NHR analysis results from the result files of OpenSees.

4.5 Optimization Methodology

As is described in Section 4.4, the computational programing of MATLAB and OpenSees can be bilaterally connected by defining a special performance function in MATLAB, indicating that the loops for running MATLAB and OpenSees will be formed as long as applying this performance function to a specific algorithm solver in MATLAB. In the case of this study, the performance function is applied to the GA solver and it can be assigned with the handle of the objective function or fitness function of GA as described in Section 4.3. The performance function could be manually adjusted in terms of different performance objectives (e.g. the maximum of peak drift, the sum of peak drift and the maximum of base shear)

While conducting the GA analysis interfacing the NRH analysis, the seismic design is considered as a complex adaptive process under the pre-defined

constraints. Each individual in the population of GA is treated as an alternative solution for designing the seismic frame. The elite individuals are the design solutions that provide superior objective performance. For a specific evolutionary process including the output function to monitor the converge process, it could be basically divided into three main steps. For the first step, a finite element model structure is built up with the help of OpenSees to provide seismic performance results from NRH analysis of the frame. For the second step, the GA framework including the fitness function, the constraint functions, the output function and the GA optional parameters, is established in MATLAB files. Finally, the results in the outputs documents obtained from NRH analysis are assigned to the results of the fitness function in MATLAB and hence the adaptive evolutionary loops are formed. The description for the evolutionary loop is illustrated in Figure 4.4.

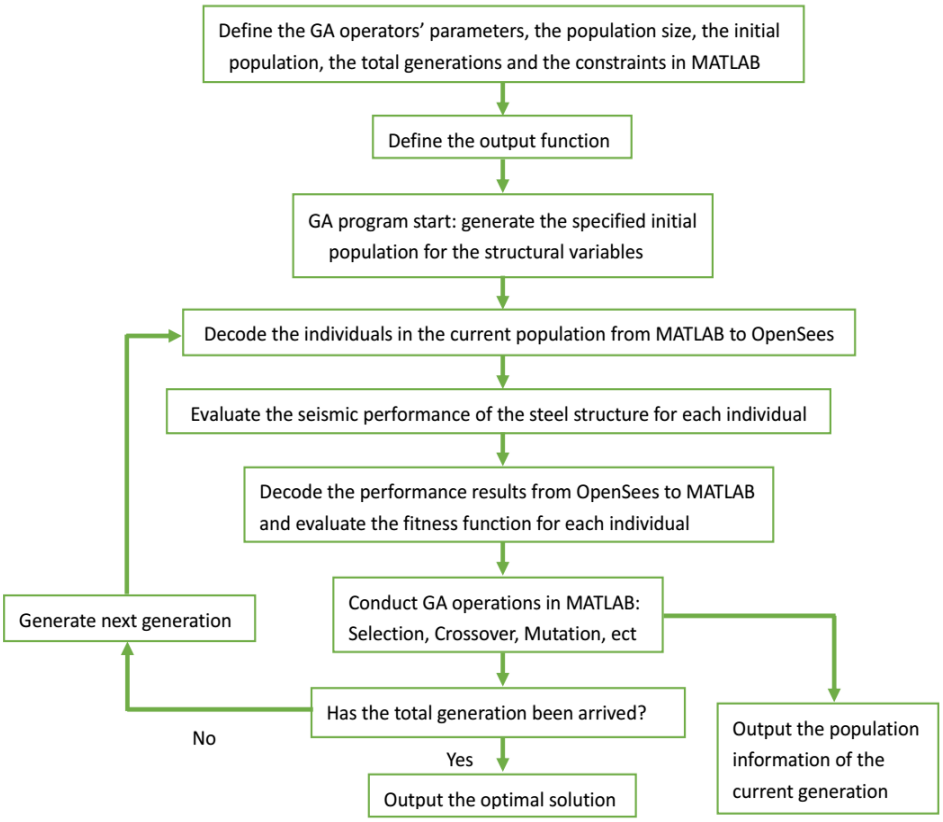

Figure 4.4 GA-NRH optimization framework

4.6 Conclusions

The genetic algorithm is a sophisticated evolutionary search algorithm based on the analogy in nature and the biological evolution. The precision of GA optimization regarding the convergence at the global optimum depends on the maintenance of adequate population diversity. In order to maintain a proper diversity during the population evolution and hence to ensure adequate exploration in the search space, the distribution of key operators of GA have to be balanced by trial and error or using recommended parameter settings. The Global Optimization Toolbox in MATLAB enables users to apply multiple advanced GA operators to the nonlinear constrained optimization problem. By creating a performance function in a sub-routine interfacing with the main routine of OpenSees, the GA solver in MATLAB can be cooperatively run with the nonlinear response history analysis. To validate the feasibility and the effectiveness of this advanced optimization framework in terms of the damper placement, the following chapter will use this method to investigate the damper optimization for a classical elastic shear building.

Charter 5

Height-wise Damper Placement Optimization with Genetic Algorithms in Elastic Shear Frames

5.0 Introduction

An integrated theoretical optimization framework interfacing GA with NRH has been explained in Chapter 4. The aim of current chapter is to evaluate the effectiveness and the efficiency of the proposed GA-NRH optimization framework with respect to the damper placement issue through an exploration on elastic shear buildings. This case study enables the reader to further understand the fundamental research concern of damper placement, and provides a straightforward and explicit description for optimizing the damper distribution using stochastic numerical analysis. Two simple shear buildings with different distributions of storey stiffnesses are involved to carried out the GA optimizations. The optimization efficiency for the examples will be evaluated by comparing the optimization achievements with other studies on the same shear buildings or with the classical damper placement methods.

The evaluation of the GA-NRH optimization framework is divided into two sections: 1. Comparison of the performance improvement of an original elastic shear frame between the GA-NRH method, the Takewaki Method (Takewaki 1997) and SSSA Method (Lopez-Garcia 2001). 2. Comparison of the performance improvement of a modified shear frame between the GA-NRH method, uniform damping method and stiffness proportional damping method. In addition to evaluating the effectiveness for GA optimization combined with NRH analysis, a central principle regarding the balance of GA parameters and the convergence at the comparable global optimum is also summarized for the users.

5.1 Model Definition for Optimization

5.1.1 Building Model A

The Building Model A as shown in Figure 5.1 is taken from Takewaki's study (Takewaki 1997), which is a six-story single-bay planar shear frame with stiff beams and a distribution of varied storey stiffnesses. In accordance to Takewaki's original model, the masses of all the storeys are defined as $m_1 = m_2 = m_3 = m_4 = m_5 = m_6 = 80000\,kg$. A viscous damper with a damping coefficient of C is placed to each storey. All damping coefficients $C_1,\ldots,C_6$ of the added viscous dampers are selected as the design variables which subject to a global constraint that the total damping C_{total} is equal to $9000\,kN \cdot s/m$. The determined lateral storey stiffnesses of the shear building model are shown in Table 5.1 and Figure 5.2. The inherent damping of the frame is neglected in Takewaki's study and the undamped fundamental natural circular frequency of the shear frame is 5.39 rad/s.

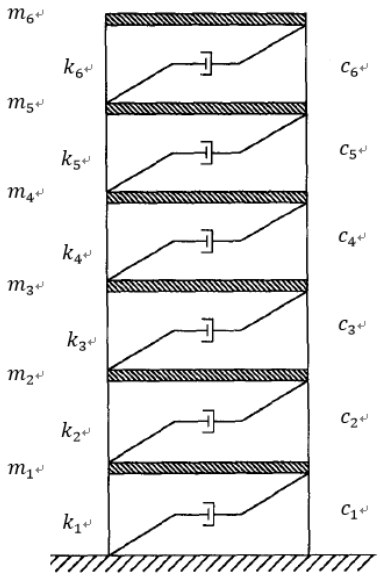

Figure 5.1 Shear frame with added viscous dampers (Takewaki 1997)

Table 5.1 Storey stiffnesses of Building Model A

Storey stiffness	k_1	k_2	k_3	k_4	k_5	k_6
(kN/m)	51310	48100	42600	34760	24440	11000

As is mentioned in Section 3.42, Lopez-Garcia (2001) proposed a heuristic method named Simplified Sequential Search Algorithms (SSSA) based on the Sequential Search Algorithms (SSA) (Zhang and Soong 1992) to explore the optimal placement of viscous dampers. In accordance to the SSSA method, the dampers are distributed sequentially where their effect on seismic response of the building is maximized. In order to verify the effectiveness of SSSA, Lopez-Garcia (2001) utilized Takewaki's building model as described above to conduct numerical simulations for the damper placement. Four realistic ground motion records including EI Centro S00E (scaled to PGA=0.369g), Kobe EW, Taft N21E and Rinaldi Northridge 318 were applied as the input excitations. For a fair comparison, Lopez-Garcia (2001) used the same performance objective and the same optimization problem as the Takewaki's (1997) study, which are to minimize the sum of the interstorey drifts in all the storeys and to optimally distribute the damping coefficient in each storey subject to a constraint of the total damping C_{total}. However, it should be noted that Takewaki's (1997) method is independent of the ground motion characteristic and Lopez-Garcia's (2001) study is based on real ground motion excitations. Additionally, Lopez-Garcia (2001) simplified his method by dividing the total added damping coefficient C_{total} into equivalent individual damping coefficients by the number of dampers n_d, and n_d was proposed as 4, 5, 6, 7 and 8. Hence, in Lopez-Garcia's (2001) study, five optimal strategies with varied dampers amount under the selected ground motions were compared to Takewaki's (1997) optimal damping distribution.

For comparing the proposed GA-NRH framework with the Takewaki Method and the SSSA Method, the ground motion record EI Centro S00E (scaled to PGA=0.369g) is selected to conduct GA optimization interfacing with nonlinear time history analysis in this study. The specific optimization problem for the GA-NRH optimization is defined as the optimal distribution of the supplemental viscous damping coefficients subject to a constrained total added damping coefficients C_{total}. The targeted performance objective is set to minimize the sum of the interstorey drifts in every storeys.

5.1.2 Building Model B

The Building Model B is a shear frame that has similar designed parameters with the Building Model A, while its storey stiffnesses are modified to a different distribution as shown in Table 5.2 and Figure 5.2. With this designed distribution of storey stiffnesses, the third storey of the building is considered as a 'soft storey', of which the stiffness is 1/10 of the others. If the seismic performance of the building could be improved in this case, the optimized add damping coefficients in the third storey (C_3) would be expected to occupy a large proportion of the total damping coefficient (C_{total}). Additionally, in order to coincide with the current design requirements in the building codes, the performance objective for optimizing the Building Model B is set to minimizing the maximum interstorey peak drift of all the storeys. For conducting the time history response analysis, this frame is considered to be subjected to the same ground motion as the Building Model A (EI Centro S00E)

For evaluating the building performance with the damper distribution optimized by the GA-NRH method, the uniform damping distribution and stiffness proportional damping distribution are involved to make the

comparison.

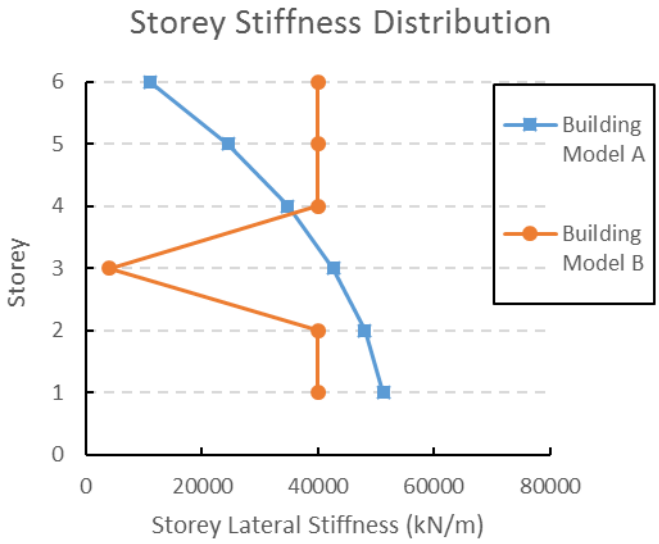

Figure 5.2 The distributions of lateral storey stiffness of the building model

Table 5.2 Storey stiffnesses of Building Model B

Storey stiffness	k_1	k_2	k_3	k_4	k_5	k_6
(kN/m)	40000	40000	4000	40000	40000	40000

5.2 Optimization Analysis

5.2.1 Modeling for NRH

In terms of establishing the finite element model for nonlinear response time history analysis, the six-storey shear frame with viscous damper as describe in Section 5.1 can be ideally simplified as six lumped masses of which each other are connected by both the elastic element and the viscous element. To start with the modeling, a bare frame without dampers is modeled with distributed lumped masses $m_1, \ldots, m_6$ as illustrated in Figure 5.3. The lumped massed on the adjacent floors are linked by the elastic elements using the 'zerolength' element and the 'uniaxialmaterial Elastic' material in the Opensees (Opensees 2016). Each elastic element is assigned with a stiffness

from k_1 to k_6 corresponding to the lateral stiffness of each storey. Regarding that inherent damping is disregarded in Takewaki's (1997) and Lopez-Garcia's (2001) study, for fair comparison, Rayleigh damping was therefore not included to model the bare frame as well as the frame with dampers.

To verify the accuracy of the established bare frame model, the undamped fundamental natural circular frequency of the frame is evaluated simply by conducting the dynamic time history analysis using a random ground motion (such as EI Centro S00E). This undamped fundamental frequency is obtained as 5.384 rad/s which is fairly closed to the one in Takewaki's study, indicating that the bare frame model is correctly modeled. After ensuring the accuracy of the bare frame model, the viscous damper is modeled to each storey of the bare frame using an additional 'zerolength' element to link the adjacent lumped masses. Each viscous element is assigned with a damping coefficient from C_1 to C_6 using the 'uniaxialmaterial viscous' material. To verify the accuracy of the established frame model with viscous dampers, the dynamic time history analysis is run by using Lopez-Garcia's (2001) optimal damping distribution with 6 dampers as can be found in Table 5.3 in Section 5.3. The output performance index (sum of interstory drifts) obtained by the time history analysis is 0.1283 m which is the same as the result of Lopez-Garcia's model. Hence, the finite element model of the shear frame with viscous dampers is well established for conducting GA optimization.

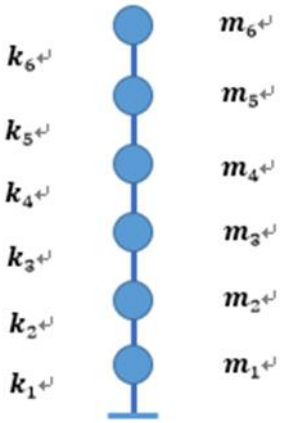

Figure 5.3 Bare shear frame modeled with lumped masses

5.2.2 Determination of GA Settings

As is described in Section 4.4 and Section 4.5, the GA framework and the NRH analysis are combined to implement the evolutionary optimization after the finite element model is built up. Before starting to run the optimization, several settings including the objective function for the optimization problem, the constrained function and the bounds for the optimized variables, and the option parameters for the GA solvers have to be appropriately determined. The objective function and constraint functions are coded in two separated 'm. file' respectively, while the file with the objective function is interfaced with the main routine of OpenSees using the method as mentioned in Section 4.4. The boundary constraints and the option parameters are defined with the main routine of the GA framework in MATLAB.

5.2.2.1 Objective Function

It has been noted in Section 5.1 that the optimization problem defined for optimizing the Building Model A is to minimize the sum of the interstorey peak drifts d_{sum} of the building by optimally distributing the supplemental damping coefficients for all the storeys. Hence, the objective function (fitness

function) expected to be minimized can express as:

$$Fitness = d_{sum} \tag{5.1}$$

While

$$d_{sum} = \sum_{j=1}^{N} d_j = \sum_{j=1}^{N} max\left(\left|D_j(t) - D_{j-1}(t)\right|\right) \tag{5.2}$$

for $0 \leq t \leq T_{total}$ *and* $j = 1, \dots, N$

where d_j is the interstorey peak drift of story j of the frame, $D_j(t)$ is the displacement relative to the ground at time t at j storey, h_j is the height of story j, T_{total} is the total duration of the earthquake excitation and N is the total number of the storeys.

In terms of the optimization problem of Building Model B, the objective function is defined as the maximum interstorey peak drifts d_{max} of the frame during the earthquake excitation, that can be expressed as:

$$Fitness = d_{max} \tag{5.3}$$

While

$$d_{max} = max\left(\left|D_j(t) - D_{j-1}(t)\right|\right) \tag{5.4}$$

for $0 \leq t \leq T_{total}$ *and* $j = 1, \dots, N$

5.2.2.2 Constrained Function and Boundary

As is described in Section 5.1, the optimized variables, which are the damping coefficients of the viscous dampers installed for every storeys, are subjected

to a total damping constraints of $9000\ kN.s/m$. This can be expressed as:

$$\sum_{j=1}^{N} C_j = C_{total} \tag{5.5}$$

Where N is the total number of the storeys, C_j is the damping coefficient of the viscous damper placed at story j of the frame, C_{total} is the sum of the added viscous damping coefficients for the building that is equal to $9000\ kN.s/m$.

Theoretically, the constrained function for the optimized variables of the optimization is the equality constraint as described in Equation 5.5. However, the GA functions in MATLAB Toolbox have a better convergence capability while solving the nonlinear constrained optimization problems with inequality constraints functions (MATLAB 2014). Regarding this concern, the equality constraint function of the optimization problems is equivalently transferred to two inequality constraint functions expressed as:

$$\sum_{j=1}^{N} C_j \geq C_{total} \tag{5.6}$$

While

$$\sum_{j=1}^{N} C_j \leq C_{total} + 0.1kN \cdot s/m \tag{5.7}$$

In order to ensure the exploration for the potential search space and avoid the convergence at local optimal points, the boundary constraints for each damping coefficient C_j are defined as:

$$0 \leq C_j \leq C_{total} \tag{5.8}$$

for $j = 1, \ldots, N$

5.2.2.3 Parameter Settings

It has been discussed in Chapter 4 that the basic evolutionary operators of GA are selection, crossover and mutation. For ensuring the search space of the optimization problem could be sufficiently explored, the characteristic diversity of the population should be appropriately maintained by balancing the operator parameters. A superior customer-defined setting for the GA parameters contributes to a better computational efficiency and a high accuracy of the convergence at global optimum. As is introduced in Section 4.3, in terms of the constrained optimization problem, MATLAB official guiding documentations (MATLAB 2014) provide some basic recommendations for distributing the option parameters of various sophisticated operator functions. Based on these fundamental recommendations, a set of efficient settings for the GA parameters are developed by using try-and-error. More specifically, the superior parameters for activating the evolution of the population is determined by monitoring the intermediate variation of the evolutionary population of each tested optimization. The effective parameters settings enable the population jump out of the local optimum during the evolution. As is illustrated in Figure 4.4, the monitoring of the GA population is implemented by outputting the population information within each evolutionary loop using the output function.

The proposed parameters settings for the optimization of the Building Model

A and Building Model B are presented in Table 5.3 and Table 5.4 respectively. With these customer settings, the optimizations initialize with random populations and the optimization problems for both the analysis cases ideally converge within 30 generations.

Table 5.3 The settings of the GA parameters for Building Model A

Option Parameters	**Value**
'PopulationSize'	50
'Generations'	15
'SelectionFcn'	@selectionroulette
'CreationFcn'	@gacreationlinearfeasible
'CrossoverFcn'	{@crossoverintermediate, 20}
'CrossoverFraction'	0.6
'MutationFcn'	@mutationadaptfeasible
'MigrationInterval'	20
'MigrationFraction'	0.2
'EliteCount'	3
'TolCon'	1e-20
'TolFun'	1e-20

Table 5.4 The settings of the GA parameters for Building Model B

Option Parameters	**Value**
'PopulationSize'	100
'Generations'	40
'SelectionFcn'	@selectionroulette
'CreationFcn'	@gacreationlinearfeasible
'CrossoverFcn'	{@crossoverintermediate, 20}
'CrossoverFraction'	0.5
'MutationFcn'	@mutationadaptfeasible
'MigrationInterval'	50
'MigrationFraction'	0.2
'EliteCount'	3
'TolCon'	1e-1000
'TolFun'	1e-1000

5.3 Results Discussion and Comparison

5.3.1 Building Model A

In terms of the optimizing the damping distribution of Building Model A, the optimization problem can converge at around 13 generations with the GA parameters settings as described in the Table 5.3. The results for the damping distribution obtained from GA optimization and the associated objective performance values are as shown in Table 5.5 and Table 5.6 respectively. For evaluating the effectiveness of the GA results, the damping distributions and the corresponding objective performances obtained from Takewaki's (1997) and Lopez-Garcia's (2001) results are presented in Table 5.5 and Table 5.6. The structural performance values from these damping distributions are simply verified with that from the original studies (Takewaki 1997, Lopez-Garcia 2001) by substituting the damping coefficients values to the building model and performing corresponding NRH analyses. In addition, the results for the traditional uniform damping distribution and the stiffness proportional damping distribution are also involved in the tables to make comparisons with the GA damping distribution. Except for the results from the GA optimization, all the structural performance values (d_{sum}) of the presented damping distributions shown in Table 5.6 are in line with the results from Lopez-Garcia's (2001) study.

As can be seen from Table 5.5, the damping distributions based on different methods vary greatly. Since the mass of each storey is equal in this case, the uniform damping proportional is indeed the mass proportional damping distribution. Table 5.6 reveals that the GA optimization produces a better performance index compared to other damping distribution methods, although the differences between the values of the performance indexes are minute while using d_{sum} as the objective performance index. This indicates

that the capability of the GA method for exploring the search space is indeed stronger than the SSSA method and the Takewaki method. On the other hand, since the GA method does not bring significant reduction to the performance index relative to the traditional damping distribution (uniform damping distribution and stiffness proportional damping distribution), the improvement obtained from the GA optimization should not be exaggerated in this case.

Table 5.5 Comparison between the damping distributions obtained by GA, SSSA, Takewaki Method, uniform damping distribution and stiffness proportional damping distribution.

Floor	**Damping coefficients (kN.s/m)**								
	Takewaki	**Lopez-Garcia (SSSA)**					**Uniform**	**Stiffness propotional**	**GA**
		Number of Applied Dampers							
		4	5	6	7	8			
6	1373.0	2250.0	1800.0	1500.0	1285.7	2250.0	1500.0	466.5	1003.0
5	1682.0	2250.0	1800.0	3000.0	2571.4	2250.0	1500.0	1036.5	1439.9
4	1851.0	2250.0	1800.0	1500.0	2571.4	2250.0	1500.0	1474.2	1498.5
3	1919.0	0	1800.0	1500.0	1285.7	1125.0	1500.0	1806.7	1617.0
2	876.5	2250.0	1800.0	1500.0	1285.7	1125.0	1500.0	2040.0	1720.9
1	1298.0	0	0	0	0	0	1500.0	2176.1	1720.8

Table 5.6 Comparison between the sum of peak interstory drifts obtained by GA, SSSA, Takewaki Method, uniform damping distribution and stiffness proportional damping distribution.

Sum of interstory drifts d_{sum} (m)				
Takewaki	**Lopez-Garcia (SSSA)**	**Uniform**	**Stiffness**	**GA**

							propotional	
	Number of Applied Dampers							
	4	5	6	7	8			
0.122	0.130	0.123	0.128	0.125	0.128	0.121	0.125	0.120

5.3.2 Building Model B

While optimizing the damping distribution of Building Model B, the global optimization problem approximately converges at around 26 generations by setting the GA parameters as described in the Table 5.4. The damping distribution strategies obtained from the GA optimization, the uniform damping method and the stiffness proportional damping method are compared in Table 5.7. The corresponding optimized performance index are also presented in Table 5.7 to make comparison. As it is seen from the table, the uniform damping distribution does not give a particular attention to strengthening the weak storey (3rd storey) by allocating larger supplemental damping, while the stiffness proportional damping distribution conversely provides much less added damping to the weak storey. The results from GA show that the weak storey is appropriately considered by the 'intelligence' of GA, as a large proportion of added damping is moderately allocated to the weak storey to counteract the lack of storey stiffness. The performance results corresponding to the damping distributions expose that the GA distribution indeed improves the seismic performance of the frame, while the maximum interstorey drift is reduced by more than 50% compared to the uniform damping distribution and the stiffness proportional damping distribution.

The evolution processes that describe the intermediate information for the values of the objective function and optimization variables are presented in Figure 5.4 – Figure 5.10. As can be seen from Figure 5.4, the maximum drift

of the frame which is used to represent the fitness of the solution individuals, is dramatically optimized from approximately 0.07m to 0.024m over 40 generations. The reduction for the optimized performance index is over 65% between the initial generation and the final generation, indicating that the GA solver can easily detect the global optimum with these parameter settings. Figure 5.5 describes that the damping coefficient of the weak story is directively increased from lower than 1000 kN.sec/m to around 5750.8 kN.sec/m. This also indicates that the damping coefficient of the weak storey is not occasionally increased allocated. The strategically evolved damping distribution reveals the powerful search capability of the GA solver applied to the optimization problem. Figure 5.6 – Figure 5.10 show that the intermediate explorations of the potential variables for other storeys are extremely flexible. As can be seen from Figure 5.7 and Figure 5.9, the fitness values for the evolved individuals could fluctuate widely between the adjacent generations. This indicates that the adjusted GA solver contains sufficient means to maintain the population diversity and to jump out of the local optimum within the search space.

Table 5.7 Comparison between the maximum interstory drifts obtained by GA damping distribution, uniform damping distribution and stiffness proportional damping distribution.

	Damping coefficients distribution ((kN.s/m)						**Maximum interstory**
	C1	C2	C3	C4	C5	C6	**drifts d_{max} (m)**
Uniform	1500.0	1500.0	1500.0	1500.0	1500.0	1500.0	0.064
Stiffness proportional	1764.7	1764.7	176.5	1764.7	1764.7	1764.7	0.056
GA	2457.4	752.3	5750.8	12.3	26.6	0.7	0.024

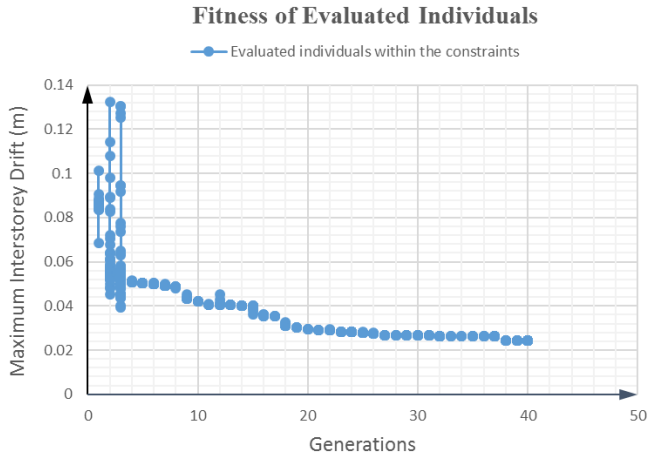

Figure 5.4 Evolution process of the fitness of individuals

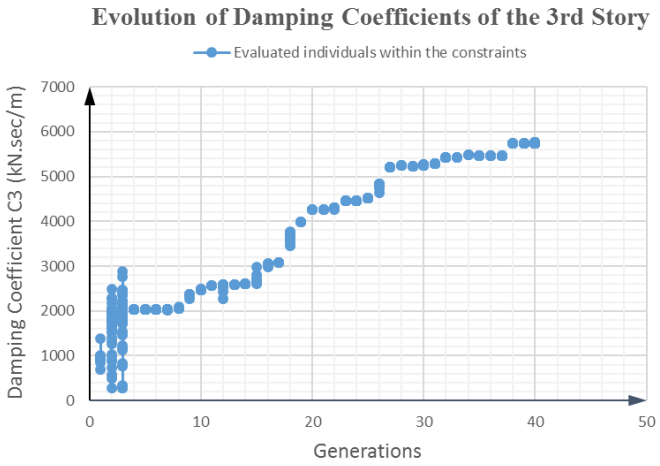

Figure 5.5 Evolution process of the damping coefficients of the weak story

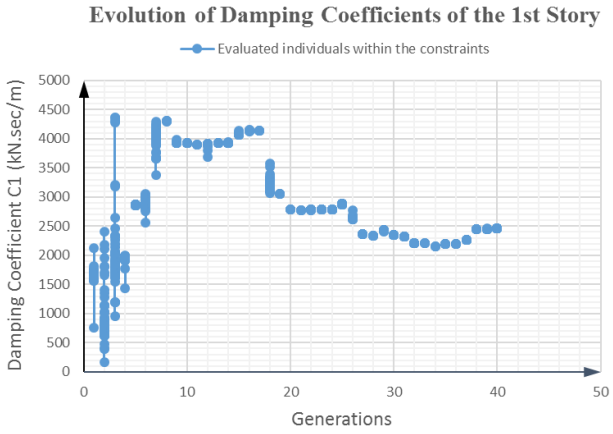

Figure 5.6 Evolution process of the damping coefficients of the 1st story

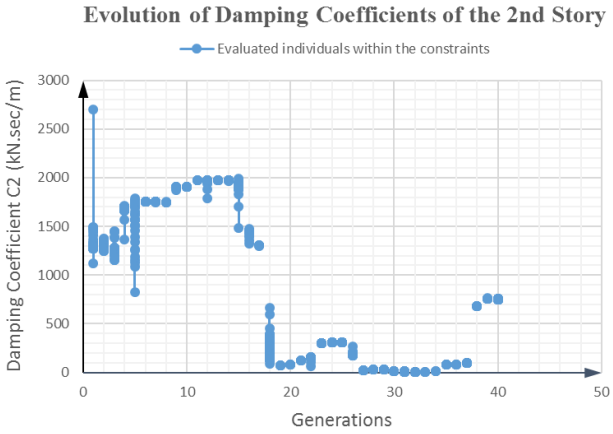

Figure 5.7 Evolution process of the damping coefficients of the 2nd story

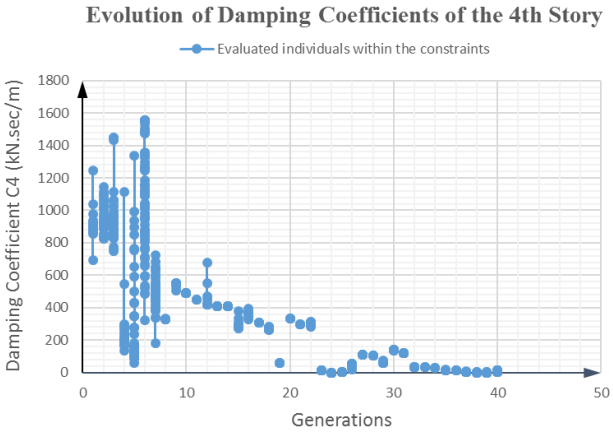

Figure 5.8 Evolution process of the damping coefficients of the 4th story

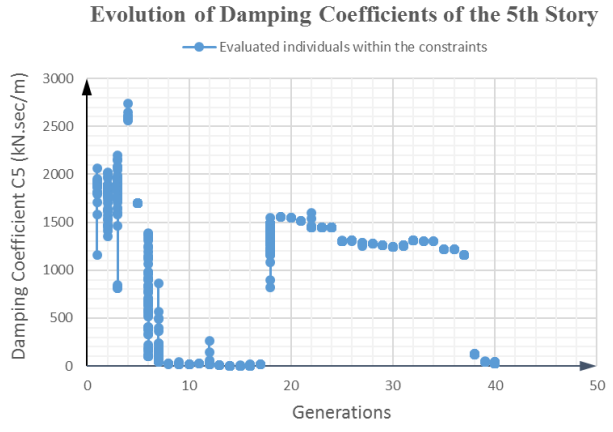

Figure 5.9 Evolution process of the damping coefficients of the 5th story

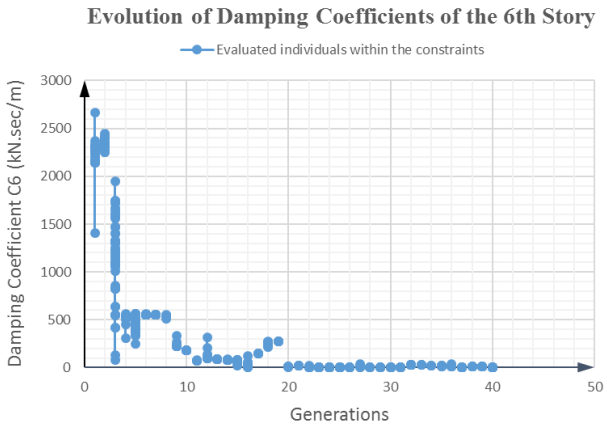

Figure 5.10 Evolution process of the damping coefficients of the 6th story

5.4 Parameters Control Principle

Since the settings of the GA parameters can significantly affect the convergence of the global optimum and the computational time consumed for the convergence, several principles for balancing the parameters of the GA solver are identified based on the practical optimization test and the general knowledge of GA.

As is mentioned in Chapter 4, the capability of GA for fully exploring the search space depends on maintaining an appropriate diversity of the individuals in the population during the evolution. Generally, this can be achieved by increasing the size of the initial population and adjusting the evolutionary operators which could produce new individuals or new genes (e.g. crossover and mutation). In the practical optimization with MATLAB, the excessive increase of the population size can sharply increase the total calculations of the functions in the GA solver that undesirably enlarges the computational time. Therefore, considering the computational efficiency, it is recommended to ensure the population diversity by adjusting the parameters of the evolutionary operators rather than solely using a huge population size.

In accordance to the recommendation of the MATLAB official guiding documentations (MATLAB 2014), the mutation option needs to be set with the default mutation function '@mutationadaptfeasible' to satisfy the bounds and the constraints while dealing with a constrained optimization problem. With this mutation function, the intensity of the mutation is not allowed to assign and hence the users are not allowed to adjust the diversity of the population by modifying the probability of mutation. However, the default crossover function '@crossoverintermediate', which is set for the crossover option when there are linear constraints, enable the users to specify the weights for creating children individuals by a single parameter 'ratio'. By enlarging the value of this parameter, the children individual created by the parents can randomly include new characteristics and hence enhances the population diversity.

In addition to ensure the diversity of the population during the evolution to explore potential search space, the superior characteristics of some elite individuals should be properly retained otherwise the superior characteristics will be occasionally lost during the selection process. In this case, the elite number is set by the parameter 'EliteCount' as shown in Table 5.3 and Table 5.4. Base on the practical test, the 'EliteCount' is suitable to be set at the value from 3 to 5, while considering its negative effect to maintain the population diversity.

5.5 Conclusions

This chapter presents a baseline study on the optimal distribution of viscous dampers in elastic frames with the help of genetic algorithms interfaced with nonlinear response analysis. For an elastic frame designed with regular distribution of storey stiffness, the GA-NRH method is slightly superior to

other damping distribution strategies including the Takewaki Method, the SSSA Method, the uniform damping method and the stiffness damping distribution method. For an elastic frame designed with irregular distribution of storey stiffness, for example the frame with weak storeys, the GA is relatively effective and efficient to detect the weak points of the structure and to improve the structural seismic response by strategically allocating supplemental damping. In contrast with the GA-NRH method, the traditional damping distribution methods could not intelligently consider the weakness of the elastic frame and the seismic response is not optimally improved.

It can be concluded that the genetic algorithm is a powerful tool to conduct the global optimization for the damper distribution problem under random earthquakes. The ability of GA for exploring the search space is identified to be stronger than other approaches. Given that GA is efficient to mitigate the seismic response of elastic frames with irregular stiffness distribution, the frames designed in practice are generally in accordance to regular distribution of lateral stiffness. In addition, the realistic buildings undergo inelastic behaviors under seismic excitations, while the elastic building could not accurately represent the nonlinear behaviors in the realistic buildings.

The following chapter will focus on investigating the damper optimization techniques with GA for moment resisting frames which is subjected to performance-based design. The nonlinear behaviors of the beams and columns of the frames will be explicitly considered, while the effectiveness of GA for optimum distribution of viscous fluid damper under strong earthquakes associated with collapse will be further explored.

Charter 6

Height-wise Damper Placement Optimization with Genetic Algorithms in Steel Moment Resisting Frames

6.0 Introduction

The aim of this chapter is to explore the effectiveness and the feasibility of the GA and NRH analysis in optimizing dampers distribution in the code-compliant inelastic steel buildings under strong earthquakes. As discussed in Chapter 3, a few of previous studies initially show that the damper optimization throughout the floors does not play a significant role with respect to the structural performance parameters under the DBE. Hence, the steel buildings investigated in this study are optimized for a seismic environment under various intensity levels, especially under higher intensity levels. In addition, since the damper optimization under strong earthquakes triggering building collapses has never been evaluated in previous studies, Incremental Dynamic Analyses (IDA) are introduced to this study to assess the collapse performance of the retrofitted building. Furthermore, both far-fault and near-fault earthquakes are considered in this work and steel MRF buildings of different stories are involved to explore the influence of higher modes.

In this chapter, two steel MRF buildings designed in accordance to the Eurocode are described. The design criteria and the modeling assumptions for these prototype MRFs are specifically presented. Based on the existing method of evaluating the total supplemental viscous damping, both of the MRFs are designed with supplemental fluid viscous dampers, of which the damping coefficients are distributed according to stiffness proportional damping distribution throughout the height of the building. In order to

perform collapse simulations for comparing collapse performance between the optimized frames and the original designed frames, a set of far-fault ground motions and a set of near-fault ground motions are considered for the seismic environments respectively.

6.1 Building Design

Two steel MRF buildings without dampers or with dampers, were designed based on the Force-based Seismic Design procedure in accordance to Eurocode 3 (BS EN 1993-1-1:2005) and Eurocode 8 (BS EN 1998-1:2004). All specific rules in the building provisions for the steel structures are enforced to design the buildings. Both of the buildings are designed with regular distributions of storey mass and lateral stiffness as conventional buildings in practice, hence to investigate the effectiveness of GA for optimizing dampers in practical and realistic buildings. By providing the building with more storeys, the variation for the damping distributions along the floors is therefore increased. Hence, the effect on the search space due to the complex vibration modes could be comprehensively explored.

6.1.1 Building Geometry

The plan view of a typical prototype office steel building as shown in Figure 6.1 is first determined for both the MRF structures, Structure A and Structure B. Structure A is a 10-storey, 5-bay by 3-bay steel building with two lateral seismic resisting MRFs in the X direction of the perimeter frames, while Structure B is a 20-storey MRF building which has the same plan view as Structure A. Additionally, gravity frames are placed in the interior of the structures. Both the structures have storey height of 4m for the first storey, while the story height of the rest storeys are all equal to 3.2m. Figure 6.2 (a) and Figure 6.2 (b) show the elevations of the lateral seismic resisting MRFs.

6.1.2 Design Concerns and Assumptions

As can be seen from Figure 6.1, the buildings are designed to be symmetric, for conducting two-dimensional analysis in the X direction. While considering the seismic excitation in the X direction, it is assumed that a half of the total building mass is assigned to each lateral resisting MRFs and a half

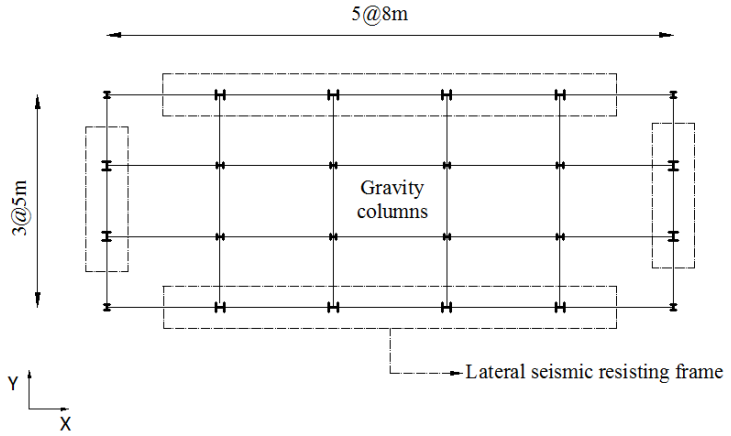

Figure 6.1 The Plan view of the prototype building

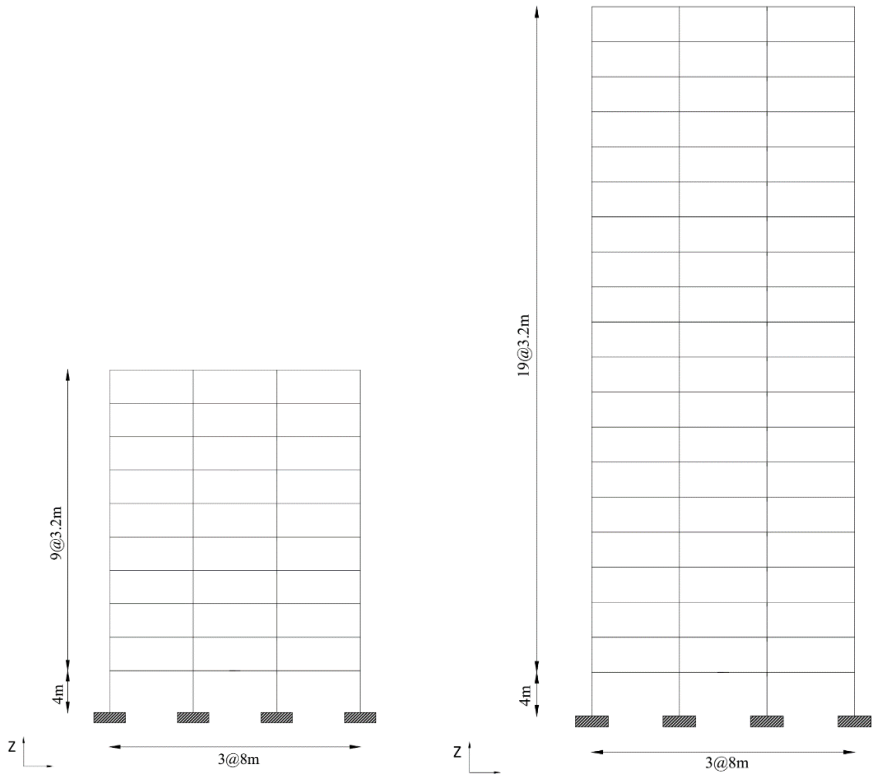

(a) (b)

Figure 6.2 The elevation view of the MRF in (a) Structure A and (b) Structure B

of the total plan area is hence assigned to the 2-D building model as the tributary area. For the design of the MRF, a lean-on column is arranged to simulate the P-Δ effects resulting from the gravity load imposed on the tributary area of the MRF. The cross-sectional stiffness of the lean-on column is defined to be equal to the sum of the cross-sectional stiffness of the gravity columns subject to the tributary area of a MRF. In addition, the nodes at each floor are horizontally constrained to account for the diaphragm effect of the composite slab. The lean-on column is designed to be pinned at the base and its degree of freedom is laterally slaved to that of each MRF columns along the floors.

For the design of the prototype office buildings, typical dead loads (G) and live loads (Q) excluding the gravity loads of the beams and the columns are chosen in accordance to European building design practice as shown in Table 6.1. The loads for the beams and the columns are calculated based on the determined beam and column sizes during the design process. Tributary area method is used to determine the concentrated joint loads applied to the prototype MRFs. It is assumed that the gravity loads are transmitted through the slabs to the beams and through the beams to the columns. The lean-on columns are assumed to carry the gravity loads and the seismic mass of the buildings which are not directly applied to the MRFs. It is assumed that the seismic loads combination $(E + G + 0.3Q)$ control the design of the MRFs, while the gravity columns are designed using the gravity load combination $(1.35G + 1.5Q)$ to consider the introduced axial loads. For each internal gravity columns at a floor, the axial load considered is equal to 450kN. The external gravity columns are designed with the same cross section as the internal columns. For the seismic combination of both the designed buildings, the gravity loads introduced to the structural elements of the MRFs are given

in Table 6.2.

Table 6.1 Gravity loads considered for the prototype office buildings

Load Category	Load Type	Load Value (kN/m^2)
slab	Dead Loads (vertical)	2.5
light partitions	Dead Loads (vertical)	0.5
Girders	Dead Loads (vertical)	0.3
Electrical	Dead Loads (vertical)	0.5
Perimeter glasses	Dead Loads (horizontal)	2.1
Cover	Dead Loads (vertical)	1.2
Office	Live Loads (vertical)	3

Table 6.2 Seismic loads and seismic mass for the prototype MRFs

Floor	External Column Load (kN)	Internal Column Load (kN)	Beam Distributed Load (kN/m)	Lean on Column Load (kN)	Lateral Seismic Mass (tons)
First Floor	126.2	67.2	14.8	1491.3	227.5
Other Floors	112.8	53.8	14.8	1452.6	218.1

In accordance to damage limitation requirement in Eurocode 8 (BS EN 1998-1:2004, 4.4.3.2), the serviceability limits of the peak interstorey drift ratio under the frequently occurred earthquake (FOE) for both the frames are selected to be 0.75% which could be expressed by:

$$\frac{q \cdot d \cdot v}{h} \leq 0.75 \tag{6.1}$$

While q is the behavior factor, d is relative displacement of a storey under

the DBE, v is the reduction factor account for seismic hazard levels (e.g. equal to 0.4 for FOE). This selected serviceability limits also achieves the performance-based design level of Immediate Occupancy under the FOE in accordance to FEMA356 (ASCE 2000). It should be noted that the intensity of FOE is equal to 40% of the intensity of the design basis earthquake (DBE), and the intensity of the maximum considered earthquake (MCE) is equal to 150% of the intensity of the DBE. The DBE is determined by the elastic acceleration design spectrum in Eurocode 8 (BS EN 1998-1:2004, 3.2.2.5) with site condition of type B and peak ground acceleration (PGA) equal to 0.35g. A high behavior factor equal to 6.5 was used for both the buildings to provide a high-ductility class for the design. In addition, 3% inherent damping is assumed for the MRFs and all the beams and the columns of the frames are with steel grade of S275 and S335.

Furthermore, according to the ultimate limit requirement in Eurocode 8 (BS EN 1998-1:2004, 4.4.2.2) for considering the P-Δ effects, the story drift sensitivity coefficient θ is limited to be less than 0.20.

To force the plastic hinges into the beams and hence to prevent the soft storey mechanism, the weak beam-strong column design principle is strongly recommended by current design provisions. In accordance to EC8, this design concern is addressed by satisfying the condition as:

$$\sum M_{Rc} \geq 1.3 \sum M_{Rb} \tag{6.2}$$

While $\sum M_{Rc}$ is the sum of design bending moments resistance of the columns linking the joint, $\sum M_{Rb}$ is the sum of the design bending moments resistance of the beams linking the joint.

In order to ensure the stiffness of the vertical elements and the plastic resistance of the plastic hinges in the columns and the beams, other design criteria for the capacity design of the columns and the beams are enforced. For example, the design shear force in the columns are limited to be less than 50% of the corresponding design plastic resistance of shear force; the design bending moments in the beams are limited to be less than the corresponding design plastic resistance of bending moments; the design axial force in the beams are limited to be less than 15% of the corresponding design plastic resistance of axial force; the design shear force in the beams are limited to be less than 50% of the corresponding design plastic resistance of shear force.

6.1.3 Analysis/Design Procedure

After the building geometry, the gravity loads, the design criteria and the assumptions are well specified, the prototype buildings are analyzed and redesigned with the aid of SAP2000 (CSI 2009) to perform the modal response spectrum analysis under the static loads and the design response spectrum. The seismic weights directly attributed to the MRFs are applied to the 2-D MRF model as concentrated joint forces on the columns and the distributed forces on the beams, while the seismic mass of the buildings which are not directly attributed to the MRFs are assigned to the lean-on columns. The beam-column connections and column-base connections are assumed to be rigid for the preliminary MRF model in SAP2000. Other specific definitions for modeling the MRFs are in accordance to the descriptions in Section 6.1.2. The design of the MRFs is considered as a redesign process based on several iterations of response spectrum analysis. After each iterative analysis, the design criteria as mentioned in Section 6.1.2 are accordingly checked and the corresponding inadequate members are redesigned. Then the new analysis is run with the redesigned member sizes. After a few iterations,

the design process is terminated when all the design requirements are satisfied.

6.1.4 Design of MRFs without Dampers

The final design of the bare MRFs without dampers, including the member selections for the columns, the beams and the gravity columns of the buildings, are shown in Table 6.3 and Table 6.4 respectively. The designed building properties, including the maximum interastorey peak drift ratio of the MRFs under the intensity levels of FOE and DBE, the total equivalent damping ξ_{total} and the fundamental natural period T_1, are presented in Table 6.5. It should be noted that the maximum interstorey peak drift θ_{max} are obtained based on the design response spectrum. Additionally, it should be noted that the interstorey drift ratio obtained from spectrum analysis were corresponding to an equivalent damping ratio of 5% in accordance to the provisions. Hence, for the equivalent damping ratio of 3% in this case, the calculated drifts of the structure should be divided by a damping coefficient B equal to 1/1.154.

Table 6.3 Building design of Structure A (without dampers)

Storey	Column	Beam	Gravity Columns
1	W24X192	W24X76	HEB360
2	W24X146	W30X90	HEB360
3	W24X117	W24X84	HEB360
4	W24X117	W24X84	HEB280
5	W24X94	W24X76	HEB280
6	W24X84	W24X76	HEB280
7	W24X84	W21X68	HEB220
8	W24X76	W24X62	HEB220
9	W24X62	W24X55	HEB220
10	W24X62	W24X55	HEB220

Table 6.4 Building design of Structure B (without dampers)

Storey	Column	Beam	Gravity Columns
1	W24X370	W30X99	HEB800
2	W24X279	W33X130	HEB800
3	W24X229	W33X118	HEB800
4	W24X207	W33X118	HEB600
5	W24X192	W30X116	HEB600
6	W24X176	W30X116	HEB600
7	W24X176	W30X108	HEB450
8	W24X162	W30X108	HEB450
9	W24X162	W30X108	HEB450
10	W24X146	W30X99/	HEB360
11	W24X146	W30X99	HEB360
12	W24X131	W30X90	HEB360
13	W24X131	W30X90	HEB280
14	W24X131	W30X90	HEB280
15	W24X117	W27X84	HEB280
16	W24X117	W24X84	HEB220
17	W24X94	W24X76	HEB220
18	W24X76	W21X68	HEB220
19	W24X68	W24X62	HEB220
20	W24X68	W24X62	HEB220

Table 6.5 Building properties of the designed buildings (without dampers)

Building	$\boldsymbol{\theta_{max,FOE}}$ **(%)**	$\boldsymbol{\theta_{max,DBE}}$ (%)	$\boldsymbol{\xi_{total}}$ **(%)**	$\boldsymbol{T_1}$ **(s)**
Structure A	0.62	1.54	3	2.159

Structure B	0.41	1.02	3	3.257

The lateral storey stiffness is an essential property for applying the stiffness proportional damping distribution. An approximate distribution of lateral storey stiffness is obtained by applying a triangular load pattern throughout the floors of the building and is derived by the following expression:

$$K_j = \frac{\sum V_j}{\Delta u_j} \tag{6.3}$$

Where K_s is the lateral storey stiffness of storey j, $\sum V_j$ is the sum of shear forces V_j in the columns of storey j, Δu_j is the interstorey drift (relative displacement) of the storey j. Table 6.6 gives the calculated distributions of the lateral storey stiffness for both the buildings.

Table 6.6 Storey stiffness of the designed buildings (without dampers)

Storey	Lateral Storey Stiffness (kN/m)		Normilized first mode	
	Structure A	*Structure B*	*Structure A*	*Structure B*
1	126911	342406	0.09	0.04
2	97168	254022	0.19	0.07
3	82787	227358	0.29	0.12
4	73173	207243	0.41	0.16
5	64955	188408	0.53	0.21
6	59000	171757	0.65	0.27
7	53113	162940	0.77	0.32
8	46371	152712	0.87	0.38
9	40803	148170	0.95	0.44
10	33956	137726	1.00	0.50
11	-	130900	-	0.55
12	-	121302	-	0.61
13	-	115514	-	0.67
14	-	110701	-	0.72
15	-	98622	-	0.78
16	-	86206	-	0.83

17	-	72200	-	0.88
18	-	58342	-	0.93
19	-	47711	-	0.97
20	-	35389	-	1.00

6.1.5 Design of MRFs with Dampers

In order to design the realistic MRFs with dampers, a typical damper-brace typology is selected to install the passive dampers in the frames. As illustrated in Figure 6.3, a horizontal damper is installed to each storey of the MRFs in the interior bay through a chevron-braced frame. In this chapter, the passive dampers are selected as fluid viscous dampers (FVDs). As this work focuses on investigating the optimum distribution of an added total viscous damping, the selected typology of chevron-braced FVDs can ideally represent the fundamental and simple design case for the damper optimization philosophy.

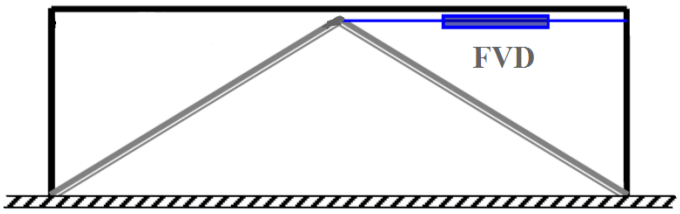

Figure 6.3 Damper-brace typology for the installation of FVD

As mentioned in Section 2.2.4, the force-velocity relationship of a FVD can be expressed by:

$$P(t) = C|\dot{u}(t)|^{\alpha}\text{sgn}[\dot{u}(t)] \tag{6.4}$$

Where $P(t)$ is the output damper force; C is the damping coefficient; $\dot{u}(t)$ is the piston velocity; sgn[ ] is the signum function; α is an velocity exponent; For $\alpha = 1$, the physical model of the damper can be described as a linear viscous dashpot (Symans et al. 2008). In this work, the velocity exponent of

all the FVDs installed in the buildings are selected to be equal to 1 which means the FVDs can be modeled as linear viscous dashpots.

As defined above, the inherent damping of the MRFs without dampers are equal to 3%. For the MRFs with dampers in this work, a total damping ratio β equal to 20% at the fundamental period of vibration are proposed for both of the frames. It should be noted that the total damping ratio β can be expressed by:

$$\beta = \beta_i + \beta_v \tag{6.5}$$

Where β_i is the inherent viscous damping ratio of the frames and β_v is the supplemental equivalent viscous damping ratio account for the total added viscous damping at the fundamental period. Therefore, a β_v equal to 17% is expected to be achieved by the added FVDs. In accordance to Whittaker et al. (2003), β_v can be calculated by:

$$\beta_v = \frac{T_1}{4\pi} \cdot \frac{\sum_j C_j \cdot \left(\varphi_j - \varphi_{j-1}\right)^2}{\sum_j m_j \cdot \varphi_j^2} \tag{6.6}$$

Where T_1 is the fundamental period of vibration of the MRF; C_j is the damping coefficient of the viscous damper installed at storey j; φ_j and φ_{j-1} are the first mode modal coordinate of storey j and $j-1$; m_j is the seismic storey mass of storey j.

Based on Equation 6.6, various of distributions of C_j throughout the floors can achieve the same total supplemental damping ratio (in this case equal to 17%). For the final design of the initial MRFs with dampers, the damping

coefficient C_j of the FVD placed in each floor are designed according to the stiffness damping proportional distribution where the relationship between the damping coefficients of the dampers in adjacent storeys are enforced by:

$$\frac{C_j}{C_{j-1}} = \frac{K_j}{K_{j-1}} \tag{6.7}$$

Where K_j and K_{j-1} is the lateral storey stiffness of the adjacent storeys. With compromising these criteria, the final designed distributions of the damping coefficients for the FVDs in both the structures are given as shown in Table 6.7. The sum of the damping coefficients for the FVDs placed in all the floors are calculated as 79321 kN.s/m and 366153.9 kN.s/m respectively. In addition, stiff braces are designed to support the FVDs in the MRFs. As the bare frames are well designed, the braces are not expected to buckle due to the peak damper force. The final design of the MRFs with dampers are shown in Figure 6.4 and Figure 6.5 respectively. The building properties of the designed buildings with dampers are given in Table 6.8.

Table 6.7 Designed damping distribution of Structure A and Structure B

Story	Damping Coefficients (kN.s/m)	
	Structure A	*Structure B*
1	14842.4	43689.7
2	11363.9	32412.3
3	9682.1	29010.0
4	8557.7	26443.4
5	7596.6	24040.1
6	6900.2	21915.5
7	6211.7	20790.5
8	5423.2	19485.5
9	4772.0	18906.0
10	3971.2	17573.3
11	-	16702.4
12	-	15477.7
13	-	14739.1

14	-	14125.0
15	-	12583.8
16	-	10999.6
17	-	9212.5
18	-	7444.2
19	-	6087.8
20	-	4515.5

Table 6.8 Building properties of the designed buildings (with dampers)

Building	$\theta_{max,FOE}$ **(%)**	$\theta_{max,DBE}$ (%)	ξ_{total} **(%)**	T_1 **(s)**
Structure A	0.37	0.92	20	2.156
Structure B	0.24	0.59	20	3.248

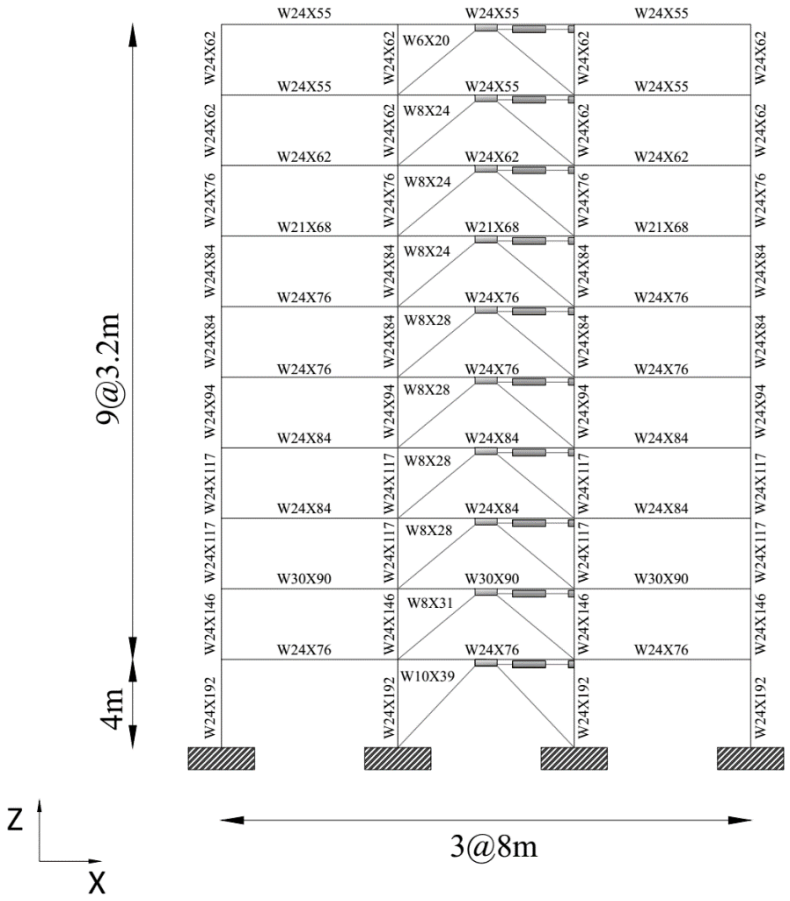

Figure 6.4 Final design of the MRF in Structure A (with dampers)

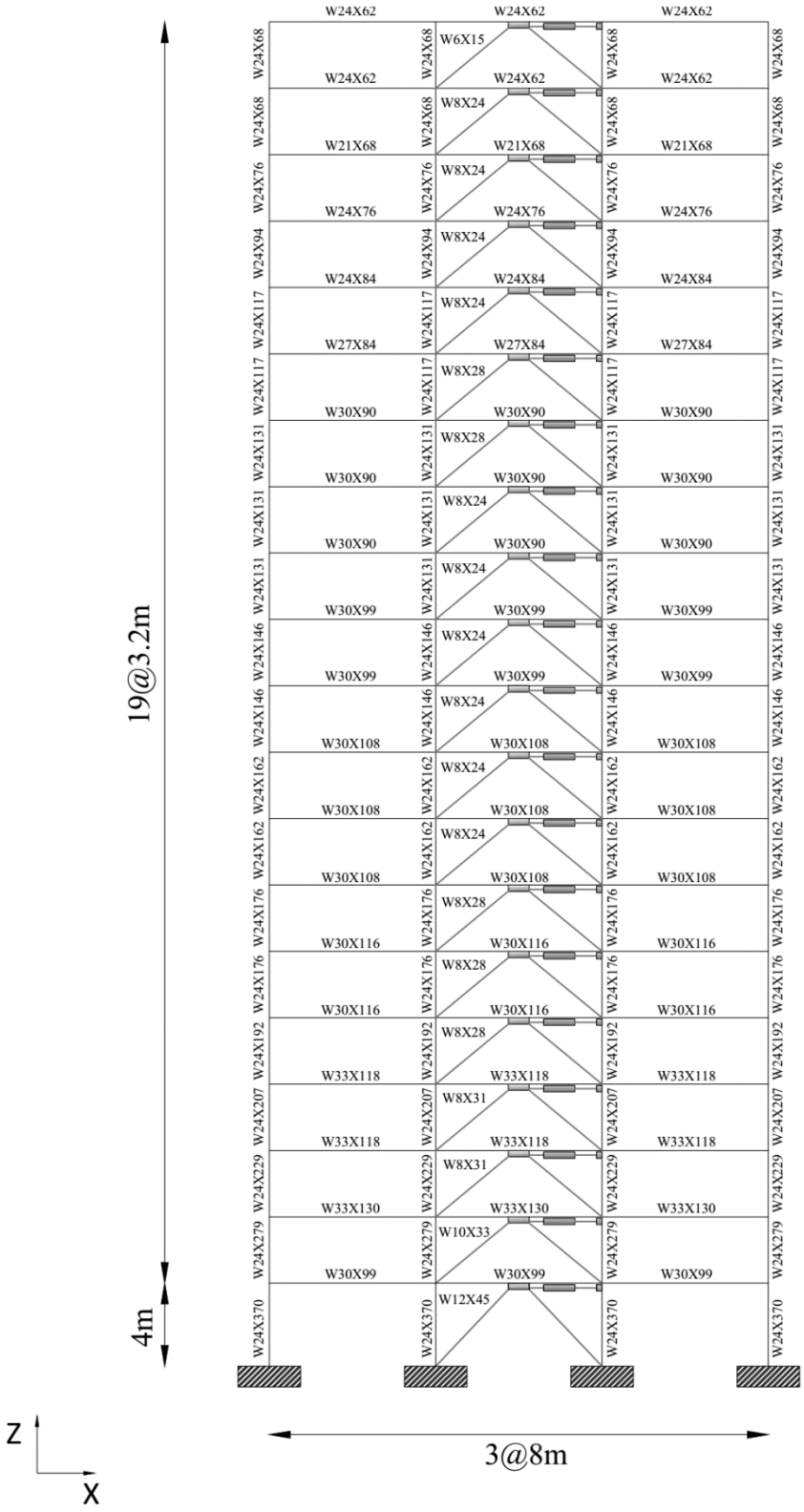

Figure 6.5 Final design of the MRF in Structure B (with dampers)

6.2 Model Details for Nonlinear Dynamic Analysis

In the present work, OpenSees (2016) software is utilized to develop nonlinear dynamic models and to preform nonlinear time series analysis for the buildings without dampers and with FVDs. The columns of the frames are modeled using the nonlinear force-based fiber elements that contains distributed plasticity to account for the moment-axial force interaction effect. According to the study of Newell an Uang (2006), deep columns with low-slenderness flanges and webs do not buckle and experience cyclic deterioration under large drifts. Hence, the heavy columns of the designed buildings in this study are not expected to undergo local bucking and the cyclic strength and the stiffness deterioration are therefore not considered for modeling the columns in the frames. The fibers of the column elements are assumed to experience bilinear elastoplastic stress-strain behavior while the 'Steel01 Material' in OpenSees (2016) is used to define the fiber element with a 0.002 strain-hardening ratio.

The beams of frames are modeled as elastic elements while two zero-length plastic flexural hinges are located at both ends of the beams. Based on the rules decribed by the Modified Ibarra-Krawinkler Deterioration Model (Lignos and Krawinkler 2011, Lignos et al. 2011), analytical rotational springs which exhibit bilinear hysteretic behavior are used to represent these zero length plastic hinges in the beams. This phenomenological model of can be described by a monotonic backbone curve with a defined reference boundary in terms of the hysteretic behavior undergone by the rotational springs. A set of rules regarding the nonlinear behavior within the strength and the deformation bounds of the springs are established by this deterioration model. A bilinear hysteretic response can be specifically characterized by three cyclic deterioration modes that are the basic yield strength deterioration,

the post-capping strength deterioration, and the unloading/reloading stiffness deterioration. As illustrated in Figure 6.6, the backbone curve regarding the three modes in the Modified Ibarra-Krawinkler Deterioration Model is defined by three strength parameters and four deformation parameters which are:

$M_y =$ effective yield strength;

$M_c =$ capping strength;

$M_r =$ residual strength $= \kappa \cdot M_y$ (κ is residual strength ratio);

$\theta_y =$ yield rotation;

$\theta_p =$ pre-capping plastic rotation;

$\theta_{pc} =$ post-capping plastic rotation;

$\theta_u =$ ultimate rotation capacity;

A detailed description for determining the parameters of the modified IK model or constructing the 'Bilin Material' in the OpenSees (2016) software refers to the study of Lignos and Krawinkler (2011).

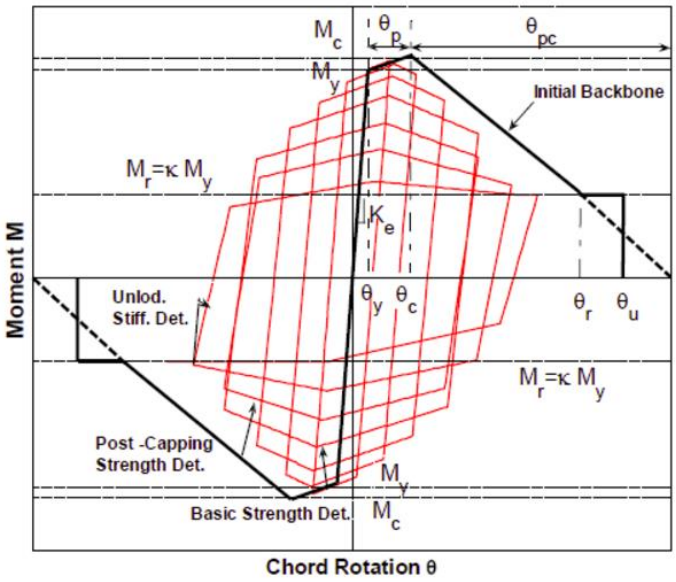

Figure 6.6 The illustration of Modified IK Deterioration Model provided by Lignos et al. (2011)

For modeling the panel zones of the MRFs, Krawinkler model (Krawinkler 1978) are used to simulate the nonlinear behavior of beam-column joints. As presented in Figure 6.7, this phenomenological model is described by four connected rigid links with four compound nodes at the corners and four single nodes at the middle. The stiffness and strength of the panel zone web are simulated by a rotational spring placed at the compound node located at the upper left corner. The column flange bending resistance is represented by an analytical rotational spring placed at the compound node located at the lower right corner. The compound nodes located at the upper right and lower left corner are considered as true flexural hinges and they are set to have no stiffness. It is summed up to be twelve nodes to represent a single Krawinkler model. Each corner of the model utilizes two nodes (equal to one compound node) to constrain x-y and rotational degrees of freedom. A detailed description for the numerical equations determined the required properties of the panel zone refers to the study of Krawinkler (1978).

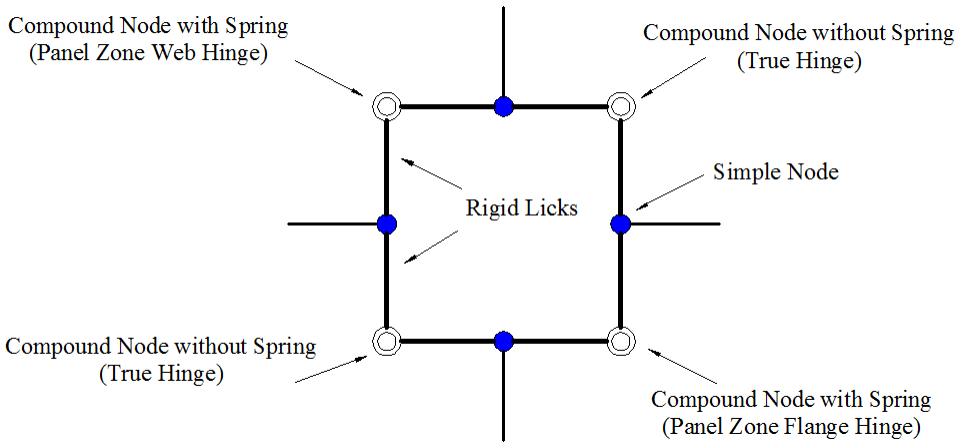

Figure 6.7 The illustration of Krawinkler model

As discussed in Section 6.1.5, the linear FVDs defined in this study can be modeled as simple linear viscous dashpots using ‘zerolength’ element in OpenSees (2016) software. Additionally, the damper limit states, potentially

occur when the piston of the damper reaches its stroke limit due to the seismic response, are not considered for the nonlinear model established for collapse simulation. This assumption is identified to be very important for evaluating the collapse performance of the frames with FVDs (Miyamoto et al. 2010). It should also be noted that the stroke limit of typical dampers is around ± 100mm while the strokes of FVDs can be extensible to ±900mm based on customer request in the market (Taylor Devices 2017). Hence, with an extended stroke limit, the FVDs presented in this work do reach its limit states even the buildings undergo a huge drift under the collapse state.

As mentioned in Section 6.1.5, stiff sections of chevron braces are designed to support the dampers and it is assumed that the braces are strong enough to resist the maximum damper forces and avoid buckling. Therefore, the diagonal braces are modeled with elastic truss elements (OpenSees 2016) with confidence.

Elastic beam column elements are used to the model the 'lean-on' column with assigned seismic storey mass in each floor. Considering the diaphragm effect, truss elements (OpenSees 2016) are utilized to constrain the x direction displacement of the nodes in the beams to the node in the 'lean-on' column at the same floor level.

The Rayleigh damping for the MRFs is defined with 3% damping ratio at first mode and second mode to account for the designed 3% inherent critical damping (Chopra 1995). The Newton-Raphson algorithm set with tangent stiffness and the Newmark method defined with constant accelerations are utilized to solve the numerical dynamic equations while calculating the seismic response of the MRF model.

6.3 Ground Motions for Nonlinear Dynamic Analysis

6.3.1 The Selection of Ground Motion Suite

In order to evaluate the effectiveness of the GA optimization with respect to the collapse performance in general seismic environments, multiple far-fault and near-fault earthquakes are considered in this work to explore the dynamic sensitivity of the retrofitted structures regarding different seismic characteristics. For the far-fault earthquakes, a ground motion suite of 22 recorded ground motions pairs (i.e. 44 individual components) is used to conduct nonlinear dynamic time series analysis and collapse simulations. This set of far-fault ground motions as presented in Table 6.9 were analytically selected by FEMA 695 (ATC 2009) from the PEER-NGA (PEER 2005) database to perform collapse simulations of structures with fundamental period less than 4s. It has been widely applied by engineers to conduct incremental dynamic analysis in the research and industrial field. For the near-fault earthquakes, a ground motion suite of 20 near-fault ground motions records is developed. This set of ground motions as shown in Table 6.10 are based on the set of 91 pulse-like ground motion records selected by Baker (2007) from the PEER-NGA database (PEER 2005). The set of 20 near-fault ground motions are screened out based on the critical region of the earthquake pulse period with respect to buildings' collapse capacity. According to the study of Champion (2012), when the ratio between the pulse period and the fundamental period of structure (T_p/T_1) is larger than 2, the collapse capacities of the buildings under the near-fault earthquakes decrease dramatically. In this chapter, the fundamental period used to develop near-fault earthquakes is the T_1 of Structure A. Specifically, the records in this near-fault ground motion suite are selected in series subjected to the region $2.00 \leq T_P/T_1 \leq 3.50$. It should be noted that this near fault ground motion suite is also applied to preform nonlinear time series analysis and IDA on

Structure B, while the region in this case is given as $1.38 \leq T_P/T_1 \leq 2.31$. Detailed explanations for the selections of the 44 far-fault ground motion records and the 91 near-fault ground motions in terms of collapse simulation refer to FEMA 695 (ATC 2009) and Baker's (2007) study respectively.

6.3.2 The Scaling of Ground Motion Suite

In order to evaluate the structural performance at a specific intensity level (i.e. DBE, MCE or 2MCE), the earthquakes within the selected ground motion suite are normalized to the same hazard level with the help of scale factor. For example, the scale factor for a ground motion at DBE is given by dividing the pseudo-spectral acceleration (PSA) at building's fundamental period (T_1) and 3% inherent damping at DBE, by the PSA in terms of this ground motion record at T_1 and 3% damping. The PSA of a building under DBE can be obtained from the design spectrum in Eurocode 8 (BS EN 1998-1:2004, 3.2.2.5), while the PSA in terms for the ground motions can be obtained by the Duhamel integral solution. The PSA of Structure A and Structure B under DBE at the corresponding fundamental vibration periods are calculated as 0.2608g and 0.1149g respectively. The DBE scale factor of the buildings with respect to the selected ground motions are presented in Table 6.9 and Table 6.10.

Table 6.9 The properties of far-fault ground motions selected for the collapse optimization

ID No.	Ground Motion	Station	Location	Component	Duration (s)	PGA (g)	DBE Scale Factor (Structure A)	DBE Scale Factor (Structure B)
FE1	Manjil 1990	Abbar	Iran	ABBAR--L	113.64	0.51	1.12	1.35
FE2	Manjil 1990	Abbar	Iran	ABBAR--T	106.04	0.50	0.55	0.63
FE3	Kocaeli 1999	Arcelik	Turkey	ARC000	45.01	0.22	6.39	2.16
FE4	Kocaeli 1999	Arcelik	Turkey	ARC090	45.01	0.15	4.21	1.74
FE5	Friuli 1976	Tolmezzo	Italy	A-TMZ000	51.36	0.35	4.71	4.38
FE6	Friuli 1976	Tolmezzo	Italy	A-TMZ270	51.36	0.31	5.25	3.83
FE7	Superstition Hills 1987	El Centro Imp. Co.	USA	B-ICC000	55.01	0.36	1.52	1.56
FE8	Superstition Hills 1987	El Centro Imp. Co.	USA	B-ICC090	55.01	0.26	0.82	1.03
FE9	Duzce 1999	Bolu	Turkey	BOL000	85.92	0.73	0.97	0.70
FE10	Duzce 1999	Bolu	Turkey	BOL090	85.92	0.82	0.92	0.98
FE11	Superstition Hills 1987	Poe Road (temp)	USA	B-POE270	52.32	0.45	1.41	1.13
FE12	Superstition Hills 1987	Poe Road (temp)	USA	B-POE360	52.32	0.30	1.21	0.82
FE13	Loma Prieta 1989	Capitola	USA	CAP000	54.985	0.53	1.80	2.20
FE14	Loma Prieta 1989	Capitola	USA	CAP090	54.985	0.44	2.83	3.22
FE15	Chi-Chi 1999	CHY101	Taiwan	CHY101-E	105.01	0.35	1.01	0.25
FE16	Chi-Chi 1999	CHY101	Taiwan	CHY101-N	105.01	0.44	0.43	0.38
FE17	Landers 1992	Coolwater	USA	CLW-LN	35.48	0.28	4.42	2.38
FE18	Landers 1992	Coolwater	USA	CLW-TR	35.48	0.42	2.49	3.02

FE19	Kocaeli 1999	Duzce	Turkey	DZC180	42.21	0.31	0.70	0.49
FE20	Kocaeli 1999	Duzce	Turkey	DZC270	42.21	0.36	0.70	1.08
FE21	Loma Prieta 1989	Gilroy Array #3	USA	G03000	54.96	0.56	3.03	1.45
FE22	Loma Prieta 1989	Gilroy Array #3	USA	G03090	54.96	0.37	0.87	1.11
FE23	Imperial Valley 1979	Delta	USA	H-DLT262	129.97	0.24	1.45	0.59
FE24	Imperial Valley 1979	Delta	USA	H-DLT352	129.97	0.35	1.14	0.88
FE25	Imperial Valley 1979	El Centro Array #11	USA	H-E11140	54.06	0.36	1.14	0.74
FE26	Imperial Valley 1979	El Centro Array #11	USA	H-E11230	54.06	0.38	2.15	1.37
FE27	Hector Mine 1999	Hector	USA	HEC000	75.37	0.27	2.07	1.87
FE28	Hector Mine 1999	Hector	USA	HEC090	75.37	0.34	1.32	1.39
FE29	Northridge 1994	Canyon Country-WLC	USA	LOS000	50.02	0.41	0.80	1.27
FE30	Northridge 1994	Canyon Country-WLC	USA	LOS270	50.02	0.48	1.66	1.50
FE31	Northridge 1994	Beverly Hills - Mulhol	USA	MUL009	60.02	0.42	1.21	1.39
FE32	Northridge 1994	Beverly Hills - Mulhol	USA	MUL279	60.02	0.52	1.63	1.61
FE33	Kobe 1995	Nishi-Akashi	Japan	NIS000	71.02	0.51	1.13	2.02
FE34	Kobe 1995	Nishi-Akashi	Japan	NIS090	71.02	0.50	1.37	1.83
FE35	San Fernando 1971	LA - Hollywood Stor	USA	PEL090	58.02	0.21	2.75	1.08
FE36	San Fernando 1971	LA - Hollywood Stor	USA	PEL180	58.02	0.17	2.07	2.47
FE37	Cape Mendocino 1992	Rio Dell Overpass	USA	RIO270	96.04	0.39	2.06	2.58
FE38	Cape Mendocino 1992	Rio Dell Overpass	USA	RIO360	96.04	0.55	3.72	3.25
FE39	Kobe 1995	Shin-Osaka	Japan	SHI000	71.02	0.24	1.73	1.29

FE40	Kobe 1995	Shin-Osaka	Japan	SHI090	71.02	0.21	2.50	2.52
FE41	Chi-Chi 1999	TCU045	Taiwan	TCU045-E	105.01	0.47	1.97	2.23
FE42	Chi-Chi 1999	TCU045	Taiwan	TCU045-N	105.01	0.51	1.53	2.01
FE43	Landers 1992	Yermo Fire Station	USA	YER270	104.04	0.24	1.53	1.14
FE44	Landers 1992	Yermo Fire Station	USA	YER360	104.04	0.15	2.33	1.24

Table 6.10 The properties of near-fault ground motions selected for the collapse optimization

ID No.	Ground Motion	Station	Location	Component	Tp (s)	Duration (s)	PGV (cm/s)	DBE Scale Factor (Structure A)	DBE Scale Factor (Structure B)
NE1	Imperial Valley 1979	El Centro Array #10	USA	H-E10233	4.5	51.99	46.92	1.14	0.61
NE2	Imperial Valley 1979	El Centro Array #11	USA	H-E11233	7.4	54.05	41.10	2.32	1.50
NE3	Imperial Valley 1979	El Centro Array #3	USA	H-E03233	5.2	54.56	41.10	2.58	0.85
NE4	Imperial Valley 1979	El Centro Array #4	USA	H-E04233	4.6	54.01	77.93	0.76	0.33
NE5	Imperial Valley 1979	El Centro Array #8	USA	H-E08233	5.4	52.57	48.55	1.40	0.55
NE6	Imperial Valley 1979	El Centro Differential Array	USA	H-EDA233	5.9	53.97	59.61	1.02	0.55
NE7	Imperial Valley 1979	Holtville Post Office	USA	H-HVP233	4.8	52.76	55.15	1.60	0.55
NE8	Loma Prieta 1989	Saratoga - Aloha Ave	USA	STG038	4.5	54.97	55.58	0.93	0.70
NE9	Landers 1992	Lucerne	USA	LCN239	5.1	63.14	140.27	0.84	0.32
NE10	Landers 1992	Yermo Fire Station	USA	YER225	7.5	104.04	53.23	2.10	1.01
NE11	Kocaeli 1999	Gebze	Turkey	GBZ184	5.9	43.01	51.96	2.97	0.69
NE12	Chi-Chi 1999	CHY101	Taiwan	CHY101289	4.8	105.01	85.45	1.11	0.33

NE13	Chi-Chi 1999	TCU029	Taiwan	TCU029306	6.4	105.01	62.34	1.87	0.72
NE14	Chi-Chi 1999	TCU031	Taiwan	TCU031306	6.2	105.01	59.86	1.37	0.49
NE15	Chi-Chi 1999	TCU036	Taiwan	TCU036277	5.4	105.01	62.43	1.57	0.83
NE16	Chi-Chi 1999	TCU038	Taiwan	TCU038277	7	105.01	50.86	1.59	0.59
NE17	Chi-Chi 1999	TCU040	Taiwan	TCU040277	6.3	105.01	52.99	2.03	0.62
NE18	Chi-Chi 1999	TCU065	Taiwan	TCU065272	5.7	105.01	127.68	0.36	0.32
NE19	Chi-Chi 1999	TCU075	Taiwan	TCU075271	5.1	105.01	88.44	0.64	0.32
NE20	Chi-Chi 1999	TCU098	Taiwan	TCU098306	7.5	105.01	32.74	0.91	0.98

6.4 Evaluation for Probability of Collapse

In terms of evaluating the collapse performance of buildings with various damper placement strategies, IDA ((Vamvatsikos and Cornell 2002) is employed to assess the probability of collapse of the buildings. As introduced in Section 2.1.4, to obtain the relationships between the engineering demand parameter (EDP) and the intensity measure (IM), each ground motion within a ground motion suite is increasingly scaled to conduct nonlinear time series response analysis until the structure reaches its collapse state. For this chapter, the spectral acceleration at the building's fundamental period $S_a(T_1)$, which dominates the intensity levels of the ground motions, is defined as the IM. The maximum interstorey peak drift θ_{max}, which is considered as one of the most critical parameters for monitoring the dynamic instability of structures (ATC 2009), is set to be the EDP. To explore the variations of the collapse performance of the buildings under different seismic environments, both the selected far-fault and near-fault ground motion suites are used to perform IDA in this work. Specifically, the $S_a(T_1)$ is increasing scaled with an increment of 0.005g until the seismic force causes collapse of the MRF model. According to FEMA P695 (ATC 2009), the criteria of simulated collapse modes and non-simulated collapse modes should both considered for the collapse simulation. For the simulated collapse modes, the cyclic deterioration modes (Lignos and Krawinkler 2011) of plastic hinges and the Krawinkler model (Krawinkler 1978) of panel zones have been applied. In terms of the criterion of simulated collapse, it is assumed that the phenomenon of the dynamic collapse occurs when the time-integration scheme in OpenSees fails to converge (Vamvatsikos 2002). For the criterion of non-simulated collapse, the limit state check for the structural performance parameter measured by the nonlinear analysis should be defined. In this case, the limit state check is based on monitoring the upper boundary of the θ_{max}

at 15%. This means it is assumed that the building reaches its collapse state when the θ_{max} reaches 15% and the non-convergence of the NRH analysis has not occurred.

After each run of a IDA, the values of $S_a(T_1)$ measure at the collapse state can be collected. To provide a straightforward evaluation for the relationship between the probability of collapse and the $S_a(T_1)$, a fragility curve can be plotted by fitting a lognormal cumulative distribution function (Porter 2007). The collapse margin ratio (CMR) as introduced in Section 2.1.4 can be also evaluated for each collapse simulation. In accordance to FEMA P695 (ATC 2009), CMR is an important parameter for the collapse evaluation and the seismic design. It is defined to represents the median seismic intensity level that would cause collapse by a half of the ground motions in the natural world. As presented in Equation 6.8, the ratio is expressed by normalizing the median spectral acceleration at fundamental period of vibration and 5% effective damping $\hat{S}_{a,C}(T_1)$ by the spectral acceleration under the MCE at fundamental period $S_{a,MCE}(T_1)$. It should be note that the $S_a(T_1)$ directly collected from IDA is for the MRF with 3% effective damping. To account for the 5%-damped $\hat{S}_{a,C}(T_1)$, the measured $S_a(T_1)$ at 3% damping should be divided by a damping coefficient B equal to 1/1.154.

$$CMR = \frac{\hat{S}_{a,C}(T_1)}{S_{a,MCE}(T_1)} \tag{6.8}$$

6.5 Computational Optimization

As described in Section 4.4, Section 4.5 and Section 5.2.2, the computational optimization for this chapter is also implemented by interfacing the GA framework set up in the MATLAB files with the NRH framework established

in the OpenSees (2016). The specific evolutionary optimization process is similar to the one of the elastic shear frame which is presented in Chapter 5.

6.5.1 Optimization Problem

For evaluating the performance objective of the retrofitted MRFs with different damping distributions, an objective fitness function with constraints is defined to assess the critical index for the structural seismic performance. In terms of the code-compliant designed building, the maximum interstorey peak drift θ_{max} is considered as one of the most important performance index to account for the limitations of serviceability and collapse failure (Takewaki 1997, Lavan and Levy 2009). Therefore, the fitness function which needs to be minimized for the optimization is expressed as:

$$Fitness = \ \theta_{max} = max\left(\frac{\left|d_j(t) - d_{j-1}(t)\right|}{h_j}\right) \tag{6.9}$$

for $0 \leq t \leq T_{total}$ *and* $j = 1, \dots, N$

Where $d_j(t)$ and $d_{j-1}(t)$ is the displacement relative to the ground at time t at storey j and storey $j-1$ respectively; h_j is the height of story j; T_{total} is the total duration of the earthquake time series; N is the total number of the floors of the building.

As mentioned in Section 6.1.5, the viscous dampers of the MRFs have been well designed according to the stiffness proportional damping distribution and the total damping coefficients of the FVDs placed in every floors are calculated as 79321 kN.s/m and 366153.9 kN.s/m for the Structure A and the Structure B respectively. For a fair comparison between the optimized damping distributions and the stiffness damping proportional distribution, it

is assumed that the retrofitted frames are provided with the same total damping coefficients of the FVDs. Hence, the optimization problem defined for this chapter could be basically described as: to minimize the θ_{max} of the MRFs under the constraints of the total damping coefficients of the FVDs initially designed by adaptively distributing the damping coefficients in all the stories. It should be noted that the term θ_{max} here specifically refer to the peak drift under a representative earthquake in terms of a selected ground motion suite, or refer to the median peak drift in terms of a selected ground motion suite. Similar to the optimization of the elastic shear frame presented in Chapter 5, the theoretical constrained function for the damper optimizations in this chapter can be defined as:

$$\sum_{j=1}^{N} C_j = C_{total} \tag{6.10}$$

Where C_j is the damping coefficient of the FVD placed at story j of the MRF; C_{total} is the sum of the damping coefficients of the FVDs placed in all the floors; N is the total number of the storeys.

As presented in Section 5.2.2.2, the equality constraint function described by Equation 6.10 is equivalently transferred to two inequality constraint functions for a better convergence capability of the GA solver in MATLAB Toolbox. These two inequality constraint functions implemented by the GA solver in this work for the C_{total} equal to 79321 kN.s/m are specifically expressed as:

$$\sum_{j=1}^{N} C_j \geq C_{total} - 1kN \cdot s/m \tag{6.11}$$

While

$$\sum_{j=1}^{N} C_j \leq C_{total} \tag{6.12}$$

The two inequality constraint functions for the C_{total} equal to 366153.9 kN.s/m are specifically expressed as:

$$\sum_{j=1}^{N} C_j \geq C_{total} - 10kN \cdot s/m \tag{6.13}$$

While

$$\sum_{j=1}^{N} C_j \leq C_{total} \tag{6.14}$$

In addition, the boundary constraints for the damping coefficient C_j of each damper are defined as:

$$0 \leq C_j \leq C_{total} \tag{6.15}$$

for $j = 1, \dots, N$

6.5.2 Optimization Cases and Intensity Levels

Based on the combination of the buildings and the selected ground motion suite, four optimization cases can be identified in this chapter. Case 1 is the Structure A under the 44 far-fault ground motions; Case 2 is the Structure A under the 20 near-fault ground motions; Case 3 is the Structure B under the 44 far-fault ground motions; Case 4 is the Structure B under the 20 near-fault ground motions. As discussed in the Section 3.4.4, previous research initially

shows that damping distribution optimized at lower intensity levels such as DBE are not efficient to improve the seismic performance under higher intensity levels (Whittle et al. 2012a). This work therefore considers multiple intensity levels for the damper optimization of the seismic buildings. For exploring the effectiveness of the optimization with respect to the collapse performance, high intensity levels that are closed to the collapse state of the buildings are mainly focused. For the damper optimization of Case 1, the intensity levels considered for the ground motions are selected as DBE, 3DBE (i.e. 3 times of DBE or 2 times of MCE) and 4MCE (i.e. 4 times of MCE or 6 times of DBE). It should be noted that 4MCE is the medium seismic intensity level for the IDA fragility curve of the Structure A with the stiffness proportional damping distribution. That means approximately half of the far-fault earthquakes within the ground motion suite have resulted in collapse of the building in this case. For the GA optimization of Case 2, Case 3 and Case 4, the objective intensity levels are selected as MCE&2MCE, 5MCE and 5MCE respectively. The upper intensity levels are all closed to the corresponding medium seismic intensity levels.

6.5.3 Representative Ground Motions Considered for Optimization

For each optimization case at an associated intensity level, a targeted ground motion within the corresponding ground motion suite is selected to perform single objective optimization with respect to the optimization problem described in Section 6.5.1. Since this work aims to improve the collapse performance regarding a given seismic environment (i.e. the corresponding ground motion suite), this selected targeted ground motion should be able to represent the characteristics with respect to the structural response of this seismic environment. According to FEMA P695 (ATC 2009), the average or the median drift in terms of a ground motion suite for a collapse simulation is

treated as an important criterion to predict and evaluate the collapse performance of the building within this ground motion suite. Hence, the targeted representative ground motion used to perform objective optimization is determined by comparing the drift resulted from each ground motion with the median drift or the average drift regarding the entire ground motion suite. If a ground motion causes a drift which is closed to the median drift or average drift, this ground motion could be selected as the targeted representative ground motion to represent the ground motion suite in terms of the dynamic sensitivity on the structural performance. It should be noted that the dynamic sensitivity of structures with respect to the seismic performance could slightly vary with the magnitude of the ground motion. Therefore, the representative ground motions for an optimization case could be different for different objective intensity levels.

Specifically, the representative target ground motion for an optimization case at an objective intensity level is determined by evaluating the maximum interstorey peak drift θ_{max} of the initial designed building under each ground motion within the corresponding ground motion suite. Hence, before the optimization process, the IDA program for the buildings with initial designed dampers (i.e. stiffness proportional damping distribution) are run in terms of the proposed optimization cases. Based on these IDA results, the θ_{max} for each ground motion at the objective intensity level can be obtained. In addition, the median/average values of the θ_{max} for all the ground motions which do not cause collapse at the objective intensity level can be accordingly calculated. Here, the ground motions that haven't cause collapse of the building at an intensity level are briefly called as the ground motions 'survive' under this intensity level. For the IDA result that provides more than 20 ground motions 'survive' under the objective intensity level, the median

value of the θ_{max} is used to dominate the selection of the representative ground motion. For the IDA result that provides less than 20 ground motions 'survive' under the objective intensity level, the average value of the θ_{max} is calculated to consider the selection of the target ground motion. Considering the mathematic discreteness, it is assumed that the median value of a set is more representative than its mean value when the number of the individuals in this set is larger than 20.

The candidate representative ground motions, which produce θ_{max} identified to be closed to the median/average θ_{max} of the ground motions, are presented in Table 6.11-6.14 for each optimization scenario. Based on the comparison between the peak drift from the candidate representative ground motions and the corresponding median/average peak drift, the targeted representative ground motion used for each optimization scenario are determined as shown in Table 6.15.

Table 6.11 Candidate quakes for selecting the representative quakes of Case 1 optimization (DBE, 3DBE and 4MCE)

Median Interstorey Peak Drift	**Median of 44 Quakes** θ_{max} (DBE)	**Median of 44 Quakes** θ_{max} (MCE)	**Median of 44 Quakes** θ_{max} (1.5MCE)	**Median of 21 Quakes** θ_{max} (4MCE)
	0.96%	**1.49%**	**2.37%**	**5.24%**

Candidate Quakes	θ_{max} (DBE)	θ_{max} (MCE)	θ_{max} (1.5MCE)	θ_{max} (4MCE)
FE25	0.90%	1.45%	1.92%	5.24%
FE9	1.04%	1.32%	1.91%	4.94%

FE27	**0.68%**	**1.06%**	**1.45%**	**5.57%**
FE31	**1.24%**	**1.89%**	**2.56%**	**6.33%**
FE30	0.82%	1.23%	1.67%	4.85%
FE10	0.91%	1.36%	1.87%	4.85%

Table 6.12 Candidate quakes for selecting the representative quakes of Case 2 optimization (MCE and 2MCE)

Average Interstorey Peak Drift	**Mean of 20 Quakes** θ_{max} (DBE)	**Mean of 20 Quakes** θ_{max} (MCE)	**Mean of 18 Quakes** θ_{max} (1.5MCE)	**Mean of 13 Quakes** θ_{max} (2MCE)
	1.21%	**2.24%**	**3.97%**	**5.50%**

Candidate Quakes	θ_{max} (DBE)	θ_{max} (MCE)	θ_{max} (1.5MCE)	θ_{max} (2MCE)
NE4	**1.30%**	**2.27%**	**4.38%**	**8.36%**
NE19	1.24%	2.21%	4.05%	7.70%
NE6	**1.19%**	**2.15%**	**3.52%**	**5.23%**
NE7	1.47%	1.98%	4.08%	8.12%
NE1	1.00%	1.85%	3.33%	5.24%

Table 6.13 Candidate quakes for selecting the representative quakes of Case 3 optimization (5MCE)

Median Interstorey Peak Drift	**Median of 44 Quakes** θ_{max} (DBE)	**Median of 44 Quakes** θ_{max} (MCE)	**Median of 44 Quakes** θ_{max} (1.5MCE)	**Median of 24 Quakes** θ_{max} (5MCE)
	0.62%	**0.91%**	**1.36%**	**4.93%**

Candidate Quakes	θ_{max} (DBE)	θ_{max} (MCE)	θ_{max} (1.5MCE)	θ_{max} (5MCE)
FE3	0.48%	0.71%	1.03%	4.90%
FE10	0.64%	0.92%	1.19%	4.96%
FE16	0.61%	0.94%	1.88%	5.09%
FE19	0.51%	0.75%	1.30%	5.06%
FE27	0.49%	0.72%	1.30%	5.14%
FE29	**0.76%**	**1.12%**	**1.40%**	**5.15%**

Table 6.14 Candidate quakes for selecting the representative quakes of Case 4 optimization (5MCE)

Average Interstorey Peak Drift	Mean of 20 Quakes θ_{max} (DBE)	Mean of 20 Quakes θ_{max} (MCE)	Mean of 20 Quakes θ_{max} (1.5MCE)	Mean of 10 Quakes θ_{max} (5MCE)
	0.56%	**0.84%**	**1.45%**	**6.32%**

Candidate Quakes	θ_{max} (DBE)	θ_{max} (MCE)	θ_{max} (1.5MCE)	θ_{max} (5MCE)
NE4	0.52%	0.76%	1.24%	6.88%
NE7	0.55%	0.81%	1.50%	5.86%
NE11	**0.54%**	**0.79%**	**1.29%**	**6.18%**

Table 6.15 Representative ground motion selected for each optimization scenario

Optimization Case	Building	Ground Motion Suite	Intensity Level	Representative Ground Motion

Case 1	Structure A	44 Far-fault	DBE	FE31
	Structure A	44 Far-fault	3DBE	FE31
	Structure A	44 Far-fault	4MCE	FE27
Case 2	Structure A	20 Near-fault	MCE	NE4
	Structure A	20 Near-fault	2MCE	NE6
Case 3	Structure B	44 Far-fault	5MCE	FE29
Case 4	Structure B	20 Near-fault	5MCE	NE11

6.5.4 GA Parameter Settings

As described in Section 5.2.2.3, a set of efficient settings of GA parameters are proposed for conducting the single objective optimization of each optimization scenario. With these parameter settings as presented in Table 6.16, the optimization problems for all the analysis scenarios can efficiently converge within 40 generations. It should be noted that the initial populations for the GA solver is set as 'damp0' in this chapter, while 'damp0' is the initial designed damping distribution of the building. (i.e. stiffness proportional damping distribution). This setting enables the GA population to start its evolution from a point comparably optimal and hence saves a large amount of computational time consumed for the global convergence.

Table 6.16 The settings of the GA parameters for the optimization of Structure A and Structure B

Option Parameters	**Value**
'InitialPopulation'	damp0
'PopulationSize'	50
'Generations'	40
'SelectionFcn'	@selectionroulette
'CreationFcn'	@gacreationlinearfeasible
'CrossoverFcn'	{@crossoverintermediate, 30}
'CrossoverFraction'	0.5

'MutationFcn'	@mutationadaptfeasible
'MigrationInterval'	100
'MigrationFraction'	0.2
'EliteCount'	3
'TolCon'	1e-1000
'TolFun'	1e-1000

6.6 Results and Discussion

6.6.1 Optimization for the Representative Ground Motions

Based on the optimization framework as illustrated in Figure 4.4 and the parameter setting provide in Table 6.16, the GA optimization for each optimization scenario can approximately converge within 40 generations in terms of minimizing the maximum peak interstorey drift. In order to monitor the convergence process, the intermediate evolutionary information for each optimization case is output using an additional output function coded in the MATLAB file. For the Case 1 optimization, Figure 6.8(a-c) show the evolutionary processes of the individuals within the GA population. Figure 6.8(d-e) present the evolutions of the individual's fitness for the Case 2 optimization while the evolutionary processes for the Case 3 optimization and the Case 4 optimization are illustrated in Figure 6.8(f) and Figure 6.8(g) respectively. The intermediate evolutionary information in these diagrams indicate that the GA solver achieves significant performance in terms of avoiding convergence at local optimum for this specific optimization problem. The value of the fitness function (i.e. maximum peak drifts) for both the buildings are reduced by at least 10% under the far-fault representative ground motions and improved by approximately 18% under the near-fault representative ground motions. This optimization achievement in terms of a given earthquake is comparably better than that from the work of Whittle et al. (2012) while they used other optimization algorithms.

The distributions of the damping coefficients obtained from the GA optimizations for all the optimization schemes are presented in Figure 6.9(a-d). As shown in the figures, the distributions of the damping coefficients obtained by the GA optimization is relatively different from the initial designed damping distribution, given that the GA program initiates the search from stiffness proportional damping distribution. These significant differences between the initial designed damping distributions and the optimized damping distributions indicate that the GA solver performs so well on exploring the deep search space and leading the population to the global optimum.

Table 6.17-Table 6.22 give the maximum interstorey peak drift of the rettrofitted frames under the corresponding representative earthquake. In addition to seismic performance under the targeted intensity levels considered for the GA optimizations, other intensity levels are also involved to make comparisons between the stiffness proportional damping distributions and the optimized damping distributions. As can be seen from the tables, the mamximum interstorey peak drifts of the frames at the associated targeted intensity levels are improved sharply by the GA optimization. However, the peak drifts under other intensity levels which are not considered for the optimization, are not signficantly improved and even increased slightly.

(a)

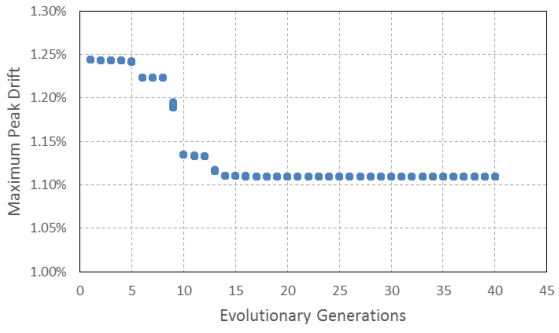

(b)

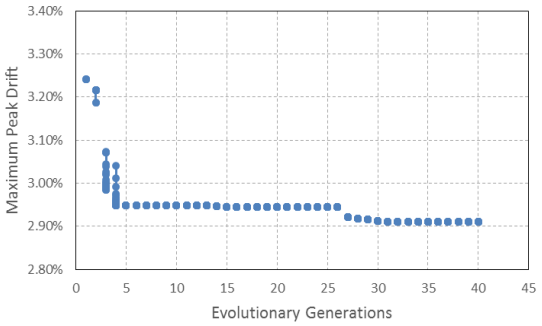
3.40%
3.30%
3.20%
3.10%
3.00%
2.90%
2.80%
Maximum Peak Drift
0
5
10
15
20
25
30
35
40
45
Evolutionary Generations

(c)

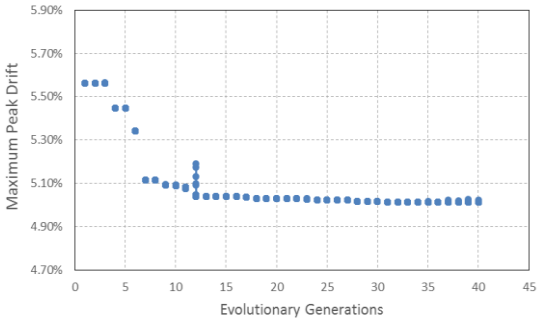
5.90%
5.70%
5.50%
5.30%
5.10%
4.90%
4.70%
Maximum Peak Drift
0
5
10
15
20
25
30
35
40
45
Evolutionary Generations

(d)

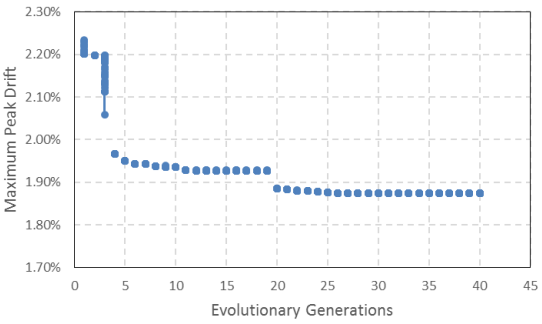
2.30%
2.20%
2.10%
2.00%
1.90%
1.80%
1.70%
Maximum Peak Drift
0
5
10
15
20
25
30
35
40
45
Evolutionary Generations

(e)

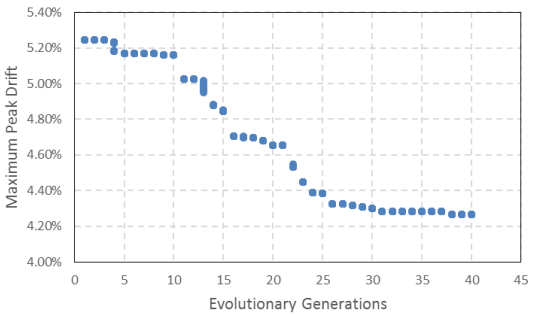
5.40%
5.20%
5.00%
4.80%
4.60%
4.40%
4.20%
4.00%
Maximum Peak Drift
0
5
10
15
20
25
30
35
40
45
Evolutionary Generations

(f)

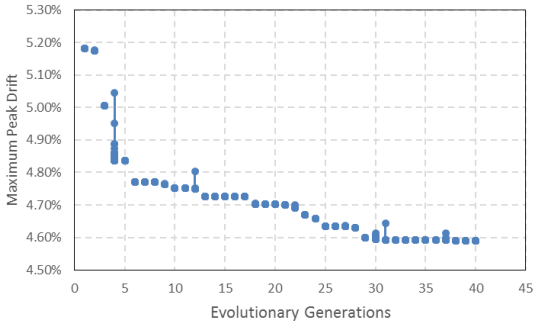

(g)

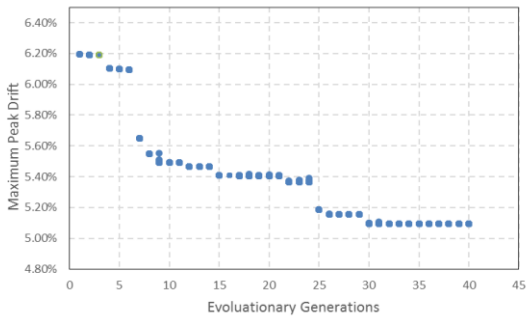

Figure 6.8 The evolutionary fitness of (a) Case 1-DBE-FE31 optimization, (b) Case 1-3DBE-FE31 optimization, (c) Case 1-4MCE-FE27 optimization, (d) Case 2-MCE-NE4 optimization, (e) Case 2-2MCE-NE6 optimization, (f) Case 3-5MCE-FE29 optimization, (g) Case 4-5MCE-NE11 optimization.

(a)

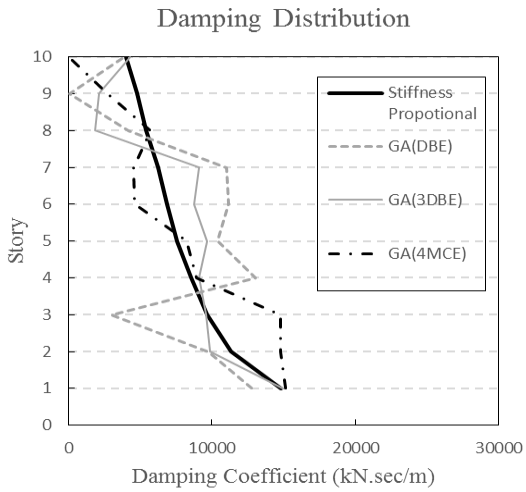

(b)

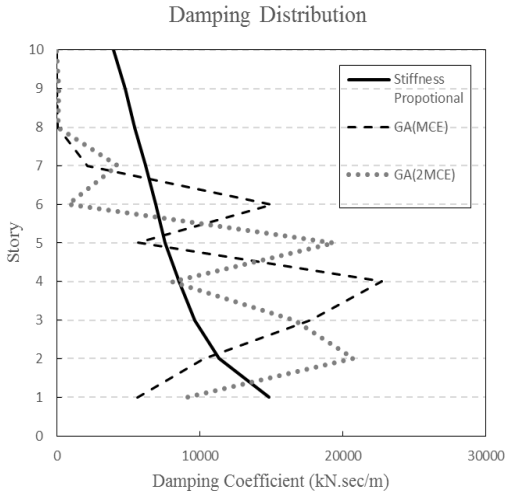

(c)

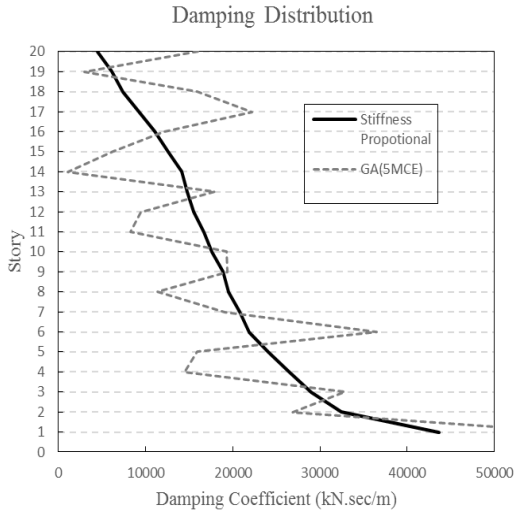

(d)

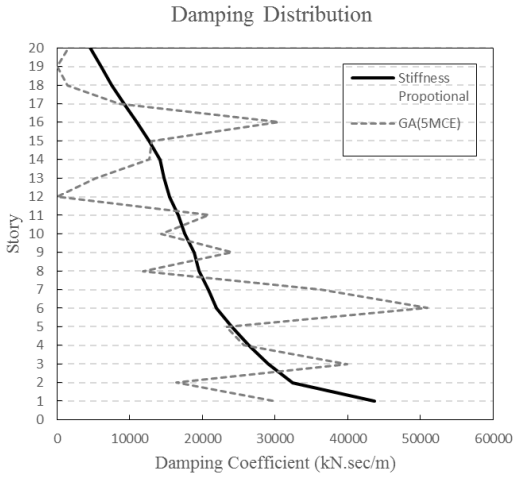

Figure 6.9 The distribution of the damping coefficients obtained from (a) Case 1 optimization (DBE,3DBE and 4MCE), (b) Case 2 optimization (MCE

and 2MCE), (c) Case 3 optimization (5MCE) and (d) Case 4 optimization (5MCE).

Table 6.17 Peak drifts of the representative ground motion (Case1-FE31) for the GA(DBE) and the GA(3DBE) optimization in terms of different damping distributions

Building	IDR_{DBE}	IDR_{3DBE}
Stiffness	1.24%	3.24%
GA (DBE)	1.11%	3.23%
GA (3DBE)	1.18%	2.91%

Table 6.18 Peak drift of the representative ground motion (Case 1-FE27) for the GA(4MCE) optimization in terms of different damping distributions

Building	IDR_{DBE}	IDR_{MCE}	IDR_{2MCE}	IDR_{3MCE}	IDR_{4MCE}
Stiffness	0.68%	1.06%	2.23%	3.56%	5.57%
GA (4MCE)	0.73%	1.08%	2.29%	3.61%	5.01%

Table 6.19 Peak drift of the representative ground motion (Case 2-NE4) for the GA(MCE) optimization in terms of different damping distributions

Building	IDR_{DBE}	IDR_{MCE}	$IDR_{1.5MCE}$	IDR_{2MCE}
Stiffness	1.31%	2.28%	4.41%	8.53%
GA	1.18%	1.87%	4.23%	7.98%

Table 6.20 Peak drift of the representative ground motion (Case 2-NE6) for the GA(2MCE) optimization in terms of different damping distributions

Building	IDR_{DBE}	IDR_{MCE}	$IDR_{1.5MCE}$	IDR_{2MCE}
Stiffness	1.20%	2.16%	3.53%	5.25%
GA	1.17%	1.96%	3.10%	4.26%

Table 6.21 Peak drift of the representative ground motion (Case 3-FE29) for the GA(5MCE) optimization in terms of different damping distributions

Building	IDR_{DBE}	IDR_{MCE}	IDR_{2MCE}	IDR_{3MCE}	IDR_{4MCE}	IDR_{5MCE}
Stiffness	0.76%	1.13%	1.95%	2.96%	3.78%	5.18%
GA (5MCE)	0.82%	1.23%	2.16%	3.27%	4.05%	4.59%

Table 6.22 Peak drift of the representative ground motion (Case 4-NE11) for the GA(5MCE) optimization in terms of different damping distributions

Building	IDR_{DBE}	IDR_{MCE}	IDR_{2MCE}	IDR_{3MCE}	IDR_{4MCE}	IDR_{5MCE}
Stiffness	0.54%	0.82%	1.70%	2.80%	4.46%	6.20%
GA (5MCE)	0.54%	0.80%	1.57%	2.42%	3.82%	5.09%

6.6.2 Optimization for the Probability of Collapse

For evaluating the collapse performance of the rettrofitted buildings with different damping distributions, the IDA programs that are described in Section 6.4 are run for all the optimization scenarios to consider the sideway collapse mechanism. The steel MRFs without installing dampers are also involved to conduct IDA to make comparisons with the rettrofited frames. The fitted fragility curves describing the probability of collapse versus the seismic intensity (i.e. the normalized spectral acceleration at fundamental period of vibration) are accordingly plotted for all the rettrofitted frames including the bare frames. Figure 6.10(a-d) present the fragility curves which describe the collapse performance of the buildings with respect to different damping distributions under a given seismic environment. As a sample illustration, Figure 6.11 provides a set of IDA curves for the 10-storey frame with stiffness proportional damping distribution under 44 far-fault ground motions. In this figure, the relationships between the maximum interstorey drift θ_{max} and the spectral acceleration under first mode $S_a(T_1)$ are described for the designed building under various ground motions with increased intensity levels until collapse. The simulated and the non-simulated collapse state of the buildings can be intuitively identified from the IDA

curves. In addition, the median/average values of the maximum interstorey drift ratio (IDR) for the buildings under the far-fault ground motion suite and the near-fault ground motion suite are also given in Table 6.23-Table 6.26. It should be noted that the median IDRs provided in the tables are with lower intensity levels where none of the earthquakes within the ground motion suites causes collapse of the building. The collapse margin ratios (CMR) as expressed by Equation 6.8 are also presented in Table 6.23-Table 6.26 for the evaluation of the collapse performance of the frames.

Figure 6.10(a) shows the fitted fragility curves of the probability of collapse for the Case 1 optimization (i.e. 10-storey building under 44 far-fault ground motions) under the intensity level of DBE,3DBE and 4MCE and the fragility curves for the bare frame and the designed frame with stiffness proportional damping distribution. As can be seen, the fragility curve for the bare frame is dramatically shifted to left with respect to that for the retrofitted MRFs with dampers. This indicates that all these damper placement strategies considered can significantly improve the collapse performance of the building. However, the probabilities of collapse for these damping distribution schemes vary slightly under a same intensity level. The fragility curve for the designed MRF (i.e. with the stiffness proportional damping distribution) coincides exactly with that for the optimization under the 3DBE. Given that the collapse performance for the optimization under 4MCE is slightly improved, the optimization under DBE even results in marginally greater likelihood of building collapse with respect to the initial designed MRF. The CMR values presented in Table 6.23 provide a straightforward comparison for the variations of the overall collapse performance between different damping distribution strategies. In addition, the median maximum interstorey peak drifts provided in Table 6.23 shows that the critical seismic performances of

the MRFs under the far-fault ground motions are relatively closed at the lower intensity levels (e.g. DBE and MCE) in terms of the considered damping distributions.

The fragility curves for the Case 2 optimization (i.e. 10-storey building under 20 near-fault ground motions) are illustrated in Figure 6.10(b). As can be seen from this figure, the probability fragility curves for the frame optimized under the MCE are similar to that for the frame with the stiffness proportional damping distribution. The fragility curve for the frame optimized under the 2MCE is observed to be slightly shifted to right compared to that with stiffness proportional damping distribution. In addition, it is observed from the Table 6.24 that both the values of the CMR and the averaged maximum interstorey drift are slightly improved by the optimization under the 2MCE.

Figure 6.10(c) shows the fragility curves of the frame with the damping distribution optimized by the Case 3 optimization (i.e. 20-storey building under 44 far-fault ground motions). It is observed that the probability fragility curve for the frame optimized under the 5MCE approximately coincides with that for the initial designed frame. In addition, the median peak drifts at lower intensity levels (i.e. DBE, MCE and 1.5MCE) as presented in Table 6.25 are even slightly amplified by the distribution optimized under the 5MCE.

As shown in Figure 6.10(d), the fragility curve for the Case 4 optimization (i.e. 20-storey building under 20 near-fault ground motions) under the 5MCE is dramatically shifted to the left of that for the stiffness proportional damping distribution at higher intensity levels. This indicates that the Case 4 optimization under the 5MCE even results in greater likelihood of building collapse at higher intensity levels (e.g. 8MCE). Additionally, Table 6.26

shows that the average peak drifts at lower intensity levels are relatively closed between the optimized damper distribution and the stiffness proportional distribution.

(a)

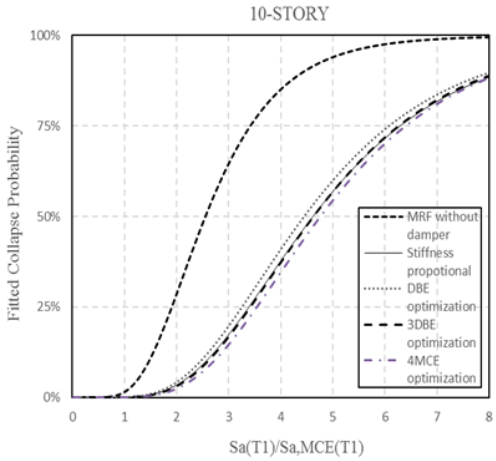

(b)

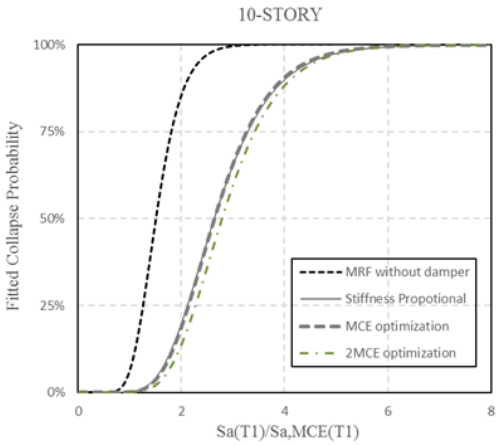

(c)

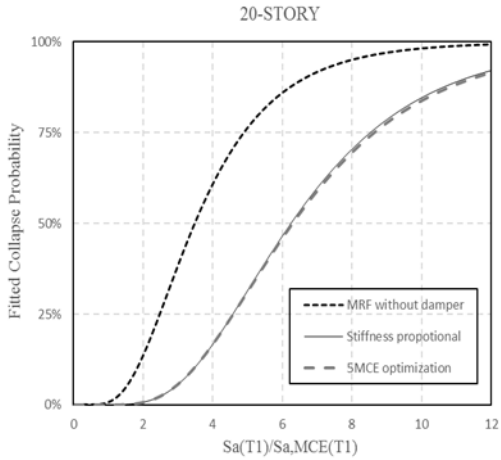

(d)

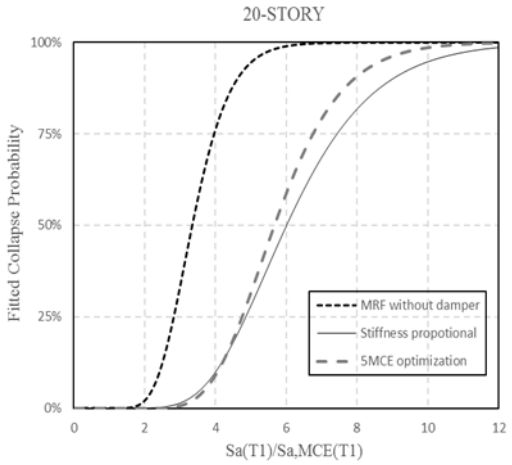

Figure 6.10 Fitted probability of collapse for the MRFs in (a) Case 1 optimization, (b) Case 2 optimization, (c) Case 3 optimization and (d) Case 4 optimization

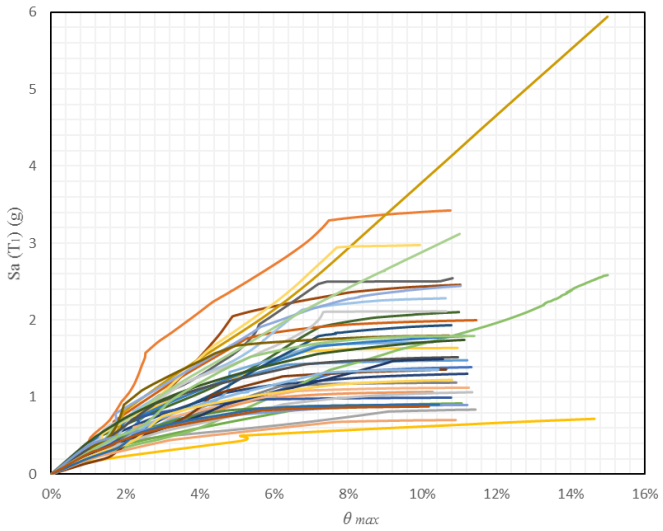

Figure 6.11 IDA curves for the 10-storey buildings with stiffness proportional damping distribution under 44 far-fault ground motions

Table 6.23 Median peak drifts of 44 far-fault ground motions in terms of different damping distributions (Case 1 optimization)

Building	CMR	IDR_{DBE}	IDR_{MCE}	$IDR_{1.5MCE}$
Bare MRF	2.55	2.02%	2.60%	-

Stiffness	4.62	0.96%	1.49%	2.37%
GA (DBE)	4.45	0.95%	1.52%	2.40%
GA (3DBE)	4.63	0.97%	1.50%	2.30%
GA (4MCE)	4.77	0.98%	1.50%	2.36%

Table 6.24 Average peak drifts of 20 near-fault ground motions in terms of different damping distributions (Case 2 optimization)

Building	CMR	IDR_{DBE}	IDR_{MCE}
Bare MRF	1.50	2.22%	5.27%
Stiffness	2.63	1.26%	2.38%
GA (MCE)	2.64	1.21%	2.31%
GA (2MCE)	2.78	1.22%	2.19%

Table 6.25 Median peak drifts of 44 far-field ground motions in terms of different damping distributions (Case 3 Optimization)

Building	CMR	IDR_{DBE}	IDR_{MCE}	$IDR_{1.5MCE}$
Bare MRF	3.49	1.89%	2.25%	-
Stiffness	6.26	0.62%	0.91%	1.36%
GA (5MCE)	6.29	0.69%	1.00%	1.52%

Table 6.26 Average peak drifts of 20 near-fault ground motions in terms of different damping distributions (Case 4 optimization)

Building	CMR	IDR_{DBE}	IDR_{MCE}	$IDR_{1.5MCE}$
Bare MRF	3.35	1.03%	1.58%	-
Stiffness	6.02	0.55%	0.81%	1.43%
GA (5MCE)	5.67	0.56%	0.84%	1.45%

In order to evaluate the effectiveness of the GA optimization on the collapse performance, the boundary intensity level that cause the building collapse under each representative ground motion is presented in Table 6.27 in terms of the considered damping distribution. As can be seen from the table, the

boundary intensity level for the optimization scenario Case 1-FE27-4MCE is improved by approximately 9% under the far-fault representative ground motion (i.e. FE27). For the optimization scenario Case 2-NE6-2MCE, the boundary intensity level of the 10-storey building is increased up to 6% under the near-fault target ground motion (i.e. NE6). However, the collapse intensity levels for the building associated with the optimization scenario of Case 1-FE31-DBE, Case 1-FE31-3DBE, Case 2-NE4-MCE are not significantly improved. This indicates that the optimization at a high intensity level closed to the collapse state are more effective to improve the collapse performance of the building than the optimization under a lower intensity levels. The boundary intensity level of collapse is solely improved by 1% for the optimization scenario Case 3-FE29-5MCE and even reduced by about 2% for the Case 4-NE11-5MCE optimization. It is observed that the collapse performance of the optimized MRF under a target representative ground motion approximately coincide with that of the optimized frame under the corresponding ground motion suite, indicating that the target ground motions used for the optimizations can basically represent the characteristics of the ground motion suites with respect to the seismic response.

It can be summarized from the results that the GA optimization is able to provide a damper distribution which achieves the collapse performance as acceptable as that achieved by the stiffness proportional damping distribution. However, considering the essential computational time and the variation of the seismic characteristics, the GA distribution cannot efficiently improve the collapse performance of the building under a given intensive seismic environment. Although the structural performance of the building under a given single earthquake can be improved under a target intensity level, this improvement should not be exaggerated as the structural performance under

other intensity levels or under other ground motions might not be consistent. It should also be noted that the GA optimization with respect to the seismic context under a lower intensity level is less effective to improve the ultimate collapse intensity of the structure. It is also observed that the GA optimization under both the far-fault and near-fault ground motion suites are less effective to improve the collapse performance of taller building than that of the shorter building. This phenomenon could be explained by the amplified problem search space and the increased complexity of the vibration mode due to the increase of the storeys. The amplification of the search space for the optimization could increase the difficulty of the convergence at global optimum. Most importantly, the increased complexity on the vibration mode would amplify the structural response of the building without the decoupled damping matrix of the Rayleigh-type damping distribution (e.g. stiffness and mass proportional damping distribution).

Table 6.27 Collapse intensities and the maximum interstorey peak drift ratios under the DBE intensity level of the representative earthquake

Building	**Damping distribution**	**Earthquake**	**IDR_{DBE}**	**Collapse Intensity (m/s2)**
10-story	GA(DBE)	FE31	1.11%	2.04
	GA(3DBE)	FE31	1.18%	1.945
	Stiffness proportional	FE31	1.24%	1.94
	GA(4MCE)	FE27	0.73%	2.32
	Stiffness proportional	FE27	0.68%	2.125
	GA(MCE)	NE4	1.17%	0.84
	Stiffness proportional	NE4	1.30%	0.815
	GA(2MCE)	NE6	1.17%	1.195
	Stiffness proportional	NE6	1.19%	1.13

20-story	GA(5MCE)	NE29	0.82%	1.035
	Stiffness proportional	NE29	0.76%	1.02
	GA(5MCE)	NE11	0.54%	1.205
	Stiffness proportional	NE11	0.54%	1.235

6.7 Conclusions

This chapter presents a baseline study on investigating the effectiveness of the GA for the optimization of the height-wise damper distribution in code-compliant steel building. Since most of the previous studies mainly focus on evaluating the structural performance of the damper optimization under individual seismic context associated with a design-based intensity level, this work evaluates the optimized performance for design-level structural performance to building collapse performance and extends the scope of investigation from a single earthquake to a ground motion suite including multiple seismic characteristics. In addition, the work focused on optimizing dampers for large drifts of the buildings associated with high intensity levels to explore the efficiency of the objective optimization on the building collapse. To establish the model of a realistic frame, two MRF buildings are designed based on the Eurocode and the buildings are designed with fluid viscous dampers based on classical stiffness proportional damping distribution. The supplemental damping distribution of the nonlinear frame models are optimized by using the GA solver along with the nonlinear time history analysis. For evaluating the optimization in terms of the collapse performance, collapse simulation with the help of Incremental Dynamic Analyses are accordingly conducted. To evaluate the effectiveness of the optimization, the structural performance of the buildings optimized by GA is compared with that installed with the classical damping distribution.

The results show that the GA stochastic optimization regarding the damper distribution along the floors cannot efficiently improve the building collapse for a given seismic context (i.e. a ground motion suite). In terms of the damper optimization for the buildings with different storeys, it is found that the collapse performance of the taller building is more difficult to be improved by optimizing the vertical damper distribution with the GA stochastic optimization. Considering that the search efficiency of GA has been demonstrated to be superior among the stochastic optimization algorithms, this conclusion could be also applied to other vertical damper optimization techniques which utilize the stochastic search algorithms. Compared to the GA damping distributions, the stiffness proportional damping distribution presented in this study shows a greater stability on reducing the seismic response and the collapse performance of the buildings under various earthquake excitations. Given that the GA distributions to some extend improve the structural response under an individual ground motion at a target intensity level, this improvement should not be overstated by previous researchers, as the reduction on the structural response could not be consistent under different ground motions and different intensity levels.

Since the stiffness proportional damping distribution is demonstrated to be one of the most effective and practical vertical damper distribution methods regarding the building collapse performance, based on this vertical damping distribution the next chapter will investigate the optimum damper placement strategy for the horizontal damper distribution (i.e. damper-brace distributed in different bays) with respect to the collapse performance.

Charter 7

Horizontal Damper Placement Techniques in Steel Moment Resisting Frames

7.0 Introduction

In the previous chapter, the effectiveness of stochastic optimization for determining the optimal vertical damper distribution with respect to the collapse resistance under strong earthquakes was explored. It is found that the classical stiffness proportional damping distribution method is more superior than other damping distributions methods which obtain the optimum damping distribution using stochastic objective optimization algorithms. In the present chapter, the horizontal distribution of dampers regarding the collapse resistance of building is investigated by attempting various brace-damper arrangements in different bays of the MRFs, based on the vertical damper placement of stiffness proportional damping distribution. In addition, the global plastic mechanisms associated with the structural performance for the horizontal retrofitted frames are further investigated in this chapter.

7.1 Background

In Chapter 6 a damping distribution throughout the height of the building was investigated based on the installation of chevron-braced dampers in the central bay of the prototype MRFs. According to this practical installation of dampers, the damper reaction forces are transfer throughout the chevron braces to the frame system. Previous researches show that the damper reaction forces contributed to the column axial loading can affect the seismic performance of the building, while the arrangement of the damper-brace in different bays is known to influence the transfer path of the damper reaction force in the columns. A review for the influence of the damper reaction force

on the column axial force and the concern of the horizontal brace-damper arrangement is provided in the present section.

7.1.1 The Influence of Damper Reaction Force

Constantinou and Symans (1993b) mention that the vertical component of the damper reaction force transferred to the supported brace can increase the axial forces in the columns of the frames. Base on their studies, apart from the supplemental damping device with viscous dampers, the added axial force developed by other damper devices could be in-phase with the bending moment and the peak drift, that potentially influence the stability of the base columns in terms of seismic loading. While the vertical component of the damper reaction force is considered as a critical design concern, the horizontal component is identified to be less critical as it can be resisted by the lateral resisting system in the frames.

Lee et al. (2009) utilized a MRF building modelled with elastomeric dampers (i.e. in-phase damper device) to explore the overstressed effects in base column that are caused by the damper reaction force. This research shows that the installation of in-phase dampers indeed induces significant axial column force at the ground floor during the seismic response of the steel structure. For the dampers with the out-of-phase behavior, Constantinou and Symans (1993b) claim that the vertical component of the damper reaction force is not critical for the seismic design of the steel frames with linear FVDs which are out of phase with the peak drifts. However, other researchers found that the MRF buildings with linear FVDs can experience significant additional axial column loadings in the base columns when the effective damping ratio of the building is over 20% (Uriz and Whittaker 2001, Kim and Choi 2006).

7.1.2 The Concern of Horizontal Brace-damper Arrangement

According to traditional horizontal damper arrangements, the brace-dampers are normally placed to interior bays of the frame that claims to utilize their reverse axial capacity to sustain the additional axial column forces. Since the horizontal distribution of the brace-dampers in each floor is known to affect the transfer path of the additional axial loads and hence affect the accumulation of the axial column loads in the base column, a number of studies engaged to reduce the axial base column loads by strategically distributing brace-dampers in different bays. The study of Apostolakis and Dargush (2010), regarding the optimal distribution of friction dampers and energy-dissipating braces in steel MRFs, founds that the seismic structural performance can be reduced by a combination of interior and exterior damper-brace bays as shown in Figure 7.1.

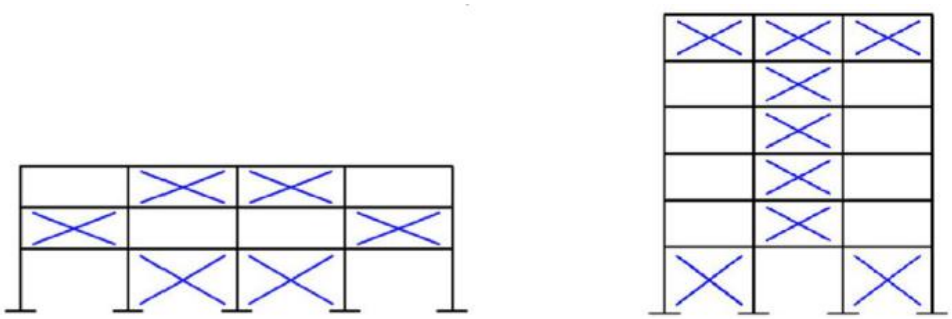

Figure 7.1 The optimal horizontal brace-damper arrangements (Apostolakis and Dargush 2010)

Mezzi (2010) proposed several horizontal brace-damper arrangements for the building frame installed with two energy-dissipating braces in each floor as shown in Figure 7.2. According to his study, the column bending moments and column axial forces can be to some extend reduced by directly linking the braces (i.e. IN, XD, SP), while the brace-damper arrangement with connected the braces in adjacent floors (i.e SP) achieves the best structural

performance.

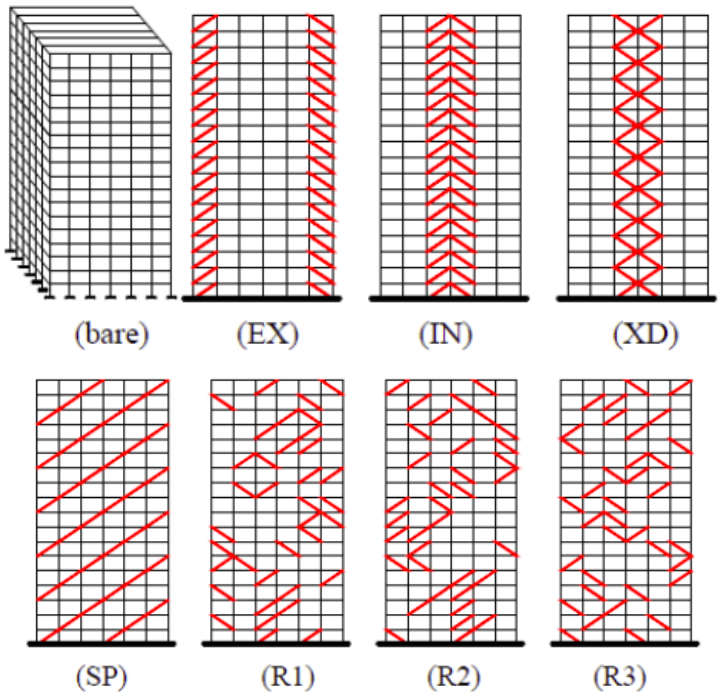

Figure 7.2 The proposed horizontal brace-damper arrangements (Mezzi 2010)

Whittle et. al (2012b) proposed a force counteraction approach to distribute the brace-dampers in each floor of a 10-storey steel MRF with linear FVDs. As illustrated in Figure 7.3, this approach highlights that some of the additional axial forces in the interior columns could be potentially counteracted if the braces in the adjacent floors are appropriately arranged. Based on this method, the unbalanced axial forced accumulated in the base columns can be calculated and used to identify the superior brace-damper arrangements. In addition, Whittle et. al (2012b) investigated five horizontal damper distributions (as shown in Figure 7.4) of the MRF with the uniform vertical damping distribution under the design-level earthquakes. They found that the linear FVDs can cause additional axial forces to the frame system, however, the structural performance under the DBE is slightly improved by the best horizontal brace-damper arrangements (i.e. A3).

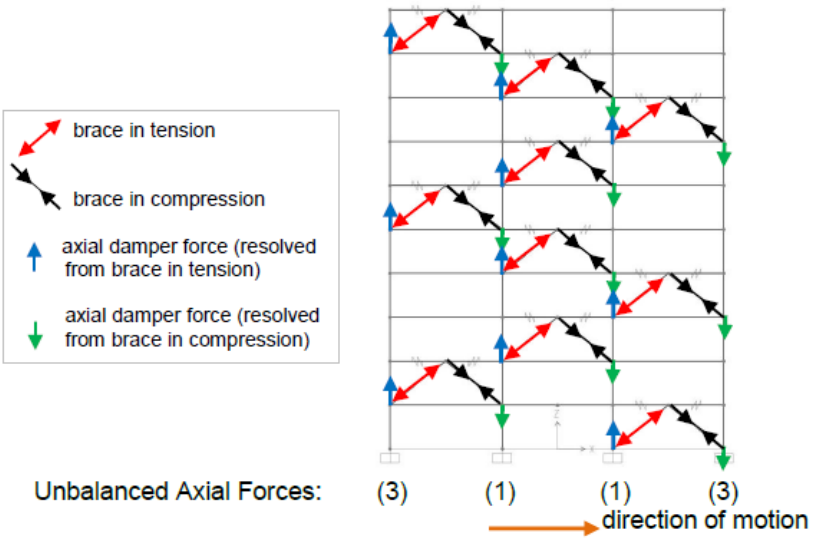

Figure 7.3 Force counteraction approach for the additional column axial loads (Whittle et.al 2012b)

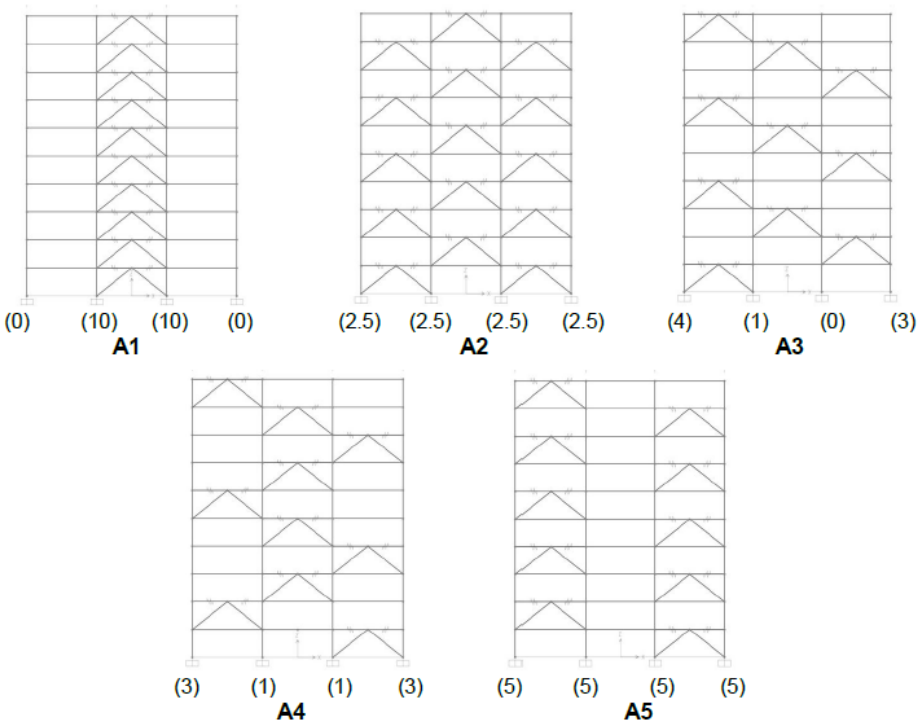

Figure 7.4 Five horizontal damper distributions (Whittle et.al 2012b)

7.2 Methodology

As it is known from Section 7.1, the column axial loading of the steel MRFs

with linear FVDs can be influenced by the distributions of the brace-dampers in different bays. However, the study of Whittle et. al (2012b) shows that the structural performance of the frames with linear FVDs is only slightly affected by the horizontal damper distribution under the design-level earthquakes. Therefore, this chapter aims to explore whether the collapse resistance of the MRFs could be significantly improved by strategically distributing the brace-damper in multiple bays. Furthermore, the developments of the plastic hinges in the retrofitted frames are also investigated to identify the superior damper arrangement strategies. Both the evaluation for the collapse performance and the plastic mechanism are based on the IDA results of the retrofitted MRFs investigated in this chapter. It should be noted that the steel MRFs utilized to explore the horizontal damper arrangements in this chapter are based on the two prototype buildings and the associated modeling details for the collapse simulation presented in Chapter 6.

In this section, the load path of the damper reaction force in a single bay of the prototype MRFs is discussed. Several brace-damper arrangements are proposed based on the considered load path of the damper forces and the accumulation of the vertical damper forces in the base columns. The seismic environments of IDA and the associated design information that are considered for the buildings models in this chapter are stated. For evaluating the plastic mechanism of the retrofitted frames, the methodology for identifying the plastic hinges in the columns is discussed.

7.2.1 Load Path of the Damper Reaction Force

Before considering the load path of the additional axial column force in the adjacent storeys, the load path of the damper reaction force in a single bay of

the prototype MRFs is explored. Figure 7.5 provides the illustration of the relationships between the damper reaction force F_D and axial brace force F_B for a chevon-braced single damper. As can be seen from the figure, both the axial brace force F_B in the left brace and the right brace are equal to $F_D / \cos\theta$ where θ is the angle between the braces and the floor. The axial brace force in the left brace is a compression force with respect to the left beam-column joint while the axial force in the right brace is identified as a tension force with respect to the right beam-column joint. Therefore, the axial force in the left braces result in an upward additional axial column force equal to $F_B \cdot \sin\theta$ in the left column and the axial brace force on the right result in a downward additional axial column force also equal to $F_B \cdot \sin\theta$ (i.e. equal to $F_D \cdot \tan\theta$).

Since the general load path of the damper reaction forces of the MRFs in this research is similar to that considered in the force counteraction approach (as shown in Figure 7.3) proposed by Whittle et.al (2012b), this study intends to reroute the additional axial column forces by optimizing the horizontal damper distribution based on this approach. The specific description for rerouting the axial damper forces (i.e. the damper reaction forces resolved from braces to columns) is illustrated in Figure 7.3 which shows the load path for the additional axial column forces of a 10-story MRF with brace-dampers installed in different bays. With this arrangement of damper braces, more than 50% of the additional axial column force in the base columns caused by the dampers could be counteracted by the couples of axial forces in the adjoining bays. For a simplification that all the axial reaction forces from dampers are equivalent, the brace-damper arrangement could be determined by assessing the number of the unbalanced axial forces accumulated in the base column. As shown in Figure 7.3, three unbalanced damper axial forces are resisted by

both the exterior columns at the base and one unbalanced damper axial force is resisted by each interior base-column.

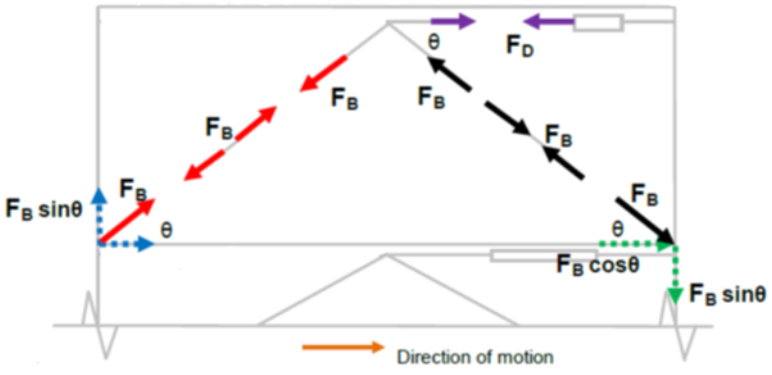

Figure 7.5 Load path of damper reaction force in a single bay

7.2.2 Considered Brace-Damper Arrangements

Based on the force counteraction approach, four critical brace-damper arrangements for the 10-story MRF (as shown in Figure 7.6) and four critical brace-damper arrangements for the 20-story MRF (as shown in Figure 7.7) are investigated to compare their collapse capacities. All these retrofitted frames are designed to potentially expose the effects of the damper axial forces on the collapse resistance of building. Hence, the design scenario maximizing the counteraction of axial damper forces and the design scenario ignoring the counteraction of axial damper forces are both explored. Table 7.1 provides the detailed numbers of the brace-dampers arranged in the exterior bays and the interior bays, and the unbalance axial forces in the base columns. As can be seen from Figure 7.6 and Table 7.7, both the A1 arrangement and the B1 arrangement are the classical brace-damper arrangement that places the dampers in the central bay of the MRF resulting in concentrated unbalance axial column loadings at the base of the interior columns. In contrast, both the A2 arrangement and the B2 arrangement are with brace-dampers installed in the exterior bays of each floor resulting uniform unbalance axial column

forces at the base. The brace-damper arrangements of A3, A4, B3 and B4 make use of the counteraction of axial damper forces in the interior columns by distributing the dampers in sequence from the bay to bay. The A3 and B3 arrangement can result in minimum unbalanced axial force in the interior column at the base, while the A4 and the B4 arrangement can provide small unbalanced axial forces in the based interior columns with comparatively uniform distribution of unbalanced forces.

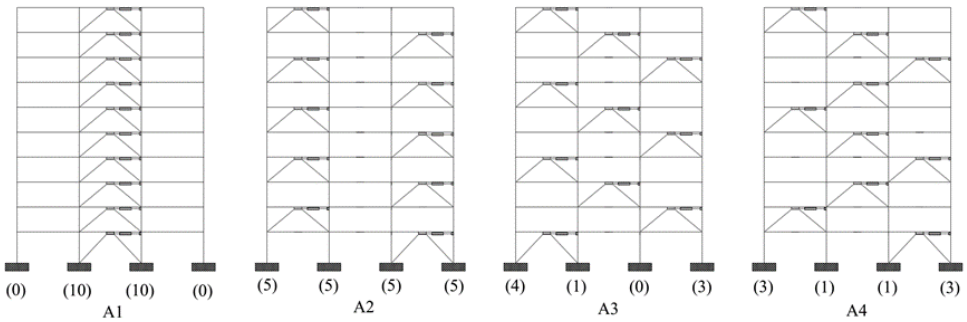

Figure 7.6 Brace-damper arrangements for 10-story MRF

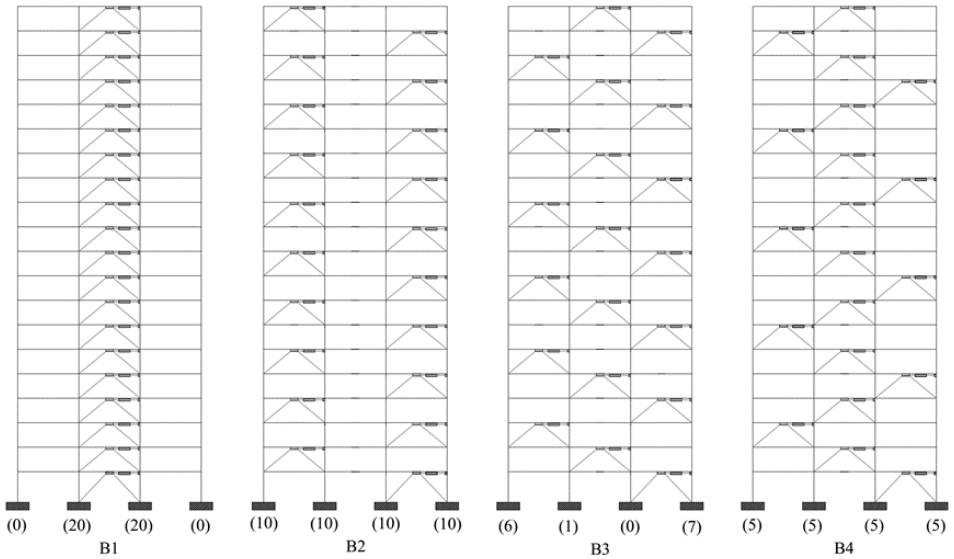

Figure 7.7 Brace-damper arrangements for 20-story MRF

Table 7.1 Numbers of brace-dampers and unit unbalanced axial forces for the MRFs

Frames	NO. of Brace-dampers		
	Left Exterior Bays	Interior Bays	Right Exterior Bays
A1	0	10	0
A2	5	0	5
A3	4	3	3
A4	3	4	3
B1	0	20	0
B2	10	0	10
B3	6	7	7
B4	5	10	5

Frames	NO. of Unit Unbalanced Axial Force			
	Column 1 (Left Exterior)	Column 2 (Left Interior)	Column 3 (Right Interior)	Column 4 (Right Exterior)
A1	0	10	10	0
A2	5	5	5	5
A3	4	1	0	3
A4	3	1	1	3
B1	0	20	20	0
B2	10	10	10	10
B3	6	1	0	7
B4	5	5	5	5

7.2.3 Building Model and Considered Ground Motions for IDA

In this chapter, both the 10-storey and the 20-storey building models for conducting the IDA program are based on the building information and the modeling details defined in Chapter 6. These include the building geometry, the design concern and assumption of the prototype buildings, the designed load combination, the design of the structural elements, the details for the nonlinear modeling and the criteria set for the IDA program. Since the stiffness proportional damping distribution of the dampers throughout the floors is demonstrated to be superior under the intensive seismic excitation associated with collapse, this classical vertical damping distributions as designed in Chapter 6 is used for all retrofitted frames in this research.

Both 44 far-fault earthquakes (refer to Table 6.9) and 20 near-fault earthquakes (refer to Table 6.10) are utilized to conduct the IDA of the frames as defined in Section 6.3.1. However, in this chapter, the ratio between the pulse period and the fundamental period (T_P/T_1) of the selected 20 near-fault earthquake records are set as 2-3.97 (i.e. the critical region for the collapse sensitivity) for the 20-story building that results in a different near-fault ground motion suite from the one selected for the 10-storey building. The property of the selected 20 near-fault ground motions is presented in Table 7.2.

7.2.4 Evaluation of Plastic Hinges Mechanism

The plastic hinge mechanism for all frames are evaluated from the result of IDA and the associated comparisons are made among different brace-damper arrangements. The number of plastic hinges in the columns of the MRF for each ground motion is calculated at different levels of maximum interstorey peak drift (θ_{max}) by performing linear interpolation on the IDA results. Then the median number of column plastic hinges for the ground motion suite is obtained for different θ_{max} levels. The percentage of plastic hinges developed in the columns of the MRF is therefore calculated by dividing the median number of column plastic hinges by the number of all possible locations of the column plastic hinges.

For evaluating the number of plastic hinges in the columns of the frames, it is assumed that each column contains two nodes at both endings which would potentially occur plastic hinges. In order to determine whether the plastic hinges occur at these nodes under a drift level, the capacity ratios of the nodes in the columns are calculated in the IDA program according to the Eurocode 3 (BS EN 1993-1-1:2005, 6.2.9.1). The capacity ratio in terms of the plastic

moment resistance is expressed by Equation 7.1, where M_{Ed} is the design value of the moment at the node in the column that can be obtained by nonlinear time series analysis within the IDA program, M_{Rd} is the design plastic moment resistance of the column element. When the capacity ratio of a plastic node is measured to be larger than 1, it can be assumed that the plastic hinge occurs at this node.

$$Capacity\ Ratio = \frac{M_{Ed}}{M_{Rd}} \tag{7.1}$$

More specifically, the design plastic moment resistance of the column M_{Rd} is determined by using the less one between the design plastic moment resistance $M_{N,Rd}$ account for the reduction due to the design axial force N_{Ed} and the design plastic moment resistance $M_{pl,Rd}$ of the gross cross-section originally obtained from the steel section table. In accordance to Eurocode 3 (BS EN 1993-1-1:2005, 6.2.9.1(5)), the design plastic moment resistance $M_{N,Rd}$ for the designed member section in this study is given by:

$$M_{N,Rd} = \frac{M_{pl,Rd} \cdot (1-n)}{1-0.5a} \tag{7.2}$$

Where

$$n = \frac{N_{Ed}}{N_{pl,Rd}}$$

$$a = \frac{A-2bt_f}{A}$$

While $N_{pl,Rd}$ is the design plastic axial force resistance of the gross cross-section, t_f is the flange thickness, b is the width of the cross section, A is the cross-sectional area.

Table 7.2 The properties of near-fault ground motions selected for the collapse optimization of the 20-storey Buildings

ID No.	Ground Motion	Station	Location	Component	Tp (s)	Duration (s)	PGV (cm/s)	DBE Scale Factor (Structure B)
NE1	Imperial Valley 1979	El Centro Array #11	USA	H-E11233	7.4	54.05	41.10	1.50
NE2	Landers 1992	Barstow	USA	BRS225	8.9	100.04	30.41	1.12
NE3	Landers 1992	Yermo Fire Station	USA	YER225	7.5	104.04	53.23	1.01
NE4	Chi-Chi 1999	TCU034	Taiwan	TCU034306	8.6	105.01	42.77	1.05
NE5	Chi-Chi 1999	TCU038	Taiwan	TCU038277	7	105.01	50.86	0.59
NE6	Chi-Chi 1999	TCU042	Taiwan	TCU042306	9.1	105.01	47.34	0.82
NE7	Chi-Chi 1999	TCU046	Taiwan	TCU046306	8.6	100.01	43.96	1.11
NE8	Chi-Chi 1999	TCU049	Taiwan	TCU049278	11.8	105.01	44.82	0.79
NE9	Chi-Chi 1999	TCU054	Taiwan	TCU054283	10.5	105.01	60.92	0.76
NE10	Chi-Chi 1999	TCU060	Taiwan	TCU060278	12	105.01	33.70	0.79
NE11	Chi-Chi 1999	TCU068	Taiwan	TCU068280	12.2	105.01	191.15	0.23
NE12	Chi-Chi 1999	TCU082	Taiwan	TCU082283	9.2	105.01	56.12	0.60
NE13	Chi-Chi 1999	TCU087	Taiwan	TCU087306	9	105.01	53.67	0.93
NE14	Chi-Chi 1999	TCU098	Taiwan	TCU098306_	7.5	105.01	32.74	0.98
NE15	Chi-Chi 1999	TCU101	Taiwan	TCU101278	10	64.01	68.39	0.72
NE16	Chi-Chi 1999	TCU102	Taiwan	TCU102278	9.7	105.01	106.57	0.39
NE17	Chi-Chi 1999	TCU103	Taiwan	TCU103277	8.3	105.01	62.18	0.62
NE18	Chi-Chi 1999	TCU104	Taiwan	TCU104278	12	105.01	31.43	0.85

NE19	Chi-Chi 1999	TCU128	Taiwan	TCU128306	9	105.01	78.66	0.41
NE20	Chi-Chi 1999	TCU136	Taiwan	TCU136278	10.3	102.01	51.82	0.80

7.3 Analyses Results and Discussions

Based on the methodology presented in Section 7.2, each considered brace-damper arrangement is analyzed by the IDA program under the far-fault and the near-fault ground motion suite. To compare the collapse resistance of the frames under various intensity levels, the probability of collapse for each retrofitted scenario is presented by the fitted fragility curve. To explore the differences of the plastic mechanism among the damper-brace arrangements, the median percentages of plastic hinges occurred in the columns of the retrofitted frames are plotted with respect to various drift levels.

Figure 7.8(a-b) show the collapse probabilities of the 10-story MRFs under 44 far-fault ground motions and 20 selected near-fault ground motions at different intensity levels. As can be seen, the fragility curves of the A2, the A3 and the A4 damper-brace arrangement schedules for both the seismic contexts solely shift slightly to right relative to the A1 arrangement, indicating that the collapse probabilities are not significantly improved by the retrofitted schedules. However, the detailed improvements reveal that the A3 and the A4 schedules are more effective than the A2 schedule for both earthquakes groups, while the collapse performance of the A2 schedule under the near-fault ground motions exactly coincides with that of the A1 schedule.

Figure 7.8(c-d) show the collapse probabilities of the 20-story MRFs under the far-fault and near-fault ground motions in terms of different intensity levels. As can be seen, the improvements of the collapse fragility curves are significant for the B2, the B3 and the B4 schedules under the far-fault earthquakes, while the B3 and the B4 arrangements have a larger shift to right compared to the B2 arrangement. The improvement of the collapse fragility curves for the B3 and the B4 schedules under the near-fault earthquakes are

more dramatic compared to that for the A3 and the A4 schedules under the near-fault motions. Similar to the 10-story MRF, the collapse performance of the B2 schedule under the near-fault earthquakes context coincides with that of the B1 schedule.

(a)

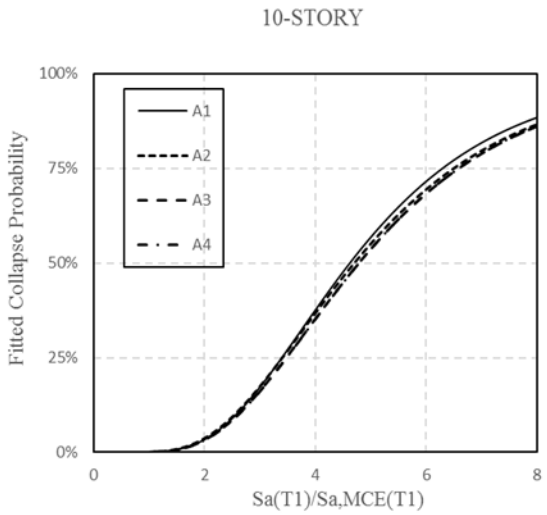

(b)

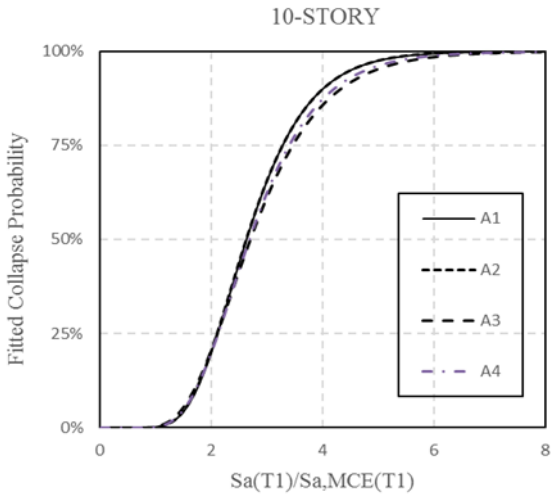

(c)

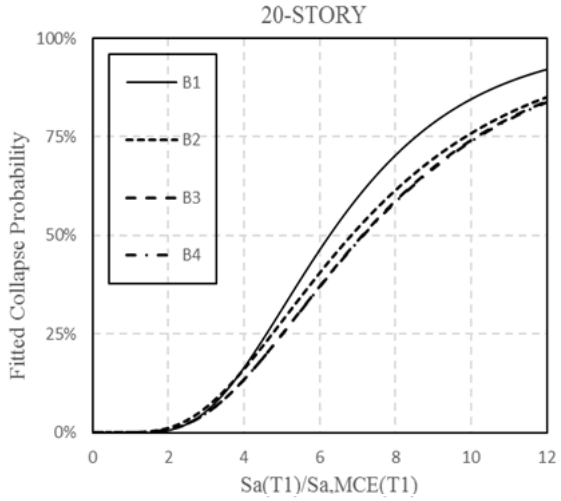

(d)

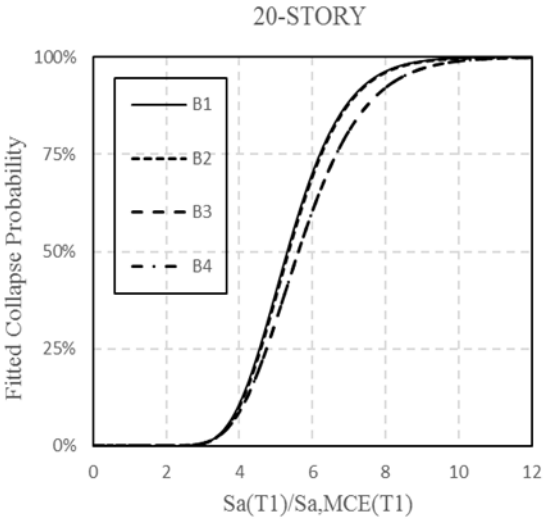

Figure 7.8 Fitted probability of collapse of 10-story MRF under the 44 far-fault quakes (a) and the 20 near-fault quakes (b); Fitted collapse probability of 20-story MRF under the 44 far-fault quakes (c) and the 20 near-fault quakes (d).

Figure 7.9(a-d) present the median values of the percentage of the plastic hinges in the columns of the 10-story and the 20-story MRFs under the 44 far-fault ground motions and the associated 20 near-fault ground motions respectively. As can be seen from Figure 7.9(a), all the braced 10-story MRFs under the far-fault quakes start to develop plastic hinges from the θ_{max} of

approximately 1.5%. While the plastic hinges of the A1 MRF increase dramatically from 1.5% to 8% for θ_{max}, the plastic hinges of the A2, A3 and A4 MRFs become stable from around 2.5% θ_{max} to 4% θ_{max}. After that the A2 frame develops the plastic hinges with a sharper increased trend relative to the A3 and the A4 frames, while the number of the column plastic hinges for the A3 and the A4 frames stay closed until 8% θ_{max}. By and large, the median plastic hinges of the A3 and the A4 MRFs have less amount than that of the A1 and the A2 MRFs. However, the plastic hinges are still significantly reduced by using the brace-damper arrangement of the A2 schedule. Figure 7.9(b) shows that the four 10-story MRFs under the near-fault earthquakes have closed median percentages of plastic hinges. While the percentage curve of the A2, the A3 and the A4 MRFs shift slightly to right from around 2% θ_{max} to 2.5% θ_{max} and from 4.8% θ_{max} to 6.3% θ_{max}, the total developed plastic hinges are significantly less than that of the A1 MRF after the θ_{max} increased to 6.3%. Figure 7.9(c) shows that the median percentage of the column plastic hinges for the MRF under the far-fault earthquakes are significantly reduced by using the B3 schedule and the B4 schedule instead of the B1 schedule. After developing the initial plastic hinges at around 1.2% θ_{max}, the percentage of the plastic hinges of the A1 MRF increases with a sharper trend than other designed MRFs. However, the accumulation of the plastic hinges for the A2 MRF speeds up at approximately 2.1% θ_{max} that makes it surpass the plastic hinges numbers at about 3.8% θ_{max}. For the θ_{max} levels between 7% to 8%, the plastic hinges of the B3 MRF has the least median percentage at around 25%, while those of the B1, the B2 and the B4 MRF are 38%, 48% and 29% respectively. As shown in Figure 7.9(d), the median percentages of plastic hinges for the B2 MRF under the near-fault earthquakes stay higher than that of other designed MRFs within the region from 1.5% θ_{max} to 3.1% θ_{max}. After that

the percentage curve of the B2 MRF increase with a smooth trend and shifts to the right of the B1 curve. For the eventual region that between 7% and 8% for θ_{max}, the least median plastic hinges percentage is achieved by the B4 schedule with approximately 12.5% θ_{max} and the largest percentage is generated by the B1 schedule with around 21% θ_{max}.

(a)

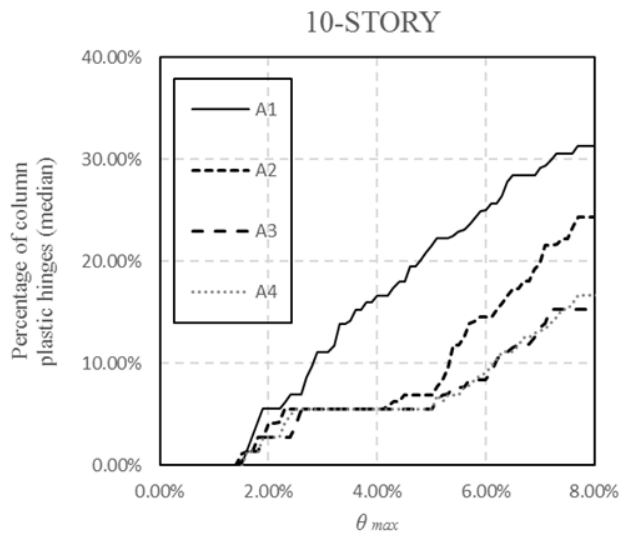

(b)

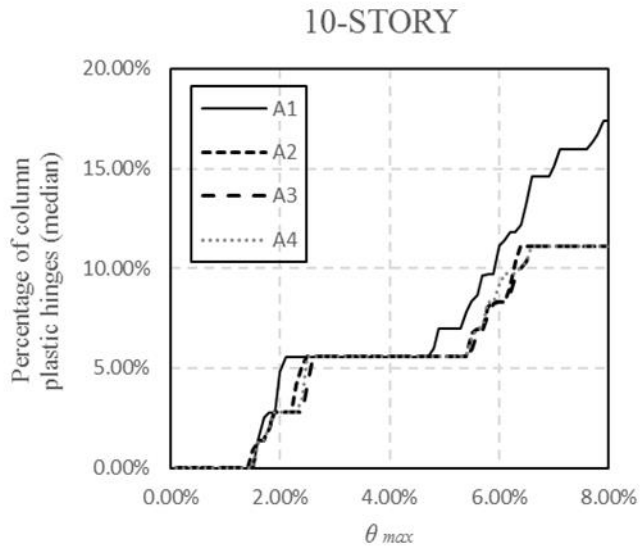

(c)

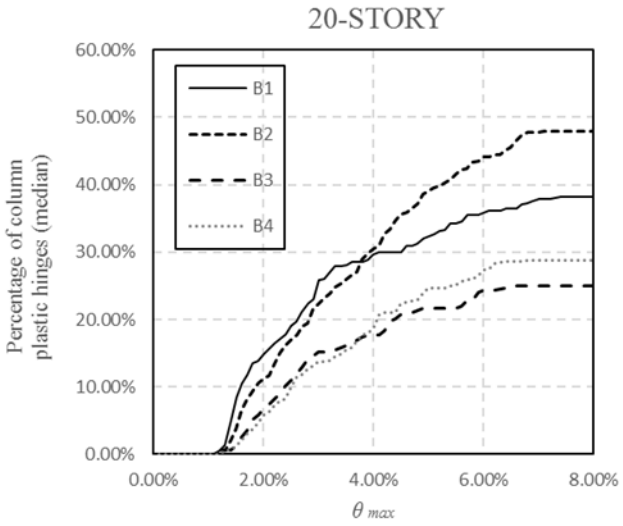

(d)

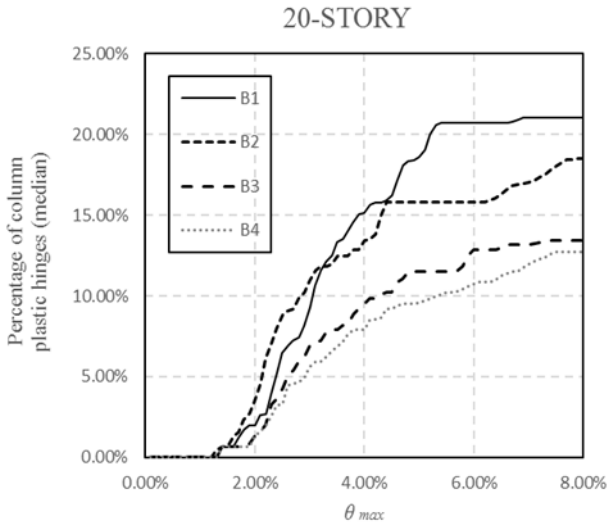

Figure 7.9 Median value of the percentage of the plastic hinges in the columns of the 10-story MRF under the 44 far-fault quakes (a) and the 20 near-fault quakes (b); Median value of the percentage of the plastic hinges in the columns of the 20-story MRF under the 44 far-fault quakes (c) and the 20 near-fault quakes (d).

7.4 Conclusions

This chapter presents a baseline study on exploring the optimum horizontal brace-damper distribution in moment resisting steel frames regarding the

collapse performance of the buildings. Several frames with different brace-damper arrangements are used to investigate the effectiveness of the axial damper force counteraction approach on improving the collapse resistance. To explore the differences of plastic mechanisms among the retrofitted frames associated with different accumulated axial damper force in the base columns, the percentages of plastic hinges occurred in the columns of the frames are evaluated and compared.

It can be summarized from the results that the horizontal distribution of dampers in different bays indeed affects the building collapse of the building and the counteraction of the additional axial forces is relatively effective to improve the building collapse. Given that the seismic performance of the buildings with different brace-damper arrangements are not with significant differences under the lower intensity levels (such as DBE and MCE), the global collapse resistances of the buildings are dramatically improved by the counteraction of the additional column axial force that are achieved by strategically distributing the dampers in the horizontal direction. It is observed that this improvement could be maximized by maximizing the counteraction of the axial damper forces in the interior columns while arranging the brace-dampers. It is also expected that taller buildings with more complex vibration modes could achieve even larger improvements on the building collapse. In addition, the percentages of plastic hinges in the buildings reveal that the plastic mechanism of buildings is significantly influenced by the horizontal damper distribution especially for taller buildings. By counteracting the additional damper forces in the interior columns, a more desirable plastic mechanism will be achieved for the steel frames. It is also observed that the frames with similar counteraction levels of the axial damper forces would have similar plastic mechanisms and collapse

resistance. In conclusion, considering the remarkable improvements on the building collapse resistance and the plastic mechanism, it is necessary to strategically distribute the brace-dampers in different bays of the tall buildings in the practical industrial design based on the force counteraction approach.

Charter 8

Conclusions

This thesis leads to final conclusions about the strategic placement of viscous dampers in steel buildings under strong earthquakes. The research background presented in Chapter 2 provides a general review of the seismic design approaches including the force-based seismic design and the performance-based seismic design (PBSD). It is pointed out that Incremental Dynamic Analysis (IDA) is an important approach to evaluate the collapse resistance of the building within the framework of PBSD. Then the general types and the applications of supplemental passive dampers are introduced. The importance and the difficulty of distributing the passive dampers in the structures are highlighted. Since the optimum placement of the passive dampers can potentially improve the structural performance and reduce the building cost, it is essential to find out an effective and efficient approach to strategically distribute the dampers in the buildings.

The basic optimization problem and the current limitations of building guidelines for damper placement is outlined in Chapter 3. The optimum distribution of dampers throughout the height of buildings is identified as the fundamental optimization problem for the issue of damper placement, while the arrangement of dampers in different bays is considered as the secondary optimization problem. Several classical damper distribution methods are introduced for the primary optimization problem, following by a literature review on existing damper distribution studies and the corresponding comparative studies. Four categories of damper optimization approaches are summarized for the current damper placement studies and the limitations of these studies are explicitly discussed. It is pointed out that most of the

previous studies do not evaluate the collapse performance of the optimized building and generally do not assess performance under large seismic intensity levels. In addition, the nonlinear behaviors of realistic buildings are seldom considered by previous researchers.

Chapter 4 presents an important and sophisticated optimization methodology which is based on the combination of genetic algorithms (GA) and the nonlinear response history (NRH) analysis. The fundamental knowledges of GA and its superiority on searching complex nonlinear optimization problems are further discussed. A detailed GA-NRH optimization framework interfacing the MATLAB program and the OpenSees program is described with specified parameter settings.

To validate the effectiveness and the efficiency of the GA on vertical damper distribution, Chapter 5 presents a baselines study on optimizing viscous dampers in the elastic shear buildings with the GA-NRH framework. Two simple shear frames with regular and irregular distribution of storey stiffness are used to explore the GA stochastic optimization under a strong earthquake excitation. By comparing the optimization results with those from other damper distribution methods, it is summarized that GA is relatively powerful on optimizing the vertical damper distribution of an elastic building under a single ground motion, especially the building is with irregular distribution of storey stiffness.

In order to investigate the effectiveness of GA in the optimization of code-compliant inelastic buildings, Chapter 6 performs a systematic study on optimizing the height-wise distribution of fluid viscous dampers (FVDs) in nonlinear MRFs with the GA-NRH framework. This study first considers the

collapse performance of the optimized buildings and establishes an integrated framework for optimizing realistic buildings under design-level ground motions and ground motions of higher intensity levels. Instead of considering a single earthquake record for the damper optimization, this research first considers a seismic context with respect to a series of ground motions. Both far-fault ground motions and near-fault ground motions are used to conduct the optimization, while the effect of higher modes is explored by using two steel buildings with different storeys. The inelastic prototype buildings are strictly designed based on the Eurocodes and modeled with considering the nonlinear behaviors in the steel MRFs. The collapse resistance for the optimized buildings are evaluated by conducting the IDA program. By comparing the results of the GA damper distribution with the stiffness proportional damping distribution, it is concluded that GA is not efficient to optimize the vertical damper distribution in code-compliant steel buildings regarding the collapse performance under a given seismic context. Furthermore, as the increase of storeys results in complex modes and large search space, it is highlighted that the height-wise damper distribution of taller realistic buildings could be less feasible to optimize by GA in terms of the collapse resistance. Since the search capability of GA is more powerful than most of other search algorithms, it is pointed out that the vertical damper distribution might be difficult to optimize by other stochastic optimization approaches as well. Compared to the GA distribution, the stiffness proportional damping distribution is more superior to control the structural response and the collapse resistance of realistic buildings under various of ground motions with different intensity levels.

At last, the horizontal damper placement (i.e. damper distribution in different bays) in the steel buildings is explored in Chapter 7. This study explores the

feasibility of the strategic brace-damper arrangements that could counteract the axial damper force in the interior columns to avoid the overstressing columns around the base of buildings. To evaluate the effectiveness of this approach, four steel MRFs with FVDs placed in different bays are used to perform the IDA and the collapse resistance of these retrofitted frames are assessed. The occurrence of the plastic hinges in the columns of the frames are also evaluated to explore the effects of the axial load path on the plastic mechanism. It is founded by this study that the brace-damper arrangement that could maximize the counteraction of the additional axial column forces can significantly increase the collapse resistance of tall buildings, even though the buildings are installed with linear FVDs that experience out of phase behavior under earthquake excitations. It is summarized from the percentages of plastic hinges in the columns that the plastic mechanisms of the retrofitted frames are varied due to the differences of the unbalanced axial damper forces in the base columns. Compared to classic horizontal damper distribution (i.e. dampers all placed in the central bays), strategically distributing dampers in different bays in accordance to the force counteraction approach is more beneficial to enhance the collapse resistance of buildings under strong earthquakes.

Detailed suggestions are provided in each analysis chapter towards the damper optimization. To sum up, GA is very effective to optimize the elastic irregular buildings under a single earthquake at a specified intensity level. For code-compliant nonlinear buildings, the stiffness proportional damping distribution of height-wise dampers is more effective than GA and other stochastic optimization approach to improve the collapse performance of buildings. Moreover, it is essential to strategically distribute passive dampers in different bays of steel frames in practical construction to improve the

collapse performance of buildings.

In summary, this thesis has treated both the primary and the secondary problem of the damper placement in the buildings under strong seismic excitations. It is the first study to investigate the damper placement issues with respect to building collapse and it is also the first attempt to optimize the vertical damper distribution in the realistic buildings regarding a large range of earthquakes and seismic intensity levels. This research has initially answered the question that whether the vertical damper distribution could be optimized by GA and whether the height-wise damper distribution of taller buildings is easier to optimize. A baseline study finds that GA is less effective to optimize the damper distribution than the practical stiffness proportional damping distribution considering the collapse resistance of buildings. The vertical damper distribution of taller buildings is unexpectedly less feasible to optimize compared to that of shorter buildings. Furthermore, for the horizontal damper distribution in steel buildings, it is necessary for structural engineers to utilize the counteraction of the axial damper force in columns to distribute the brace-dampers in different bays of steel frames. Last but not the least, a practical GA optimization framework, which is provided with explicit recommendations of option parameters, has been established for researchers and engineers to optimize damper distribution or any other nonlinear constrained optimization problem.

References

Adhikari, S., & Woodhouse, J. (2000, January). Towards identification of a general model of damping. In *Proceedings of the 18th International Modal Analysis Conference* (Vol. 1, pp. 377-383).

American Society of Civil Engineers (ASCE). (2000). *FEMA 356: Prestandard and Commentary for the Seismic Rehabilitation of Buildings.* Washington, DC, US: Federal Emergency Management Agency.

American Society of Civil Engineers (ASCE). (2006). *ASCE 7-05: Minimum Design Loads for Buildings and Other Structures*. Reston, Virginia, US: Structural Engineering Institute.

Antonucci, R., Balducci, F., Bartera, F., Castellano, M. G., Fuller, K., & Giachetti, R. (2004, August). Shaking table testing of an RC frame with dissipative bracings. In *Proceedings of 13th world conference on earthquake engineering, Vancouver, BC, Canada* (pp. 1-6).

Apostolakis, G., & Dargush, G. F. (2010). Optimal seismic design of moment‐resisting steel frames with hysteretic passive devices. *Earthquake Engineering & Structural Dynamics*, *39*(4), 355-376.

Applied Technology Council (ATC). (2009). *FEMA P695: Quantification of Building Seismic Performance Factors.* Washington, DC, US: Federal Emergency Management Agency.

Ashour, S. A. (1987). *Elastic seismic response of building with supplemental damping*. (Doctoral Dissertation). Michigan Univ., Ann Arbor (USA).

Bäck, T. (1996). *Evolutionary algorithms in theory and practice: evolution strategies, evolutionary programming, genetic algorithms*. Oxford university press.

Baker, J. W. (2007). Quantitative classification of near-fault ground motions using wavelet analysis. *Bulletin of the Seismological Society of America*, *97*(5), 1486-1501.

Bommer, J., & Stafford, P. (2009). Seismic hazard and earthquake actions. In A. Elghazouli, *Seismic Design of Buildings to Eurocode 8* (pp. 6–46). Oxfordshire: Spon Press.

Boyd, S., & Vandenberghe, L. (2004). *Convex optimization*. New York: Cambridge University Press.

BS EN 1993-1-1:2005. (2005). *Eurocode 3: Design of Steel Structures - Part 1-1: General Rules and Rules for Buildings*, British Standards

BS EN 1998-1:2004. (2004). *Eurocode 8: Design of Structures for Earthquake Resistance - Part 1: General Rules, Seismic Actions and Rules for Buildings*, British Standards.

BS EN 1998-3:2005. (2005). *Eurocode 8: Design of Structures of Earthquake Resistance - Part 3: Assessment and Retrofitting of Buildings*, British Standards.

Building Seismic Safety Council (BSSC). (2001). *FEMA 368: NEHRP Recommended Provisions for Seismic Regulations for New Buildings and Other Structures, 2000 Edition*. Washington, DC, US: Federal Emergency Management Agency.

Building Seismic Safety Council (BSSC). (2004). *FEMA 450: NEHRP Recommended Provisions for Seismic Regulations for New Buildings and Other Structures, 2003 Edition*. Washington, DC, US: Federal Emergency Management Agency.

Building Seismic Safety Council (BSSC). (2009). *FEMA P750: NEHRP Recommended Seismic Provisions for New Buildings and Other Structures,*

2009 Edition. Washington, DC, US: Federal Emergency Management Agency.

Champion, C., & Liel, A. (2012). The effect of near－fault directivity on building seismic collapse risk. *Earthquake Engineering & Structural Dynamics*, *41*(10), 1391-1409.

Chopra, A. K. (1995). *Dynamics of structures* (Vol. 3, p. 339). New Jersey: Prentice hall.

Christopoulos, C., Filiatrault, A., & Bertero, V. V. (2006). *Principles of passive supplemental damping and seismic isolation*. Iuss press.

Cimellaro, G. P., & Retamales, R. (2007). Optimal softening and damping design for buildings. *Structural Control and Health Monitoring*, *14*(6), 831-857.

Coley, D. A. (1999). *An introduction to genetic algorithms for scientists and engineers*. World Scientific Publishing Co Inc.

Constantinou, M. C. (2002). Highly Effective Seismic Energy Dissipation Apparatus. Patent No. US-6438905-B2, NY, US.

Constantinou, M.C., Soong, T., & Dargush, G. (1998). *Passive energy dissipation systems for structural design and retrofit*. Buffalo: Multidisciplinary Center for Earthquake Engineering Research.

Constantinou, M.C., & Symans, M. D. (1993a). Experimental study of seismic response of buildings with supplemental fluid dampers. *The Structural Design of Tall and Special Buildings*, *2*(2), 93-132.

Constantinou, M. C., & Symans, M. D. (1993b). Seismic response of structures with supplemental damping. *The structural Design of tall and special buildings*, *2*(2), 77-92.

Constantinou, M.C., & Tadjbakhsh, I. G. (1983). Optimum design of a first

story damping system. *computers & Structures*, *17*(2), 305-310.

Fajfar, P., & Krawinkler, H. (2004, June). Performance-based seismic design concepts and implementation. In *Proceedings of the International Workshop, Bled, Slovenia* (Vol. 28, pp. 2004-05).

Frahm, H. (1911). Device for damping vibrations of bodies. Washington, DC, US.

Gluck, N., Reinhorn, A. M., Gluck, J., & Levy, R. (1996). Design of supplemental dampers for control of structures. *Journal of structural Engineering*, *122*(12), 1394-1399.

Gürgöze, M., & Müller, P. C. (1992). Optimal positioning of dampers in multi-body systems. *Journal of sound and vibration*, *158*(3), 517-530.

Hahn, G. D., & Sathiavageeswaran, K. R. (1992). Effects of added-damper distribution on the seismic response of buildings. *Computers & structures*, *43*(5), 941-950.

Hoffman, E. W., & Richards, P. W. (2014). Efficiently implementing genetic optimization with nonlinear response history analysis of taller buildings. *Journal of Structural Engineering*, *140*(8), A4014011.

Ibarra, L., & Krawinkler, H. (2005). *Global Collapse of Frame Structures under Seismic Excitations* (Report No. 152). Berkeley, CA: Pacific Earthquake Engineering Research Center.

International Code Council. (2015). *International Building Code, 2015 Edition*. Country Club Hills, IL, US: International Code Council, Inc.

ITT (2017). *ITT Infrastructure Products*. NY, US: ITT Enidine Inc.

Karavasilis, T. L., Sause, R., & Ricles, J. M. (2012). Seismic design and evaluation of steel moment‐resisting frames with compressed elastomer

dampers. *Earthquake Engineering & Structural Dynamics*, *41*(3), 411-429.

Kim, J., & Choi, H. (2006). Displacement-based design of supplemental dampers for seismic retrofit of a framed structure. *Journal of Structural Engineering*, *132*(6), 873-883.

Kramer, S. (1999). *Geotechnical Earthquake Engineering*. United States of America: Prentice-Hall Inc.

Krawinkler, H. (1978). Shear in beam-column joints in seismic design of steel frames. *Engineering Journal*, *15*(3), 82-91.

Lavan, O., & Levy, R. (2006). Optimal design of supplemental viscous dampers for linear framed structures. *Earthquake engineering & structural dynamics*, *35*(3), 337-356.

Lavan, O., & Levy, R. (2009). Simple iterative use of Lyapunov's solution for the linear optimal seismic design of passive devices in framed buildings. *Journal of Earthquake Engineering*, *13*(5), 650-666.

Lee, K. S., Ricles, J., & Sause, R. (2009). Performance-based seismic design of steel MRFs with elastomeric dampers. *Journal of structural engineering*, *135*(5), 489-498.

Lee, D., & Taylor, D. (2001). Viscous damper development and future trends. *The Structural Design of Tall Buildings*, *10*(5), 311-320.

Levy, R., & Lavan, O. (2006). Fully stressed design of passive controllers in framed structures for seismic loadings. *Structural and Multidisciplinary Optimization*, *32*(6), 485-498.

Lignos, D. G., & Krawinkler, H. (2011). Deterioration modeling of steel components in support of collapse prediction of steel moment frames under earthquake loading. *Journal of Structural Engineering*, *137*(11), 1291-1302.

Lignos, D. G., Krawinkler, H., & Whittaker, A. S. (2011). Prediction and validation of sidesway collapse of two scale models of a 4‐story steel moment frame. *Earthquake Engineering & Structural Dynamics*, *40*(7), 807-825.

Liu, W., Tong, M., & Lee, G. C. (2005). Optimization methodology for damper configuration based on building performance indices. *Journal of Structural Engineering*, *131*(11), 1746-1756.

Lopez-Garcia, D. (2001). A simple method for the design of optimal damper configurations in MDOF structures. *Earthquake spectra*, *17*(3), 387-398.

MATLAB [Computer software]. (2014). Global Optimization Toolbox Release 2014b. Natick, MA, US: The MathWorks Inc.

Mezzi, M. (2010). Innovative configurations and morphologies using dissipating bracing systems. *9th US NCEE and 10th CanadianCEE, Toronto, Canada*.

Mitchell, M. (1998). *An introduction to genetic algorithms*. Cambridge: MIT Press.

Miyamoto, H., Gilani, A. S., Wada, A., & Ariyaratana, C. (2010). Limit states and failure mechanisms of viscous dampers and the implications for large earthquakes. *Earthquake engineering & structural dynamics*, *39*(11), 1279-1297.

Movaffaghi, H., & Friberg, O. (2006). Optimal placement of dampers in structures using genetic algorithm. *Engineering computations*, *23*(6), 597-606.

Newell, J. D., & Uang, C. M. (2006). *Cyclic behavior of steel columns with combined high axial load and drift demand* (Report No. SSRP-06/22). Department of Structural Engineering, University of California, San Diego.

Open System for Earthquake Engineering Simulation (OpenSees) [Computer software]. (2016). University of California at Berkeley, Berkeley, CA, US: Pacific Earthquake Engineering Research Center.

Pacific Earthquake Engineering Research Center (PEER). (2005). NGA Database. University of California at Berkeley, Berkeley, CA, US. Retrieved from http://peer.berkeley.edu/nga

Paola, M. D., Mendola, L. L., & Navarra, G. (2007). Stochastic seismic analysis of structures with nonlinear viscous dampers. *Journal of Structural Engineering*, 133(10), 1475-1478.

Pearl, J. (1984). Heuristics: intelligent search strategies for computer problem solving. Addison-Wesley.

Porter, K., Kennedy, R., & Bachman, R. (2007). Creating fragility functions for performance-based earthquake engineering. *Earthquake Spectra*, *23*(2), 471-489.

Priestley, M. J. N. (2000). Performance based seismic design. *Bulletin of the New Zealand society for earthquake engineering*, *33*(3), 325-346.

SAP2000 [Computer software] (2009). Static and dynamic finite element analysis of structures. Version 14. Berkeley, CA, US: Computers and Structures Inc.

Seleemah, A. A., & Constantinou, M. C. (1997). *Investigation of seismic response of buildings with linear and nonlinear fluid viscous dampers* (Report No. NCEER-97-0004). National Center for Earthquake Engineering Research.

Shukla, A. K., & Datta, T. K. (1999). Optimal use of viscoelastic dampers in building frames for seismic force. *Journal of Structural Engineering*, *125*(4), 401-409.

Şigaher, A. N., & Constantinou, M. C. (2003). Scissor-jack-damper energy dissipation system. *Earthquake Spectra*, *19*(1), 133-158.

Singh, M. P., & Moreschi, L. M. (2001). Optimal seismic response control with dampers. *Earthquake engineering & structural dynamics*, *30*(4), 553-572.

Singh, M. P., & Moreschi, L. M. (2002). Optimal placement of dampers for passive response control. *Earthquake Engineering & Structural Dynamics*, *31*(4), 955-976.

Soneji, B., & Jangid, R. (2007). Passive hybrid systems for earthquake protection of cable-stayed bridge. *Engineering Structures*, *29*(1), 57-70.

Soong, T. T., & Dargush, G. F. (1997). *Passive energy dissipation systems in structural engineering*. Wiley.

Structural Engineers Association of California (SEAOC) (1995). *Vision 2000 Committee: Performance Based Seismic Engineering of Buildings*. Sacramento, CA, US: California Office of Emergency Services.

Symans, M. D., Charney, F. A., Whittaker, A. S., Constantinou, M. C., Kircher, C. A., Johnson, M. W., & McNamara, R. J. (2008). Energy dissipation systems for seismic applications: current practice and recent developments. *Journal of structural engineering*, *134*(1), 3-21.

Takewaki, I. (1997). Optimal damper placement for minimum transfer functions. *Earthquake Engineering & Structural Dynamics*, *26*(11), 1113-1124.

Takewaki, I. (2000). Optimal damper placement for planar building frames using transfer functions. *Structural and Multidisciplinary Optimization*, *20*(4), 280-287.

Takewaki, I. (2009). *Building Control with Passive Dampers: Optimal Performance-based Design for*. John Wiley & Sons.

Taylor Devices Inc. (2017). Retrieved from http://www.taylordevices.com

Taylor, D. P. (2000). Toggle brace dampers: A new concept for structural control. In *Advanced Technology in Structural Engineering* (pp. 1-8).

Taylor, D. P. (2002). *History, design, and applications of fluid dampers in structural engineering*. NY, US: TAYLOR Devices Inc.

Taylor, D. P., & Constantinou, M. C. (1998). *Fluid dampers for applications of seismic energy dissipation and seismic isolation*. NY, US: Taylor Devices Inc.

Trombetti, T., & Silvestri, S. (2006). On the modal damping ratios of shear-type structures equipped with Rayleigh damping systems. *Journal of sound and vibration*, *292*(1), 21-58.

Uriz, P., & Whittaker, A. S. (2001). Retrofit of pre‐Northridge steel moment‐resisting frames using fluid viscous dampers. *The Structural Design of Tall and Special Buildings*, *10*(5), 371-390.

Vamvatsikos, D., & Cornell, C. (2002). Incremental dynamic analysis. *Earthquake Engineering & Structural Dynamics*, *31*(3), 491-514.

Vas, P. (1999). *Artificial-intelligence-based electrical machines and drives: application of fuzzy, neural, fuzzy-neural, and genetic-algorithm-based techniques* (Vol. 45). Oxford university press.

Whittaker, A. S., Constantinou, M. C., Ramirez, O. M., Johnson, M. W., & Chrysostomou, C. Z. (2003). Equivalent lateral force and modal analysis procedures of the 2000 NEHRP Provisions for buildings with damping systems. *Earthquake Spectra*, *19*(4), 959-980.

Whittle, J. K., Williams, M. S., Karavasilis, T. L., & Blakeborough, A. (2012a). A comparison of viscous damper placement methods for improving seismic building design. *Journal of Earthquake Engineering*, *16*(4), 540-560.

Whittle, J. K., Williams, M. S., & Blakeborough, A. (2012b). Performance of Structural Members In Seismic Retrofitted Frames with Viscous Dampers. *University of Oxford, UK*.

Wu, B., Ou, J. P., & Soong, T. T. (1997). Optimal placement of energy dissipation devices for three-dimensional structures. *Engineering Structures*, *19*(2), 113-125.

Zhang, R. H., & Soong, T. T. (1992). Seismic design of viscoelastic dampers for structural applications. *Journal of Structural Engineering*, *118*(5), 1375-1392.